Modification of biomaterials for the immobilization and release of chemokines

Zur Erlangung des Grades eines Doktors der Naturwissenschaften (Dr. rer. nat.)
Genehmigte Dissertation von Michelle Fiona Kilb aus Hanau
Tag der Einreichung: 9. Februar 2023, Tag der Prüfung: 28. März 2023

1. Gutachten: Prof. Dr. Katja Schmitz
2. Gutachten: Prof. Dr. Harald Kolmar
Darmstadt, Technische Universität Darmstadt 2023

TECHNISCHE UNIVERSITÄT DARMSTADT

Fachbereich Chemie
Clemens-Schöpf-Institut für Organische Chemie und Biochemie
Arbeitsgruppe Prof. Dr. Katja Schmitz

Modification of biomaterials for the immobilization and release of chemokines

Accepted doctoral thesis by Michelle Fiona Kilb

Date of submission: February 9, 2023
Date of thesis defense: March 28, 2023

Darmstadt, Technische Universität Darmstadt 2023

Bitte zitieren Sie dieses Dokument als:
URN: urn:nbn:de:tuda-tuprints-236410
URL: http://tuprints.ulb.tu-darmstadt.de/23641
Jahr der Veröffentlichung auf TUprints: 2023

Dieses Dokument wird bereitgestellt von tuprints,
E-Publishing-Service der TU Darmstadt
http://tuprints.ulb.tu-darmstadt.de
tuprints@ulb.tu-darmstadt.de

Die Veröffentlichung steht unter folgender Creative Commons Lizenz:
Namensnennung 4.0 International
https://creativecommons.org/licenses/by/4.0/

This work is licensed under a Creative Commons License:
Attribution 4.0 International
https://creativecommons.org/licenses/by/4.0/

For mum

Erklärungen laut Promotionsordnung

§8 Abs. 1 lit. c PromO

Ich versichere hiermit, dass die elektronische Version meiner Dissertation mit der schriftlichen Version übereinstimmt und für die Durchführung des Promotionsverfahrens vorliegt.

§8 Abs. 1 lit. d PromO

Ich versichere hiermit, dass zu einem vorherigen Zeitpunkt noch keine Promotion versucht wurde und zu keinem früheren Zeitpunkt an einer in-oder ausländischen Hochschule eingereicht wurde. In diesem Fall sind nähere Angaben über Zeitpunkt, Hochschule, Dissertationsthema und Ergebnis dieses Versuchs mitzuteilen.

§9 Abs. 1 PromO

Ich versichere hiermit, dass die vorliegende Dissertation selbstständig und nur unter Verwendung der angegebenen Quellen verfasst wurde.

§9 Abs. 2 PromO

Die Arbeit hat bisher noch nicht zu Prüfungszwecken gedient.

Darmstadt, 9. Februar 2023

Michelle Fiona Kilb

The present work was written from April 1, 2020 to February 9, 2023 in the department of chemistry at the Clemens-Schöpf-Institute of Organic Chemistry and Biochemistry at the Technical University of Darmstadt under the supervision of Prof. Dr. Katja Schmitz.

Parts of this work have already been published or presented at conferences:

Publications

Kilb, M.F.; Ritz, U.; Nickel, D.; Schmitz, K. pH-Dependent Release of Vancomycin from Modularly Assembled Collagen Laminates. Polymers **2022**, 14, 5227, doi:10.3390/polym14235227.

Kilb, M.F.; Engemann, V.I.; Siddique, A.; Stark, R.W.; Schmitz, K. Immobilisation of CXCL8 gradients in microfluidic devices for migration experiments. Colloids Surf. B Biointerfaces **2021**, 198, 111498, doi:10.1016/j.colsurfb.2020.111498.

Braun, J.; Eckes, S.; **Kilb, M.F.**; Fischer, D.; Eßbach, C.; Rommens, P.M.; Drees, P.; Schmitz, K.; Nickel, D.; Ritz, U. Mechanical characterization of rose bengal and green light crosslinked collagen scaffolds for regenerative medicine. Regen. Biomater. **2021**, 8, rbab059, doi:10.1093/rb/rbab059.

Kilb, M.F.; Moos, Y.; Eckes, S.; Braun, J.; Ritz, U.; Nickel, D.; Schmitz, K. An Additively Manufactured Sample Holder to Measure the Controlled Release of Vancomycin from Collagen Laminates. Biomedicines **2021**, 9, 1668, doi:10.3390/biomedicines9111668.

Abstracts

“Migration of THP-1 cells on immobilized IL-8 gradients in microfluidic devices“, Microfluidics: Designing the Next Wave of Biological Inquiry – Virtual Conference, EMBL, **2020**

Poster presentation

“Directed release of vancomycin from modularly assembled collagen laminates”, GDCh Biochemistry Conference, Münster, Germany, **2022**

* These authors have contributed equally to this publication.

Acknowledgments

At this point I would like to thank everyone who supported and motivated me.

In the first place, I would like to thank Prof. Dr. Katja Schmitz, who gave me the opportunity to write my PhD thesis in her research group, who supported me during my entire thesis and who gave me the opportunity to visit conferences. I also wish to thank Prof. Dr. Harald Kolmar for taking over the co-reference.

My thanks go to Anke Imrich, who helped me with the sub-cultivation and preparation of cells for microfluidic experiments. I would also like to thank the entire working group of Prof. Dr. Katja Schmitz for the pleasant working atmosphere and the nice lunch breaks. I would also like to thank the research groups Hausch and Schmidt as well as the Merck Lab, who allowed me to use their ice machine, the -80 °C freezer and the Image Analyzer LAS-3000. I specially would like to thank Dr. Asma Siddique, who prepared microfluidic channels for me and whose collaboration I always enjoyed. I also wish to thank the DFG for the financial support of the project ”CoLOsAM”. At this point I especially would like to thank Dr. Ulrike Ritz, Prof. Dr. Ing. habil. Daniela Nickel, Dr. Joy Braun and Stefanie Eckes for the pleasant cooperation. I have really enjoyed working with you.

I especially would like to thank my former research group colleagues, Stefanie Eckes, Julia Wack and Victoria Engemann for their humorous manner, their trust in me, their true friendship and their support in every situation of life.

My special thanks go to my family and friends, who supported me during my entire study and especially during my PhD thesis. I would like to thank my mum, Rhonda Kilb, who showed me that you should not give up hope until the end and I would like to thank my father, Thomas Kilb, who impresses me every day anew with his positive manner. I also wish to thank my brother Matthias Kilb, who always believes in me and is one of the smartest people I know. My special thanks go to my boyfriend Yannik Moos, who always supports and believes in me in every situation of life. I do not know what I would do without you.

Contents

List of abbreviations

APTES	(3-aminopropyl)triethoxysilane
ATH	Antithrombin-heparin complex
BMSC	Bone marrow stromal cell
BSA	Bovine serum albumin
CCL2	Monocyte chemoattractant protein (MCP-1)
CV	Column volume
CX3CL1	Fractalkine
CXCL12	Stromal cell-derived factor 1 (SDF-1)
CXCL8	Interleukin-8 (IL-8)
DAG	Diacylglycerol
DMF	Dimethylformamide
ECM	Extracellular matrix
EDC	1-Ethyl-3-(3-dimethylaminopropyl)carbodiimide
ELR	Sequence motif containing glutamate, leucine and arginine
FBS	Fetal bovine serum
FITC	Fluorescein isothiocyanate
GAG	Glycosaminoglycan
GDP	Guanosine diphosphate
GlcA	D-glucoronic acid
GlcN	Glucosamine
GlcNAc	D-N-acetylglucosamine
GPCR	G protein-coupled receptor
GTP	Guanosine triphosphate
HSPG	Heparan sulfate proteoglycan
ICAM1	Intercellular adhesion molecule 1
IdoA	Iduronic acid
IL-1	Interleukin-1
IP_3	Inositol 1,4,5-trisphosphate
LAPAP	Laser-assisted protein adsorption by photobleaching
LB	Lysogeny broth
LFA1	Lymphocyte function-associated antigen 1
LPS	Lipopolysaccharide
MAC1	Macrophage antigen 1
NHS	N-hydroxysuccinimide
OD_{600}	Optical density at a wavelength of 600 nm
PDMS	Polydimethylsiloxane
PDT	Photodynamic therapy
pI	Isoelectric point
PI3K	Phosphoinositide 3-kinase

PIP_2	Phosphatidylinositol (4,5)-bisphosphate
PIP_3	Phosphatidylinositol (3,4,5)-trisphosphate
PKC	Proteinkinase C
PLC	Phospholipase C
PSGL1	P-selectin glycoprotein ligand 1
PTB	Photoactivated tissue bonding
PTP	Photochemical tissue passivation
PTT	Photothermal therapy
RB	Rose bengal
RGX	Rose bengal and green light cross-linking
ROI	Region of interest
RT	Room temperature
SAM	Self-assembled monolayer
SSI	Surgical site infection
TNF	Tumor necrosis factor
VCAM1	Vascular cell-adhesion molecule 1
VLA4	Very late antigen 4
XCL1	Single cysteine motif-1α (SCM-1α)
XCL2	Single cysteine motif-1β (SCM-1β)

1. Abstract

The presentation of biologically active molecules by modified biomacromolecules is of scientific interest for the understanding and treatment of inflammatory processes. The focus of this work lies on the presentation of chemokines to analyze chemokine-induced cell migration and on the characterization of photodynamically modified collagen biomaterials.

In regenerative medicine, controlled drug release by modified biomaterials represents an important technique, as side effects due to systemic or excessive local drug applications can be avoided. Collagen is a commonly used biomaterial in regenerative medecine, as it provides a substrate for the adhesion of cells and is degraded to non-toxic products. Modifications of the biomaterial collagen by rose bengal and green light cross-linking (RGX) have already been described for different clinical applications, such as for orthopedics or ophthalmology. In this work RGX was used to bond stacks of different collagen materials to laminates with tailored properties for a biomedical application, e.g. a controlled drug release to avoid surgical site infections (SSIs). SSIs are the most common complications in orthopedic surgery and can be prevented by antimicrobial prophylaxis. The aim of this work was to characterize multilayered collagen laminates in terms of their swelling behavior and antibiotic release. For the fabrication of multilayered collagen laminates, two types of collagen materials were selected. The results indicated that homogeneous laminates composed of sponge-like collagen showed a lower swelling degree than a single RGX-treated, sponge-like collagen sheet. This was explained by the additional layer of rose bengal at the interface between the piled sheets. In contrast, homogeneous laminates composed of a thin collagen membrane did not show any change in their swelling degree, independent of the number of collagen layers. This was explained by the compact structure of the material. Heterogeneous collagen laminates composed of both materials reached swelling degree values in-between. For homogeneous sponge-like laminates and heterogeneous laminates the experimental swelling degrees were significantly smaller then the theoretical ones. These findings were explained by the different number of available swelling interfaces in laminates compared to individual sheets. To test the release of the model antibiotic vancomycin, an additively manufactured sample holder was developed, which allows to quantify the release of vancomycin into opposite directions. The sample holder elongated the time until half-maximal release was reached. This can be attributed to the decreased size of release areas compared to a sample in solution. Release experiments with heterogeneous, bi-layer collagen laminates under physiological conditions showed that the release of vancomycin preferentially takes place at the surface of a thin collagen film instead of sponge-like collagen, independent of the laminate's orientation or loading. Furthermore, loading of vancomycin into the sponge-like collagen layer of heterogeneous, bi-layer collagen laminates led to an elongated time of half-maximal release. Studies with triple-layer collagen laminates led to similar results, as the time for half-maximal release increased with the number of sponge-like collagen layers. Furthermore, vancomycin was again preferentially released at the surface of the thin collagen film layer. These findings can be explained by shorter diffusion pathways and a negligible effect of re-swelling for the thin collagen film in contrast to the sponge-like collagen. In detail, the higher porosity results in a higher swelling degree. Compression by insertion of the sample into the sample holder therefore has a stronger effect on the sponge-like material and leads to a larger uptake

of fluid during re-swelling that is opposed to the diffusion of vancomycin out of the collagen sheet. Consequently, vancomycin is released more slowly. In contrast to bi-layer laminates, the orientation of triple-layer heterogeneous laminates determined to which extent vancomycin was released by the thin collagen film layer. This can be explained by an increased swelling of sponge-like collagen at the bottom side of the sample holder. Similarly, an increased swelling and release at the bottom side of a triple-layer, sponge-like, homogeneous collagen laminate was observed. This can be attributed to the laminate's thickness. Overall, these findings reveal mechanisms that must be considered for the composition of collagen laminates.

Since the pH can change during wound healing or infections, release studies under alkaline (pH 8.5) or acidic (pH 5.5) conditions reported for these processes were carried out. The pH did not have any effect on the total amount of released vancomycin from single sheets of RGX-modified, sponge-like collagen or heterogeneous, bi-layer laminates. The latter showed again a preferential release at the side of the thin collagen film layer, as observed for physiological pH (pH 7.4). In addition, the release from RGX-modified single sheets and bi-layer laminates was retarded at pH 5.5, which was explained by an increased swelling degree at this pH. At pH 8.5, the release was also delayed but no changes in the swelling degree were observed between pH 8.5 and pH 7.4. These results might be explained by electrostatic interactions, as negatively charged vancomycin might interact with positively charged areas of collagen at pH 8.5. The findings of this work can be used in regenerative medicine, as sponge-like collagen would be more suitable for a delayed release of active substances that support tissue regeneration.

In summary, the results showed that the biomaterial collagen can be modularly assembled to laminates that allow a controlled and directed release of antibiotics. These findings are of biomedical interest, as sponge-like collagen may be more suitable for the delayed release of active substances at later stages of wound healing than for the fast release of antibiotics at infected sites. Further studies might include the release of proteins from collagen laminates or the cross-linking of proteins within collagen matrices with RGX for a delayed release.

The second part of this work dealt with the presentation of biologically active molecules, such as chemokines on surfaces. These small secreted signaling proteins induce and steer the migration of cells in homeostatic and inflammatory processes. Chemokines interact with corresponding receptors on the surfaces of cells, induce different signaling cascades and lead to cellular responses, such as cell migration. The latter can either occur along soluble chemokine concentration gradients, which is specified as chemotaxis, or along surface-bound gradients, a process termed haptotaxis. As chemokines are also involved in different diseases, understanding the migration of cells upon chemokine stimulation contributes to understand and treat inflammatory processes. Interleukin-8 (CXCL8) was used as a model inflammatory chemokine in this work.

In previous works, a dopamine-heparin coating had been developed that allowed a reversible immobilization of CXCL8 in microfluidic channels. In this work, reversibly immobilized CXCL8 gradients in microfluidic channels should be further characterized with respect to their suitability for different migration experiments. The results indicated that the dopamine-heparin coating led to a homogeneous distribution of CXCL8. Furthermore, the gradient stability at 37 °C was not different from previous experiments at room temperature. Cell migration experiments confirmed a directed and reproducible migration of THP-1 cells that express receptors for CXCL8 along the reversibly immobilized CXCL8 gradient towards high concentrations of CXCL8. Control experiments did not show any directed cell migration only in the presence of buffer or homogeneously distributed chemokine. Since chemokine

gradients naturally occur as a mixture of soluble and immobilized gradients, the influence of overlaid, soluble chemokine on the gradient and cell migration was examined. An overlay of the gradient with soluble chemokine that has a concentration in the same order of magnitude as initial CXCL8 used for gradient formation increased the gradient's steepness within the first 20 h of incubation and led to a delay of cell migration. In contrast, very low concentrations of soluble CXCL8 overlaid over the immobilized gradient did not influence directed cell migration. In summary, the method represents a simple setup to analyze to which extent non-covalently immobilized chemokine gradients are influenced by soluble chemokine and enables a reproducible analysis of cell migration along these gradients.

Since the coating method with dopamine and heparin only enables a non-covalent immobilization of CXCL8 that changed over the time of the migration experiment, it was attempted to covalently immobilize CXCL8 in microfluidic channels. The development of a suitable method was motivated by the fact that RGX worked well in the former project for cross-linking collagen layers and that collagen is a commonly used substrate in migration studies. However, no CXCL8 immobilization could be detected under the tested conditions. Interaction studies could not confirm an interaction of CXCL8 with collagen, while weak, non-specific interactions of RB with CXCL8 and BSA were observed. However, the interactions were apparently not sufficient to activate the protein for binding to collagen. As the immobilization of native proteins by a photodynamic process is attractive, future studies might involve the use of higher light intensities to develop an immobilization method.

2. Zusammenfassung

Die Präsentation von biologisch aktiven Molekülen durch modifizierte Biomakromoleküle ist von wissenschaftlichem Interesse für das Verständnis und die Behandlung von inflammatorischen Prozessen. Der Fokus dieser Arbeit liegt auf der Präsentation von Chemokinen zur Analyse der chemokininduzierten Zellmigration und der Charakterisierung von photodynamisch modifizierten Kollagenbiomaterialien.

In der regenerativen Medizin stellt die kontrollierte Wirkstofffreisetzung durch modifizierte Biomaterialien ein wichtiges Thema dar, da Nebenwirkungen durch systemische oder zu hohe lokale Wirkstoffapplikationen verhindert werden können. Kollagen ist ein häufig verwendetes Biomaterial in der regenerativen Medizin, da es ein Substrat für die Adhäsion von Zellen darstellt und zu nichttoxischen Produkten abgebaut wird. Modifikationen des Biomaterials Kollagen mittels Quervernetzung mit Bengalrosa und grünem Licht (RGX) wurden bereits für verschiedene klinische Anwendungen beschrieben, wie zum Beispiel für die Orthopädie und Augenheilkunde. In dieser Arbeit wurde RGX verwendet, um Stapel verschiedener Kollagenmaterialien zu Laminaten mit angepassten Eigenschaften für biomedizinische Anwendungen zu verbinden, z.B. eine kontrollierte Wirkstoffreisetzung zur Prävention von post-operativen Wundinfektionen (SSIs). SSIs stellen die am häufigsten vorkommenden Komplikationen in der orthopädischen Chirurgie dar und können durch antimikrobielle Prophylaxe verhindert werden. Ziel dieser Arbeit war es, mehrschichtige Kollagenlaminate bezüglich ihres Quellverhaltens und der Freisetzung eines Antibiotikums zu charakterisieren. Für die Herstellung mehrschichtiger Kollagenlaminate wurden zwei Arten an Kollagenmaterialien ausgewählt. Die Ergebnisse zeigten, dass homogene Laminate aus schwammartigem Kollagen ein niedrigeres Quellvermögen zeigten als eine RGX-behandelte, schwammartige Kollageneinzelschicht. Dies wurde durch die zusätzliche Schicht an Bengalrosa an der Grenzfläche zwischen den gestapelten Einzelschichten erklärt. Im Gegensatz dazu zeigten homogene Laminate aus einer dünnen Kollagenmembran keine Änderung des Quellvermögens, unabhängig von der Anzahl an Kollagenschichten. Dies wurde durch die kompakte Struktur des Laminats erklärt. Heterogene Kollagenlaminate, die aus beiden Materialien aufgebaut waren, erreichten dazwischenliegende Werte für das Quellvermögen. Für homogene Laminate aus schwammartigen Kollagen und heterogene Laminate war das experimentell bestimmte Quellvermögen signifikant kleiner als das theoretische. Diese Erkenntnisse wurden durch die unterschiedliche Anzahl an möglichen Quellungsgrenzflächen im Laminat gegenüber den einzelnen Schichten erklärt. Um die Freisetzung des Modellantibiotikums Vancomycin zu testen, wurde ein additiv gefertigter Probenhalter entwickelt, der es ermöglicht, die Freisetzung von Vancomycin in gegensätzliche Richtungen zu quantifizieren. Der Probenhalter verzögerte die Zeit, bis eine halbmaximalen Freisetzung erreicht wurde. Dies kann einer verringerten Freisetzungsfläche im Vergleich zu einer Probe in Lösung zugeschrieben werden. Freisetzungsversuche mit heterogenen, zweischichtigen Kollagenlaminaten unter physiologischen Bedingungen zeigten, dass die Freisetzung von Vancomycin bevorzugt an der Oberfläche eines dünnen Kollagenfilms statt eines schwammartigen Kollagens stattfindet, unabhängig von der Orientierung oder Beladung des Laminats. Darüber hinaus führte eine Beladung von Vancomycin in der schwammartigen Kollagenschicht von heterogenen, zweischichtigen Kollagenlaminaten zu einer verlängerten Zeit zur halbmaximalen Freisetzung. Studien mit dreischichtigen Kollagenlaminaten ergaben ähnliche Ergebnisse, da sich die

Zeit für die halbmaximale Freisetzung mit der Anzahl an schwammartigen Kollagenschichten verlängerte. Des Weiteren wurde Vancomycin wieder bevorzugt an der Oberfläche der dünnen Kollagenfilmschicht freigesetzt. Diese Erkenntnisse können durch kürzere Diffusionswege und einem vernachlässigbaren Effekt des erneuten Quellens im Gegensatz zu schwammartigen Kollagen erklärt werden. Im Einzelnen ergibt sich aus der höheren Porosität ein höheres Quellvermögen. Kompression durch die Insertion der Probe in den Probenhalter hat demnach einen stärkeren Effekt auf das schwammartige Material und führt zu einer stärkeren Flüssigkeitsaufnahme während des erneuten Quellens, die der Richtung der Vancomycinfreisetzung aus der Kollagenschicht entgegen gerichtet ist. Damit wird das Vancomycin langsamer freigesetzt. Im Gegensatz zu zweischichtigen Laminaten, bestimmte die Orientierung von dreischichtigen, heterogenen Laminaten in welchem Ausmaß Vancomycin von der dünnen Kollagenfilmschicht freigesetzt wurde. Dies kann durch eine verstärkte Quellung des schwammartigen Kollagens an der unteren Seite des Probenhalters erklärt werden. In ähnlicher Weise wurde eine stärkere Quellung und Freisetzung an der unteren Seite eines dreischichtigen, schwammartigen, homogenen Kollagenlaminats beobachtet. Dies kann der Dicke des Laminats zugeschrieben werden. Insgesamt zeigen diese Befunde Mechanismen auf, die bei der Zusammensetzung von Kollagenlaminaten berücksichtigt werden müssen.

Da sich der pH Wert während der Wundheilung oder Infektionen ändern kann, wurden Freisetzungsversuche unter alkalischen (pH 8,5) oder sauren (pH 5,5) Bedingungen durchgeführt, die für diese Prozesse beschrieben wurden. Der pH hatte keinen Einfluss auf die freigesetzte Gesamtmenge an Vancomycin aus RGX-modifiziertem, schwammartigen Kollagen oder heterogenen, zweischichtigen Laminaten. Letztere zeigten erneut eine bevorzugte Freisetzung auf der Seite der dünnen Kollagenfilmschicht, wie bei physiologischem pH (pH 7,4) beobachtet. Darüber hinaus war die Freisetzung aus RGX-modifizierten Einzelschichten und zweischichtigen Laminaten bei pH 5,5 verzögert, was mit einem erhöhtem Quellvermögen bei diesem pH erklärt wurde. Bei pH 8,5 war die Freisetzung ebenfalls verzögert, jedoch wurden keine Änderungen des Quellvermögens zwischen pH 8,5 und pH 7,4 beobachtet. Diese Ergebnisse könnten durch elektrostatische Interaktionen erklärt werden, da negativ geladenes Vancomycin mit positiv geladenen Bereichen des Kollagen bei pH 8,5 interagieren könnte. Die Erkenntnisse dieser Arbeit lassen sich in der regenerativen Medizin nutzen, da schwammartiges Kollagen besser für eine verzögerte Freisetzung von aktiven Substanzen geeignet wäre, welche die Geweberegeneration unterstützen.

Zusammenfassend zeigten die Ergebnisse, dass das Biomaterial Kollagen modular zu Laminaten zusammengesetzt werden kann, welche eine kontrollierte und gerichtete Freisetzung von Antibiotika erlauben. Diese Erkenntnisse sind von biomedizinischem Interesse, da schwammartiges Kollagen eher für die verzögerte Freisetzung von aktiven Substanzen zu späteren Zeitpunkten der Wundheilung geeignet sein könnte als für die schnelle Freisetzung von Antibiotika an infizierten Stellen. Weitere Studien könnten die Proteinfreisetzung aus Kollagenlaminaten oder die Quervernetzung von Proteinen innerhalb von Kollagenmatrixen mittels RGX für eine verzögerte Freisetzung umfassen.

Der zweite Teil dieser Arbeit behandelte die Präsentation biologisch aktiver Moleküle, wie z.B. Chemokine auf Oberflächen. Diese kleinen Signalproteine induzieren und lenken die Migration von Zellen in homöostatischen und inflammatorischen Prozessen. Chemokine interagieren mit entsprechenden Rezeptoren auf den Oberflächen von Zellen, induzieren verschiedene Signalkaskaden und führen zu zellulären Antworten, wie zum Beispiel der Zellmigration. Letztere kann entweder entlang löslicher Chemokinkonzentrationsgradienten stattfinden, was als Chemotaxis bezeichnet wird, oder entlang oberflächengebundener Gradienten, ein Prozess der Haptotaxis genannt wird. Da Chemokine auch in

verschiedenen Krankheiten involviert sind, ist das Verständnis der Migration von Zellen nach Chemokinstimulation eine Grundlage um inflammatorische Prozesse zu verstehen und zu behandeln. Interleukin-8 (CXCL8) wurde in dieser Arbeit als Modellchemokin verwendet.

In vorherigen Arbeiten wurde eine Dopamin-Heparin-Beschichtung entwickelt, die eine reversible Immobilisierung von CXCL8 in mikrofluidischen Kanälen ermöglicht. In dieser Arbeit sollten reversibel immobilisierte CXCL8-Gradienten in mikrofluidischen Kanälen in Hinblick auf ihre Eignung für verschiedene Migrationsexperimente weiter charakterisiert werden. Die Ergebnisse zeigten, dass die Dopamin-Heparin-Beschichtung eine homogene Verteilung von CXCL8 ermöglichte. Darüber hinaus war die Gradientenstabilität bei 37 °C nicht anders als bei früheren Experimenten bei Raumtemperatur. Zellmigrationsexperimente bestätigten eine gerichtete und reproduzierbare Migration von THP-1-Zellen, die Rezeptoren für CXCL8 exprimieren, entlang des reversibel immobilisierten CXCL8-Gradienten zu hohen Konzentration an CXCL8 hin. Kontrollversuche zeigten keine gerichtete Zellmigration nur in der Anwesenheit von Puffer oder homogen verteiltem Chemokin. Da Chemokingradienten natürlicherweise als Mischung von löslichen und immobilisierten Gradienten auftreten, wurde der Einfluss von überlagertem, löslichem Chemokin auf den Gradienten und die Zellmigration untersucht. Eine Überlagerung des Gradienten mit löslichem Chemokin, dessen Konzentration in derselben Größenordnung liegt wie die des CXCL8, welches zur Gradientenbildung verwendet wurde, führte zu einer erhöhten Gradientensteilheit innerhalb der ersten 20 h der Inkubation und zu einer Verlangsamung der gerichteten Zellmigration. Im Gegensatz dazu hatten sehr niedrige Konzentrationen an löslichem CXCL8, das den immobilisierten Gradienten überlagerte, keinen Einfluss auf die gerichtete Zellmigration. Zusammenfassend stellt die Methode einen einfachen Aufbau dar, um zu analysieren, in welchem Ausmaß nicht-kovalent immobilisierte Chemokingradienten durch lösliches Chemokin beeinflusst werden und ermöglicht eine reproduzierbare Analyse der Zellmigration entlang dieser Gradienten.

Da die Beschichtungsmethode mit Dopamin und Heparin nur eine nicht-kovalente Immobilisierung von CXCL8 ermöglicht, die sich über die Zeit des Migrationsexperiments verändert, wurde versucht, CXCL8 kovalent in mikrofluidischen Kanälen zu immobilisieren. Die Entwicklung einer geeigneten Methode war dadurch motiviert, dass RGX zur Quervernetzung von Kollagenschichten im ersten Projekt gut funktioniert hatte und Kollagen ein häufig verwendetes Substrat in Migrationsstudien ist. Unter den getesteten Bedingungen konnte jedoch keine CXCL8 Immobilisierung detektiert werden. Interaktionsstudien konnten keine Interaktion von CXCL8 mit Kollagen bestätigen, während schwache, unspezifische Interaktionen von RB mit CXCL8 und BSA beobachtet konnten. Die Interaktionen waren aber offenbar nicht ausreichend, um das Protein für eine Bindung ans Kollagen zu aktivieren. Da die Immobilisierung nativer Proteine durch einen photodynamischen Prozess attraktiv ist, könnten zukünftige Studien die Verwendung höherer Lichtintensitäten zur Entwicklung einer Immobilisierungsmethode beinhalten.

3. Introduction

In order to understand and treat inflammatory processes, the presentation of biologically active molecules by modified biomacromolecules is of scientific interest. The modification of biomaterials, such as collagen, has several advantages in terms of antibiotic administration and will be discussed in the following chapters. Besides biomedical application, the modification of biomaterials also enables the presentation of bio-active substances, such as chemokines. The function of chemokines in cell migration processes and tools to study chemokine-mediated cell migration will be described in the following chapters as well.

3.1. Surgical site infections

Surgical site infections (SSIs) describe infections due to microbial contamination that arise within a post-operative period of 30 days without an implant or within one year after implantation.[1, 2] SSIs include wound infection, regional extension and organ or visceral infection.[1] The frequency of infection depends on the wound classification, the surgical procedure and the surgical site.[3, 4] SSIs are divided into different types, belong to the most common complications after orthopedic surgery and increase both, healing time as well as costs.[1, 5] Different risk factors have been identified for SSIs, e.g. diabetes, smoking, the duration and microbiological contamination of operative procedures and deficient antibiotic treatment.[2, 5] Furthermore, the risk of SSIs in orthopedic procedures is increased by the usage of implants.[3] The predominant microorganism causing SSIs is the gram-positive *Staphylococcus aureus* (50.4 %), followed by the gram-negative microorganisms *Escherichia coli* (46.4 %), *Pseudomonas aeruginosa* (15.9 %) and *Citrobacter spp.* (15.9 %).[6] The most effective reported antibiotics against gram-positive bacteria, such as *Staphylococcus aureus*, are vancomycin, teicoplanin, linezolid and amikacin.[6]

3.2. Antibiotic administration

The prevention of SSIs depends on the timing of surgical antimicrobial prophylaxis and is commonly addressed by prophylactic systemic antibiotic administration.[3, 7] However, the systemic application of antibiotics, either oral or intravenous, has several disadvantages as it might lead to adverse side effects or drug resistance.[4, 8, 9] For example, Harbarth *et al.* found out that a prolonged antibiotic prophylaxis increases the risk of antibiotic resistance after cardiovascular surgery.[10] Moreover, a systemic administration also leads to low concentrations at the target site.[4, 9] In comparison, the local antibiotic administration allows a high antibiotic concentration at the injury site for a long period without systemic adverse side effects.[3] As the antibiotic exposure time and concentration can decrease cell viability, the controlled, local release of antibiotics is desirable.[4] A controlled antibiotic release allows an increase of the therapeutic activity, efficacy and reduces the toxicity of the antimicrobial drug.[11] In orthopedic surgery, the local application of antibiotics is achieved by different methods, e.g. lyophilized powder for short term exposure or bone cements loaded with antibiotics for a prolonged

antibiotic exposure.[3] On the one hand, antibiotic-loaded bone cements, e.g. fabricated from polymethylmethacrylate, are characterized by an ideal antibiotic release and bone compatibility.[12] On the other hand, they have inferior mechanical properties and require removal by additional surgery, since they are non-biodegradable.[3, 12] Consequently, the controlled release of antibiotics from biodegradable delivery systems, such as biodegradable nanoparticles, is of interest.[12] For example, Abdullah *et al.* used polycaprolactone-coated chitin-lignin gels loaded with penicillin/streptomycin for a controlled drug release without measurable cytotoxicity.[8]

In order to treat infected bone defects or SSIs, different antibiotics are available, for example tetracyclines, tobramycin and vancomycin (see figure 3.1).[9, 13] Tetracyclines belong to the polyketides and are characterized by a broad-spectrum antibacterial activity.[9] The latter is based on the prevention of aminoacyl-tRNA binding to the ribosomal acceptor site, leading to protein synthesis inhibition.[14] Tetracyclines have been used during bone grafting procedures, however, many pathogens have attained resistance against tetracyclines.[9] The aminoglycoside tobramycin is derived from *Streptomyces tenebrarius* and inhibits the mRNA translation.[9, 15] It is active against gram-negative bacteria and *Staphylococcus aureus*.[9] Vancomycin is a glycopeptide derived from *Amycolatopsis orientalis* and inhibits the cell wall synthesis.[9, 15] As opposed to tobramycin, vancomycin is only effective against gram-positive bacteria.[9] One advantage of vancomycin is that it can be applied to patients with a β-lactam allergy.[13] Furthermore, vancomycin is thermally stable, has only a low risk of allergy and a low serum protein binding.[15] Vancomycin only has a negligible effect or no inhibitory effect on the replication of cells, such as osteoblasts, up to a local concentration of 1000 µg/mL *in vitro*.[16] The release of vancomycin from different biomaterials has been reported in the literature. Hartinger *et al.* showed that carbodiimide cross-linked collagen can be used for the controlled release of vancomycin, as approximately 85 % of vancomycin were released after seven days.[17] The release kinetics of vancomycin from cross-linked gelatin as biodegradable delivery system has been studied by Tigani *et al.*[18] They used the non-zero-length cross-linker glutaraldehyde to chemically cross-link gelatin and achieved a total release from 30 % to 54 % of vancomycin after 1920 h.[18] They showed that the release properties depend on the cross-linking degree, as the time for half-maximal release increased with the degree of cross-linking and the release of vancomycin is driven by its diffusion through the polymer network.[18] In detail, the release of vancomycin from a completely cross-linked polymer, which has lost its biodegradability, can be entirely described by Fickian diffusion.[18] In contrast, the release of vancomycin from a partially cross-linked polymer that still maintains its biodegradability, is described by the Fickian diffusion through the polymer network as well as the degradation process of the polymer.[18] Furthermore, Lopez *et al.* analyzed the release of vancomycin from layered double hydroxides, which are biocompatible inorganic materials.[11] The release values varied between 40 % and 100 %, depending on the synthesize method of the complexes composed of vancomycine and layered double hydroxide.[11] Moreover, Besheli *et al.* used silk scaffolds with vancomycin-loaded silk fibroin nanoparticles as drug delivery systems, resulting in release values up to 100 % within 14 days.[19] Since vancomycin is commonly used in surgery to prevent infections [4], vancomycin was used as a model antibiotic for release experiments to analyze the antimicrobial properties of different collagen laminates.

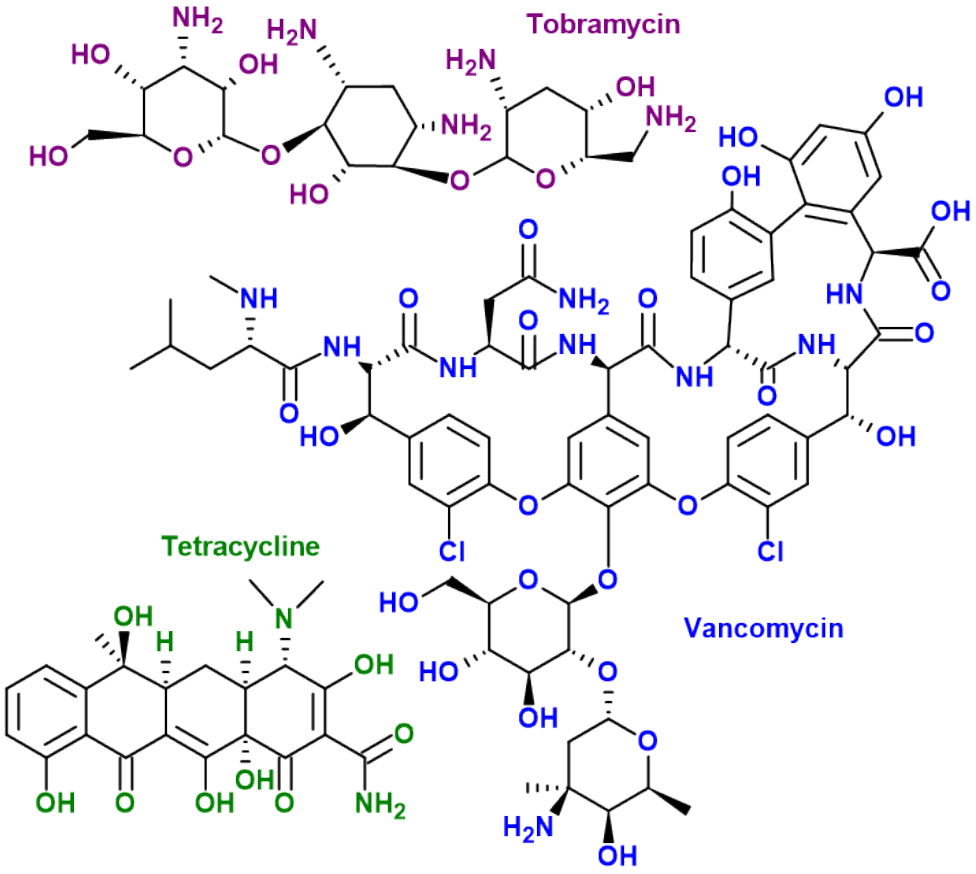

Figure 3.1.: Chemical structure of tetracycline [20], tobramycin [21] and vancomycin [22].

3.3. Biomaterials for regenerative medicine

3.3.1. Hydrogels

Hydrogels are defined as cross-linked polymer networks that contain a high amount of water.[23] They are characterized by a good biocompatibility and flexibility in size and shape.[23] Furthermore, hydrogels provide spacial and temporal control of drug release.[23] Hydrogels are classified into macroscopic hydrogels, microgels and nanogels, according to their gel size.[23] Macroscopic hydrogels can be applied as transdermal patches, epicardial implants or can be injected.[23] Injectable macroscopic hydrogels are further divided into three different types.[23] The first type, named *in situ* gelling hydrogels, are injectable macroscopic hydrogels that gel inside the body.[23] In contrast, shear-thinning hydrogels first pre-gel outside the body, followed by injection under shear stress and then recover their initial rigidity inside the body, once shear stress is not applied anymore.[23] The third type, termed macroporous hydrogels, refers to hydrogels that mechanically collapse and then reach their initial shape inside the body, once the mechanical stress is removed.[23] Microgels can either be applied by injection or by oral or pulmonary administration.[23] Nanogels are mostly applied systemically.[23]

In hydrogels, the uptake of liquid is possible due to the meshes that are open spaces between the polymer networks.[23] The exposure of a hydrogel to a compatible solvent leads to the swelling of the

hydrogel (see figure 3.2).[24] During swelling, the solvent molecules penetrate from the surface of the hydrogel into the hydrogel, separating a rubbery region from a non-solvated region with a flexible boundary.[24] This flexible boundary is described as swelling interface.[25] In the rubbery region, the mesh network expands, resulting in further diffusion of solvent molecules into the polymeric network of the hydrogel, thus, the swelling interface moves towards the non-solvated region.[24, 25] The interface separating the rubbery region from the solvent is termed polymer interface and moves outwards.[25] The swelling properties of a hydrogel depend on the type of the porous structure as well as the degree of porosity.[24] The porosity can range from hydrogels without network porosity to hydrogels with high porosity, characterized by an interconnected open-cell structure.[24] Based on the above mentioned parameters, hydrogels are divided into four classes, of which micro-porous hydrogels are mostly used in biomedical applications and controlled release technologies.[24] For micro-porous hydrogels, the major swelling mechanism combines molecular diffusion and convection in water-filled pores.[24] In the body, the swelling or de-swelling of a hydrogel depends on the difference of the osmotic pressure between the hydrogel and the tissue.[26] Khan *et al.* found out that the swelling of low viscous chitosan poly(vinyl)alcohol co-polymers decreased with an increased cross-linking by glutaraldehyde.[27]

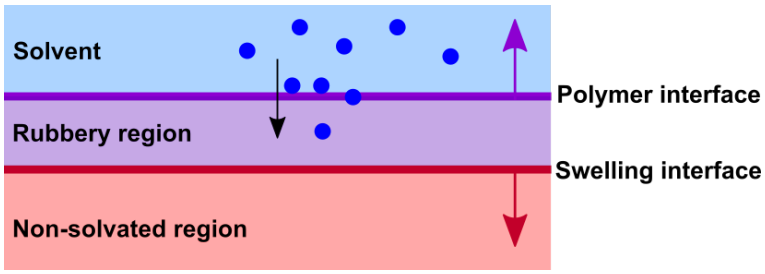

Figure 3.2.: Schematic illustration of hydrogel swelling, based on Peppas *et al.*[25] The penetration of solvent molecules (blue dots) into a hydrogel leads to the formation of a swelling interface (red line) that moves towards the non-solvated region of the hydrogel, while a polymer interface (purple line) moves to the opposite direction.

If a hydrogel is loaded with a drug, the mesh size, defined as the distance between polymer molecules in the network, has an influence on the diffusion of the drug inside the network and the drug release from the network.[23] Drugs with a smaller size than the mesh size diffuse fast and therefore have a short release time.[23] Drugs with a comparable size as the mesh size diffuse slowly.[23] If the drug size is larger than the mesh size, the drug is immobilized and can only be released by degradation, deformation or swelling of the polymer.[23]

Hydrogels are used in different medicinal fields, e.g. wound healing, oncology or immunology. For a medical application, the biocompatibility displays an important characteristic as it describes a material's ability to locally induce and promote normal wound healing, reconstruction and the integration of tissue.[26, 28] In literature, a quantitative expression of biocompatibility was proposed that depends on different parameters, e.g. the number of macrophages or angiogenesis.[28] An ideal biological scaffold due to its high tissue specificity is the native extracellular matrix (ECM).[29] One advantage of hydrogels is their structural and compositional similarity to the ECM and their ability for engineering, e.g. regarding cellular attachment control.[29] Important factors for the biocompatibility of hydrogels are pore sizes that are large enough for cell growth, cell proliferation, cell migration and diffusion of metabolites and waste.[29] Moreover, hydrogels should enable cell attachment and a sufficient

environment to enable vascularization.[29, 30] Furthermore, the degradation of the hydrogel into fragments should not be toxic, controlled and dependent on the application.[29] For example, permanent or semi-permanent scaffolds are most qualified for corneal replacement.[30] Different synthetic and biological materials are used in hydrogels in regenerative medicine. Synthetic materials such as poly(lactic acid), poly(glycolic acid) and poly(lactic-co-glycolic acid) are used for skin, cartilage, bone, vessel and other applications.[29] Natural polymers such as collagen, gelatin, hyaluronic acid or pullulan are used as hydrogel-based scaffolds for cartilage, skin, eye, vascular and many other applications.[29] Mostly collagen type I is used for the fabrication of collagen hydrogels as it is biocompatible, allows cell adhesion and provides a native viscoelastic environment for cells.[31]

3.3.2. Collagen types, structure and biosynthesis

Collagens belong to the most abundant proteins in the ECM and are the main component of the connective tissue where they contribute to tissue and organ stability.[32] Furthermore, collagens function as storage and by release of cellular mediators.[32] Based on their structure and supramolecular organization, the 28 collagen types [33] are divided into fibril-forming collagens (e.g. collagen type I and II), basement membrane collagens (e.g. collagen type IV), microfibrillar collagens (e.g. collagen type VI), anchoring fibrils (e.g. collagen type VII), hexagonal network-forming collagens (e.g. collagen type VIII), transmembrane collagens (e.g. collagen type XIII), multiplexins (e.g. collagen type XV) and fibril-associated collagens (e.g. collagen type IX).[32] The most abundant collagen subfamily are fibril-forming collagens.[32]

Structurally, collagens are characterized by a right-handed triple helix that is composed of three identical or different α-chains (see figure 3.3).[32] The above mentioned different collagen types depend on the combination of α-chains and the peptide sequence.[33] Each α-chain is characterized by a repeating sequence of glycine at every third position and a high amount of proline and hydroxyproline in-between.[32] The glycine residues enable the assembly of the three α-chains to a triple helix and are located in the center of the triple helix.[32] The latter is stabilized by intramolecular hydrogen bonds due to 4-hydroxyproline.[32] Besides the triple helical domain, the length of which varies between the different collagen types, non-collagenous domains can be found at each end of the triple helical part.[32] In detail, non-helical telopeptides at both ends of the central triple helical domain are followed by a N-propeptide or a C-propeptide, respectively.[32] Both propeptides are cleaved off during biosynthesis and are not part of the mature collagen.[32]

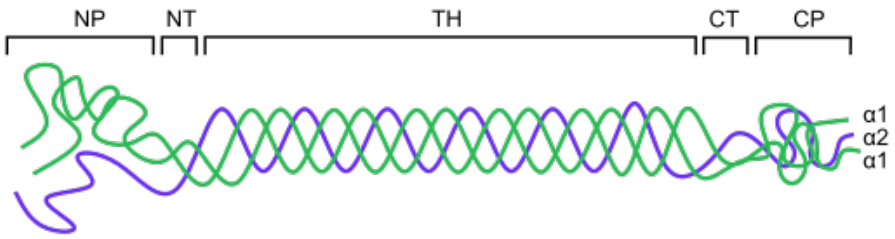

Figure 3.3.: Schematic illustration of the collagen structure based on Gelse *et al.* [32] Three α-chains assemble to a triple helix (TH) that is flanked by non-helical telopeptides (NT and CT) and propeptide domains (NP and CP) at the N- and C-terminus.

In the connective tissue, the main production of collagen takes place in the fibroblasts.[34] The biosynthesis (see figure 3.4) of collagen starts in the nucleus, where the gene is transcribed and alternative splicing occurs, to result in different collagen types.[32] The mature mRNA is transported from the nucleus to the rough endoplasmic reticulum, where the translation into pre-procollagen takes place.[32] After removal of the signal peptide the procollagen molecule is post-translationally modified by enzymatic hydroxylation of lysins and prolines as well as glycosylation of hydroxylated lysins in the rough endoplasmic reticulum.[32] After post-translational modification, the C-propeptide is stabilized by intrachain disulphide bonds and three α-chains align at the C-terminus to form a triple helix.[32] At the Golgi apparatus, the procollagen molecules are packed into secretory vesicles and released into the extracellular space.[32] In the extracellular space, the N- and C-propeptide are cleaved off and the resulting molecule is termed tropocollagen.[32, 35] Tropocollagen first self-assembles into five-stranded and then larger collagen fibrils by hydrophobic and electrostatic interactions.[32] The fibril formation is influenced by propeptides and stabilized by covalent cross-linking.[32] The cross-linking occurs due to the hydroxylation of lysines by lysyl oxidases in the telopeptide region and is of importance for the stability of the collagen molecule.[32]

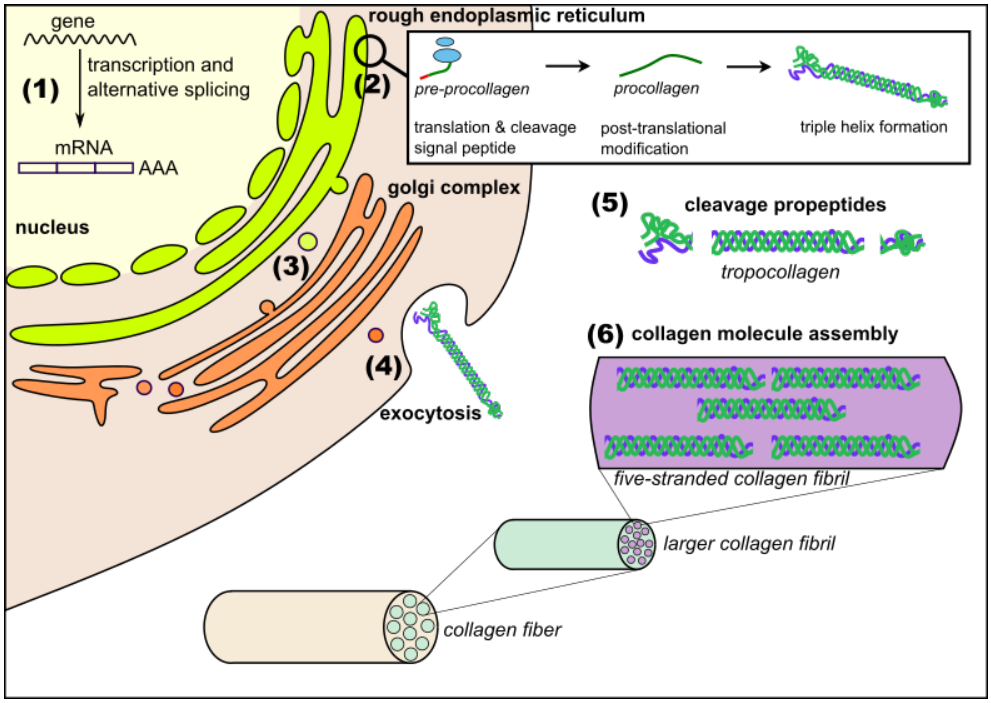

Figure 3.4.: Schematic illustration of the collagen biosynthesis based on Gelse *et al.*[32]

3.3.3. Collagen in regenerative medicine

Collagen is a commonly used biomaterial in regenerative medicine as it provides physiological interaction by cell adhesion and has mechanical strength.[33] Furthermore, it is degraded to non-toxic products and has a low immunogenicity depending on its source.[32] For example, collagen is used as a scaffold for skin wound healing, as it interacts with platelets, leading to a suitable matrix for further inflammatory cells.[33] Collagen as a biomaterial is recombinantly produced, e.g. in *Escherichia coli*, or extracted from

animal sources such as rat, pork or cow.[33] Animal-derived collagen has the main disadvantages of batch-to-batch variability, immunogenicity, disease transmission and allergies as opposed to recombinantly produced human collagen.[33] However, recombinantly produced collagen needs additional post-translational modifications, depending on the host.[33]

3.3.4. Collagen modifications

Atelocollagen

As described above, immunogenicity and the risk of allergic reactions represent a problem for the use of collagen in regenerative medicine. To overcome these problems, the telopeptide region can be removed from tropocollagen to yield atelocollagen that has a lower immunogenicity.[36, 37] However, the proteolytic cleavage of the telopeptides from the remaining triple-helical quaternary structure leads to a lower stability of the collagen molecule.[38, 39] Atelocollagen has already been used for implants, plastic surgical products and as a drug delivery system for different molecules.[36, 37]

Cross-linking of collagen

Biodegradability and biocompatibility belong to the main advantages of collagen for the application as a biomaterial. Since both, mechanical stability and protease resistance, are important properties for biomaterial implantation, different cross-linking techniques are available to improve the properties of collagen and to regulate its mechanical stability and degradation.[34] During cross-linking, covalent bonds are formed between the functional groups of the protein.[34] In the following chapters, different cross-linking techniques that have been used to modify the properties of collagen are described.

Chemical cross-linking of collagen

The formation of covalent bonds by chemical cross-linking can either be achieved by non-zero-length cross-linkers or zero-length cross-linkers. Non-zero-length cross-linkers such as glutaraldehyde remain as part of the cross-linked structure.[40] Glutaraldehyde reacts with free primary amine groups of collagen (lysine, hydroxylysine or histidine), forming a carbinolamine as intermediate that further reacts to a Schiff base under dehydration, resulting in imide cross-linked collagen fibers.[40] Glutaraldehyde reaches a high degree of cross-linking and Olde Damink *et al.* were able to show that cross-linking of aligned collagen fibers by glutaraldehyde increases collagen tensile strength.[40, 41] Tigani *et al.* used glutaraldehyde to cross-link gelatine.[18]

Zero-length chemical cross-linkers are not incorporated into the cross-linked structure.[40] One example for a zero-length chemical cross-linker is 1-ethyl-3-(3-dimethylami-nopropyl) carbodiimide (EDC) in combination with N-hydroxysuccinimide (NHS).[40] The cross-linking mechanism of EDC-NHS relies on the reaction of EDC with free carboxylic acid groups of collagen (glutamic acid or aspartic acid), forming an O-acylisourea intermediate that reacts with NHS to an activated ester. The latter further reacts with free amine groups, resulting in amide cross-linked collagen.[40] Compared to the cross-linking with glutaraldehyde, EDC-NHS results in a lower cross-linking density and a more hydrophilic surface.[40] Furthermore, EDC-NHS is less cytotoxic compared to glutaraldehyde.[40] However, cross-linking with EDC-NHS has the disadvantage that the cross-links have an influence on the integrin-recognition sequence required for the binding of cells to collagen.[40]

Besides covalent bonds, cross-linking can also be achieved by ionic bonds.[34] One example for a non-toxic, non-covalent cross-linking agent is the biopolymer chitosan, a polycationic molecule.[34] The cross-linking mechanism relies on the formation of ionic bonds between the positively charged amino groups of chitosan and the negatively charged carboxylic groups of collagen.[34] One advantage of this cross-linking method is the one-step-preparation process and the fact that chitosan itself is a biocompatible hydrogel.[34]

Enzymatic cross-linking of collagen

Enzymatical collagen cross-linking can be achieved by transglutaminases, a class of enzymes commonly found in biology and widely used in biotechnology. Transglutaminases catalyze the reaction between glutamine and lysine, forming an isopeptide bond.[40, 42] In detail, the transglutaminase binds to glutamine and forms an acyl-enzyme intermediate under release of ammonia.[40, 42] The acyl-enzyme intermediate is attacked by a primary amine and an amide bond is formed at the glutamine site (transamidation).[40, 42] One advantage of the cross-linking with transglutaminase is that no chemical residues or side-products are incorporated into the cross-linked structure.[34]

Physical cross-linking of collagen

Different methods have been reported in the literature for the formation of covalent bonds by physical cross-linking. One example is dehydrothermal treatment. The reaction is favored by removing the by-product water by heat and vacuum.[40] In this method, amino groups of collagen react with carboxylic acid, resulting in amide cross-linked collagen.[40] One disadvantage of dehydrothermal treatment is that the reaction is non-specific and that thermal degradation might occur.

Besides dehydrothermal treatment, ultraviolet radiation can be used for physical cross-linking of collagen. In this method, reactive radicals are formed, mainly by the excitation of carbonyl bonds, and simplify the formation of cross-links as they react with adjacent amino acids.[40] Compared to dehydrothermal cross-linking, ultraviolet radiation is only effective for thin and/or transparent material, needs less time and is also non-specific.[34]

Photodynamic cross-linking of collagen

Since physical and chemical cross-linking methods have some disadvantages, such as toxicity of residual reagents or side products or thermal degradation, photodynamic cross-linking is an alternative that operates under milde conditions and allows an improvement of the properties of collagen without influencing its biocompatibility.[43] Photodynamic cross-linking describes the formation of protein-protein cross-links after light-activation of a photosensitizing dye.[44] In biomedical applications methylene blue, riboflavin and rose bengal (RB, see figure 3.5) belong to commonly used photosensitizers.[45, 46] All three photosensitizers are also used for other applications, e.g. as vitamin or for the treatment of methemoglobinemia.[40, 47] Wang *et al.* used RB-conjugated gold nanorods for oral cancer treatment in a hamster model study by combining a photodynamic therapy (PDT) with a photothermal therapy (PTT).[48] In PDT, RB is activated by light and reacts with substrates or molecular oxygen to yield reactive species that damage cancer tissues.[48] In PTT, the heat generated by exposure to near-infrared light leads to the death of cancer cells.[48] Gold nanorods are well suited for PTT, as they strongly absorb light and transform the photon energy in heat.[49]

Besides the focused cross-linking of a specific region, the simple cross-linking technique and the excitation of dyes by visible light are advantages of photodynamic cross-linking.[50, 51] The cross-linking principle relies on the absorption of light by the dye, leading to the formation of excited triplet species that attack the protein, either directly or via singlet oxygen.[52] The created radicals then lead to cross-linking.[52] It follows, that a high triplet quantum yield is of importance for this kind of reaction.[53] RB (2,4,5,7-tetraiodo-3,‘4’,5’,6’-tetrachlorofluorescein) belongs to the xanthene dyes and has a triplet quantum yield of 0.786 in water.[54, 55] It has three proteolytic species, leading to pKa values of 1.89 and 3.93.[56] The absorption maximum of RB in water is at a wavelength of 548 nm while the emission maximum is at a wavelength of 566 nm.[57] The fluorescence quantum yield reaches a value of 0.018 for RB in water.[57, 58]

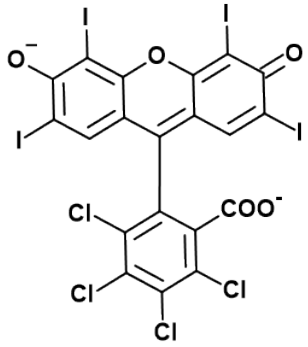

Figure 3.5.: Chemical structure of RB.[59]

The molecular mechanism of photochemical cross-linking of collagen by RB and exposure to green light (RGX) largely remain unknown.[44] In the RGX mechanism, two different pathways are distinguished from each other. In the energy transfer pathway, the light-activation of RB leads to an excited triplet state of RB and the energy is transferred from the excited triplet state of RB to oxygen, resulting in singlet oxygen.[52] The latter reacts with the protein by transferring its energy under formation of radicals that initiate protein cross-linking.[52] In the other pathway, termed electron transfer pathway, the light-activation of RB leads to an excited triplet state of RB that accepts an electron from an electron donor molecule, e.g. an amine, resulting in an excited donor molecule and an RB anion radical.[52] This radical species further initiates protein cross-linking.[52] The generation of radicals is also used in PDT. Alarcon *et al.* proposed that RB aggregates are able to bind to positively charged amino acids of collagen and if the oxygen level is low, the excited triplet state of RB accepts an electron from arginine side chains.[44] The protein cross-linking is initiated by RB anion radicals or arginine cation radicals.[44] In an environment with a sufficiently high oxygen concentration, the energy transfer pathway predominates.[60] Wertheimer *et al.* were able to show that RB prefers the energy transfer pathway if arginine and oxygen are present.[60]

The effect of RGX on different collagen materials has already been described in the literature. Chan *et al.* cross-linked collagens by using an argon laser (514 nm) together with the photosensitizing dye RB, resulting in an improvement of the properties of collagen regarding its strength, stiffness and stability.[43] Furthermore, photodynamic cross-linking has been used for several clinical applications.[51] Photo cross-linking can either take place between two tissue surfaces (wound closure), within a tissue to change its mechanical properties (biomechanical stiffening), within a tissue to change the biological response (photochemical tissue passivation (PTP)) or to modify a biomaterial (tissue engineering).[51]

In dermatology, Tsao *et al.* showed in a human study that photoactivated tissue bonding (PTB) [61] after skin excision only led to little inflammation and a better scar appearance than conventional surface stitches.[62] Furthermore, Zhu *et al.* used RGX in ophthalmology to increase the stiffness of the cornea in rabbits.[63] Photodynamic cross-linking has also been used in orthopedics, as Mazaki *et al.* used furfurylamin-conjugated gelatin cross-linked by RGX to repair osteochondral defects in rabbits.[64] In terms of changing the biological response within a tissue, Fernandes *et al.* showed that PTP can be used to prevent a capsular contraction after the insertion of breast implants.[65] Salinas *et al.* also used PTP by light-activating an RB-coated tissue to strengthen adventitial collagen, resulting in a prevention of intimal hyperplasia in a vein graft model.[66]

In our own research group, Eckes *et al.* analyzed the properties of three different, commercially available collagen sheets after RGX-treatment.[67] In detail, a thin collagen sheet named Collagen Solutions after its supplier, a compact collagen sheet named Viscofan and a sponge-like atelocollagen sheet referred to as Atelocollagen were examined.[67] RGX-treatment was performed with a 0.01 % (w/v) solution of RB and 10 min exposure to green light (565 nm).[67] According to Eckes *et al.*, RGX achieved a higher mechanical stability of sponge-like Atelocollagen, as the swelling degree was reduced and the thickness significantly changed compared to unmodified samples.[67] Furthermore, RGX led to an increased viability of osteoblasts on RGX-treated Atelocollagen and Collagen Solutions.[67] Moreover, Eckes *et al.* were able to show that RGX allows the assembly of single collagen sheets to collagen laminates. The mechanical behavior of collagen laminates as well as the response of cells to these laminates and their degradability have been systematically analyzed by Braun *et al.*[68]

3.4. Chemokines

3.4.1. Classes of chemokines

Chemokines are small signaling proteins that are secreted in response to injury or inflammation.[69] They are also named chemotactic cytokines [70], as they influence the communication and interaction of cells and induce chemotaxis.[71] Chemokines have a molecular weight of 8 kDa to 12 kDa.[72] They are mostly secreted into the extracellular space, where they form soluble or bound chemokine gradients and selectively recruit immune cells.[70, 72] There are 23 chemokine receptors and over 40 human chemokines known.[73] All chemokines share a common structure, consisting of a flexible N-terminal domain, an N-loop that leads into a three-stranded antiparallel β-sheet, followed by a C-terminal α-helix.[72] The first and the second β-strand are connected by a 30s loop and the second and third β-sheet are connected by a 40s loop.[72] Disulfide bonds stabilize the protein fold and enable the formation of a Greek key motif as a secondary structure.[69, 72] The common structure of chemokines is shown in figure 3.6.

Based on the number and location of conserved cysteines at the N-terminus and the number of amino acids between the conserved cysteines, chemokines are classified into four different groups, termed C, CC, CXC and CX3C chemokines.[74–76] The structures of the different chemokine classes are shown in figure 3.6. CXC chemokines are further subdivided into ELR+ and ELR- CXC chemokines [76], dependent on whether they have a glutamate (E)-leucine (L)-arginine (R)-motif in the N-terminus.[77, 78] The existence and proximity of the ELR-motif to the N-terminus determines whether CXC chemokines are able to attract neutrophils or not.[77, 78] Furthermore, the presence of the ELR-motif is also important for the angiogenetic activity of CXC chemokines.[79] One example for an ELR+CXC chemokine is interleukin-8 (IL-8, CXCL8) that plays an important role in the trafficking of neutrophils.[70] Stromal

cell-derived factor 1 (SDF-1, CXCL12) belongs to the ELR-CXC chemokines and functions in the homing of neutrophils to the bone marrow.[70, 74, 76] Chemokines of the CC subfamily, such as monocyte chemoattractant protein-1 (MCP-1, CCL2) also fulfill important immune functions, e.g. the inflammatory monocyte trafficking.[70] For the class of C chemokines only two variants are known, termed single cysteine motif -1α (SCM-1α, XCL1) and single cysteine motif -1β (SCM-1β, XCL2), while only one CX3C chemokine is known, named fractalkine (CX3CL1).[70]

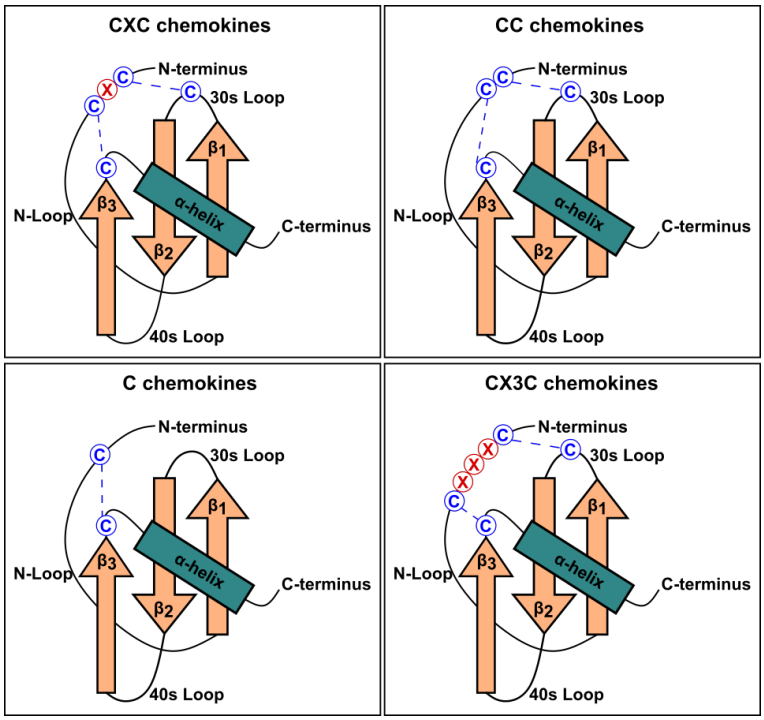

Figure 3.6.: Illustration of the four chemokine classes, modified according to Rollins *et al.* and Deshmane *et al.* [72, 76] The protein fold is stabilized by disulfide bonds (dashed lines).

3.4.2. Interleukin-8 (CXCL8)

In 1987, CXCL8 was identified by different research groups as a tissue-derived peptide that has the ability to activate neutrophils and is secreted by monocytes, T lymphocytes, neutrophils, fibroblasts, endothelial cells and epithelial cells in response to inflammation.[76, 80] CXCL8 was formerly purified from the supernatant of stimulated human blood mononuclear phagocytes [80] and belongs to the class of ELR+CXC chemokines.[76] CXCL8 is produced by mononuclear cells after environmental stress or after stimulation with lipopolysaccharide (LPS), interleukin-1 (IL-1) and tumor necrosis factor (TNF) as a 99 amino acid long precursor.[81, 82] The precursor is secreted after cleavage of a 20 amino acid long signaling sequence.[83] Extracellular processing, starting from the N-terminus, leads to four different variants.[83] The main mature variant (70 %) has a length of 72 amino acids and a molecular weight of 8 kDa [81, 84], while the other N-terminal variants have a length of 77 (17 %), 70 (8 %) or 69 amino acids (5 %).[84] For the sequence of the 72 amino acid variant, the ELR-motif is located at position four to six [78] and Lindley *et al.* showed that the 72 amino acid variant can be recombinantly produced in *Escherichia coli*.[84] The sequence [78] of the main mature variant is shown below:

SAKELRCQCIKTYSKPFEPKFIKELRVIESGPECANTEIIVKLSDGRELCLDPKENWVQRVVEKFLKRAENS

In 1989, Clore *et al.* determined the secondary structure of the CXCL8 monomer.[85] The CXCL8 monomer is able to form a dimer in solution, which is stabilized by hydrogen bonds between the first β-sheet [82] resulting in a six-stranded anti-parallel β-sheet (see figure 3.7).[85] CXCL8 binds to two different receptors, named CXCR1 and CXCR2, leading to cellular reactions of neutrophils, endothelial cells and cancer cells.[76, 86] Even though the CXCL8 monomer as well as the dimer bind to the CXCR2 receptor with similar affinities, the monomer has a higher affinity for the CXCR1 receptor than the dimer.[82] Both CXCL8 receptors share a sequence homology of 77 % and their genes are located on chromosome 2q35.[74, 87] The interaction of CXCL8 with its receptor CXCR1 is based on the interaction of the receptor's N-terminal domain with the N-loop of CXCL8 (Site-I), followed by the interaction of the chemokines ELR-motif with the second and third extracellular loop (Site-II) of CXCR1 (arg199, arg203 and asp265).[69, 88–91] The C-terminal region of CXCL8 is of importance for the binding of CXCL8 to the membrane of endothelial cells and the following emigration of leukocytes *in vivo* from the blood vessels.[92]

Figure 3.7.: Structure of the CXCL8 dimer in solution, obtained from PDB 1IL8.[93]

CXCL8 and its receptors are involved in different inflammatory diseases, such as chronic obstructive pulmonary disorder, the development of asthma, cystic fibrosis, inflammatory bowel disease, neuro-inflammatory diseases, vascular diseases, arthritis and cancer.[82, 94] The angiogenetic effect is important for the progression of a tumor, as the tumor vasculature provides a sufficient oxygen and nutrient supply.[82] In 2020, Li *et al.* also showed that the clinical scores of different patients suffering from COVID-19 correlated with the amount of CXCL8 at different time points, so CXCL8 might be used as a biomarker for COVID-19.[95]

Interaction of CXCL8 with glycosaminoglycans

Linear polysaccharides with disaccharides composed of an amino sugar and an uronic acid or galactose are described as glycosaminoglycans (GAGs).[96, 97] The attachment of one or more GAGs to a protein core by a tetrasaccharide linker leads to the formation of proteoglycans that are present at the surface of cells and in the ECM.[96] One example for proteoglycans are heparan sulfate proteoglycans (HSPGs).[98] HSPGs contain heparan sulfate that is composed of dimers of amino sugar D-N-acetylglucosamine (GlcNAc) and D-glucuronic acid (GlcA).[96, 99] The negatively-charged carboxylic acid units and sulfate groups lead to the high negative charge of GAGs.[97] HSPGs have the

ability to bind chemokines and cytokines by electrostatic and non-ionic interactions and are involved in the recruitment of leukocytes, as they are present on epithelial cells, endothelial cells and in basement membranes.[92, 97, 98] The binding of chemokines to GAGs on the surface of endothelial cells also prevents the disordering of chemokine gradients by diffusion or proteolysis.[100, 101] Closely related to heparan sulfate is heparin, which is able to bind CXCL8 by its C-terminus.[102] Heparin is composed of sulfated iduronic acid (IdoA) and sulfated glucosamine (GlcN) and has a higher sulfation degree than heparan sulfate.[99] In CXCL8, amino acids of the C-terminal helix (arg60, lys64, lys67 and arg68) and of the proximal loop (lys20) are responsible for the binding of CXCL8 to heparin.[103] Figure 3.8 shows the major disaccharide repeating units of heparin and heparan sulfate.

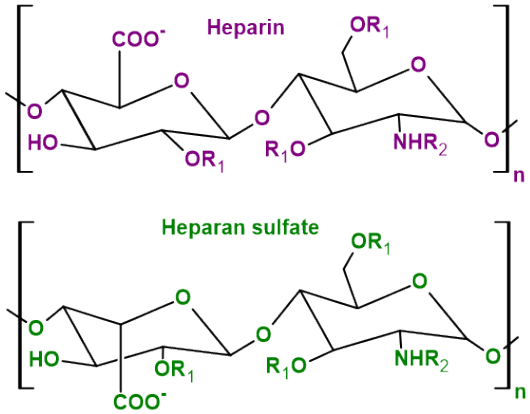

Figure 3.8.: Chemical structure of the major disaccharide repeating units of heparin and heparan sulfate (R_1 = H or SO_3^- and R_2 = H, SO_3^- or $COCH_3^-$), based on Morla.[97]

Signaling cascades induced by CXCL8

The coordination of the migration of immune cells in the body is based on the interaction of an individual chemokine with different receptors and *vice versa*.[69] Chemokine receptors are classified into two groups, G protein-coupled receptors (GPCRs) and atypical chemokine receptors.[74] The classification is based on the sequence motif DRYLAIV, which is present in the third transmembrane domain of GPCRs but not in atypical chemokine receptors.[74] The receptors have an extracellular N-terminus, seven hydrophobic transmembrane domains that are linked to each other by three extracellular and three intracellular loops and an intracellular C-terminus.[73] Chemokine GPCRs can be further classified into homeostatic receptors, inflammatory receptors or receptors that act as both, homeostatic and inflammatory receptors.[74]

The binding of CXCL8 to the rhodopsin-like class A GPCRs [104] CXCR1/2 leads to the activation of the respective receptor. In the inactivated form, heterotrimeric G protein consisting of an α_i-, β- and γ-subunit is bound to the receptor with guanosine diphosphate (GDP) located in its binding pocket.[104–106] After binding of CXCL8 to the receptor, a conformational change of the receptor takes place, leading to the exchange of GDP for guanosine triphosphate (GTP) and a dissociation of the Gα_i-subunit from the G$\beta\gamma$-subunit (see figure 3.9). As a result, different signaling pathways are induced.

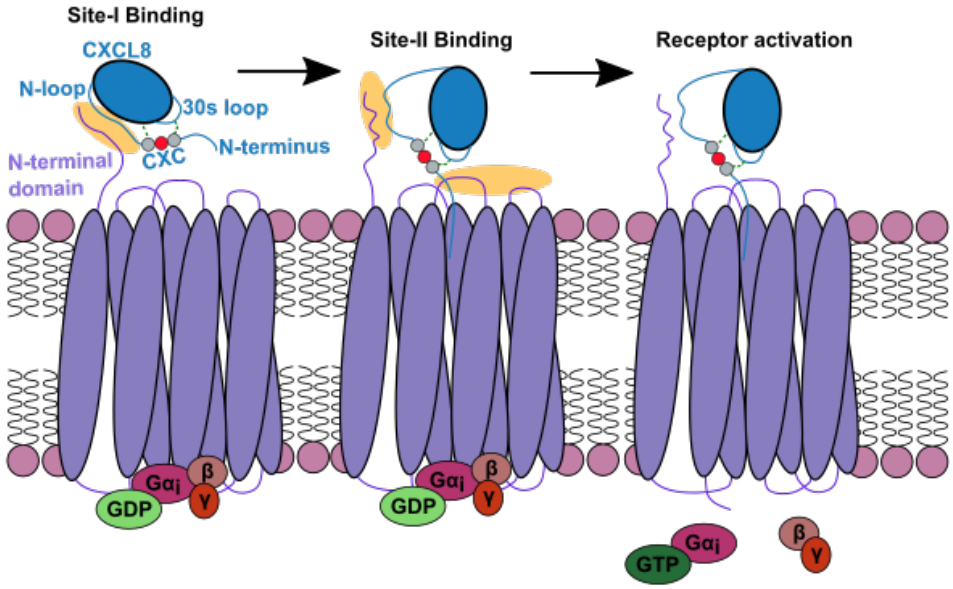

Figure 3.9.: Activation of CXCR1/2 after binding of CXCL8, modified according to Metzemaekers *et al.*, Joseph *et al.*, Xiong *et al.* and Liu *et al.* [91, 104–106] CXCL8 interacts with the receptor by two binding sites (highlighted in yellow). First, the N-loop of the chemokine interacts with the N-terminal domain of the receptor (binding site-I), followed by the additional interaction of the chemokine's ELR-motif with the receptor's extracellular loops. After binding, the receptor undergoes a conformational change, inducing further signaling pathways.

Figure 3.10 summarizes the CXCL8-induced signaling cascades that are important for neutrophil migration. The G$\beta\gamma$-subunit activates membrane-bound phospholipase C (PLC) that coverts phosphatidylinositol (4,5)-bisphosphate (PIP_2) into diacylglycerol (DAG) and inositol 1,4,5-trisphosphate (IP_3).[104, 107] DAG activates isoforms of proteinkinase C (PKC) while IP_3 leads to the release of intracellular calcium from the endoplasmic reticulum.[104, 107] The latter activates members of the RHO GTPase family.[107] The G$\beta\gamma$-subunit also activates phosphoinositide 3-kinase (PI3K) that converts PIP_2 into phosphatidylinositol (3,4,5)-trisphosphate (PIP_3).[104, 107] The local accumulation of PIP_3 at the cell front results in the activation of RHO family GTPases and actin polymerization, resulting in directed migration.[107, 108]

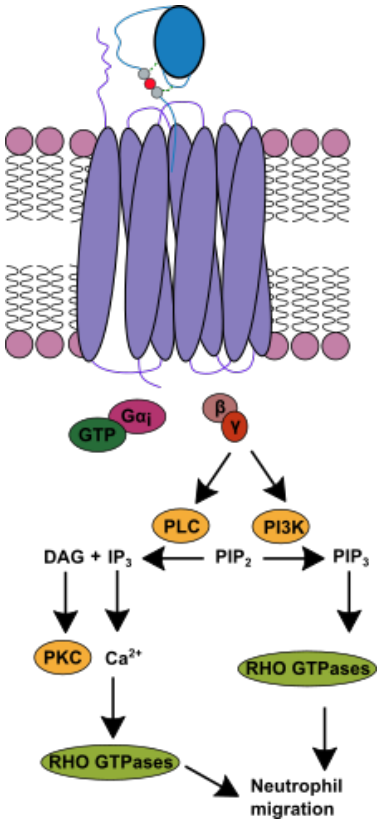

Figure 3.10.: Illustration of the signaling cascades induced by CXCL8-CXCR1/2 interaction that lead to neutrophil migration. The illustration was composed according to Metzemaekers *et al.* and Oliveira *et al.* [104, 107]

3.4.3. Cell migration

Cells can either migrate as single cells or in groups.[109] For single-cell migration, mesenchymal or amoeboid modes of migration are distinguished from each other.[109] Fibroblasts and cancer cells often use the mesenchymal cell migration mode, while for immune cells, the amoeboid mode dominates.[109] The migration of cells plays an important role in homeostatic and pathological processes, e.g. the repair of injured tissue as transmigrated neutrophils have a higher ability to defend invading pathogens or during chronic inflammatory diseases.[108, 110] As described in the previous chapter, different signaling cascades are induced after stimulation of chemokine receptors with chemokine ligands. Following the induction of different signaling cascades, neutrophils are able to recognize and directly migrate along chemotactic gradients that are either soluble or immobilized.[108, 109] The *in vivo* migration of neutrophils is induced by CXCL8 monomers and dimers.[74] Directed cell migration along soluble gradients is determined as chemotaxis while the migration along substrate bound gradients is termed haptotaxis.[108]

The amoeboid migration of cells can be considered as a cyclical process.[108, 109] In the first step, the cell transmits an external stimuli, e.g. the binding of a chemokine to its receptor, to an intracellular signal, resulting in the polarization of the cell.[108] In case of chemotactic stimuli, the cell is polarized by the intracellular accumulation of PIP_3 at the cell front.[108] This local accumulation is achieved by

the localized activation of PI3K and a low level of lipid phosphatases due to a larger number of receptor activation events than at the rear end of the cell in a chemotactic gradient.[108] The local accumulation of PIP_3 at the cell front results in the activation of RHO family GTPases and actin polymerization at the cell front, in particular the leading edge of lamellipodia or spike-like filopodia.[108] Lamellipodia are broad protrusions containing branched and linear actin filaments while filopodia are finger-like protrusions containing bundles of linear F-actin.[109] In the next step, the protrusion is stabilized by attachments of the leukocytes on the surface the cell is supposed to migrate along, e.g. the ECM.[108] Besides their stabilizing effects, these adhesion complexes also have signaling functions.[108] Following protrusion stabilization, a myosin force is generated at the cell front so that the cell is pulled towards the protrusion.[108] At the cell rear, adhesions are released and the cell tail retracts, resulting in the completion of the cell migration cycle.[108] If the actin cortex of neutrophils has a local rupture, the cells are able to switch from the protrusion-based mechanism to a contractility-based mechanism.[109] The latter describes the formation of blebs, which are spherical protrusions formed by a myosin-based contraction and pressure-driven cytosolic flow.[109]

The path of leukocyctes from the blood vessel to the site of inflammation in the tissue can be divided into several steps, termed capture, rolling, slow rolling, arrest, adhesion strengthening and spreading, intravascular crawling and transmigration (see figure 3.11).[100]

The capture and rolling of leukocytes on the endothelial cell layer is mediated by selectins, e.g. L-, P- and E-selectin that interact with P-selectin glycoprotein ligand 1 (PSGL1) and other glycosylated ligands.[100] Leukocytes express L-selectin and PSGL1 while endothelial cells express E- and P-selectin as well as PSGL1.[100] The interaction of selectins with their ligands leads to leukocyte-leukocyte and leukocyte-endothelial cell interactions under blood flow, which results in leukocyte capture or leukocyte secondary capture.[100] Besides selectins, activatable receptors termed integrins are also involved in the rolling of leukocytes.[100] For example, leukocytes express the integrin very late antigen 4 (VLA4) that interacts with the vascular cell-adhesion molecule 1 (VCAM1) that is presented by the endothelium.[100] If endothelial cells are stimulated by chemokines, they get activated, synthesize chemokines and chemoattractants and express immunoglobulin superfamily members, such as intercellular adhesion molecule 1 (ICAM1) and VCAM1 that bind the integrins expressed by leukocytes, e.g. VLA4 and lymphocyte function-associated antigen 1 (LFA1).[100] The chemokine-mediated recruitment of leukocytes to the endothelial cells is further supported by the binding of chemokines to GAGs on the surface of endothelial cells.[100] The following arrest of leukocytes on the endothelial cells is the result of conformational changes of integrin heterodimers, leading to a modulation of the integrin affinity towards its ligand.[100] The adhesion of arrested leukocytes is strengthened by the clustering of integrins that is induced by ligand binding.[100] In the next step, leukocytes crawl along the endothelial layer of the blood vessels to the proximity of the inflammation in the surrounding tissue, followed by transmigration into the injured or inflamed tissue, where high concentrations of chemokines are present.[100, 109] Intravascular crawling depends on the interaction of macrophage antigen 1 (MAC1), produced by leukocytes, and ICAM1, expressed by endothelial cells.[100] If a site for transmigration is found, leukocytes can either emigrate into the tissue by a paracellular or transcellular route.[100] The paracellular route describes the migration of leukocytes between endothelial junctions and is facilitated by the reduction of endothelial cell contacts.[100] Furthermore, increased amounts of intracellular endothelial calcium ions activate the myosin contraction and lead to an opening of endothelial cell contacts.[100] The transmigration of leukocytes through the endothelial junctions is mediated by endothelial junctional molecules, e.g. ICAM1, and the corresponding ligands expressed by leukocytes, e.g. LFA1.[100] The transcellular route describes the migration of leukocytes through

endothelial cells and takes places at areas where the endothelial layer is very thin.[100] If the leukocyte protrusion extends into the endothelial cells, ICAM1 is ligated and translocated to regions that are rich in F-actin and caveolae, resulting in the formation of vesicula-vacuolar organelles.[100] The latter facilitate the transmigration of leukocytes through endothelial cells by forming membrane-associated passageways.[100] Once the leukocytes have passed the endothelial cell layer, they have to cross the endothelial cell basement membrane and pericytes to follow increasing chemokine concentrations to the site of injury or inflammation.[100] In particular, leukocytes migrate through gaps between pericytes and through areas where only low amounts of protein are deposited within the extracellular matrix.[100] After reaching the site of inflammation or injury, granulocyte neutrophils use defense mechanisms against pathogens, such as phagocytosis of pathogens, production of reactive oxygen/nitrogen species, the release of degradative enzymes and the release of microbicidal agents by degranulation.[104]

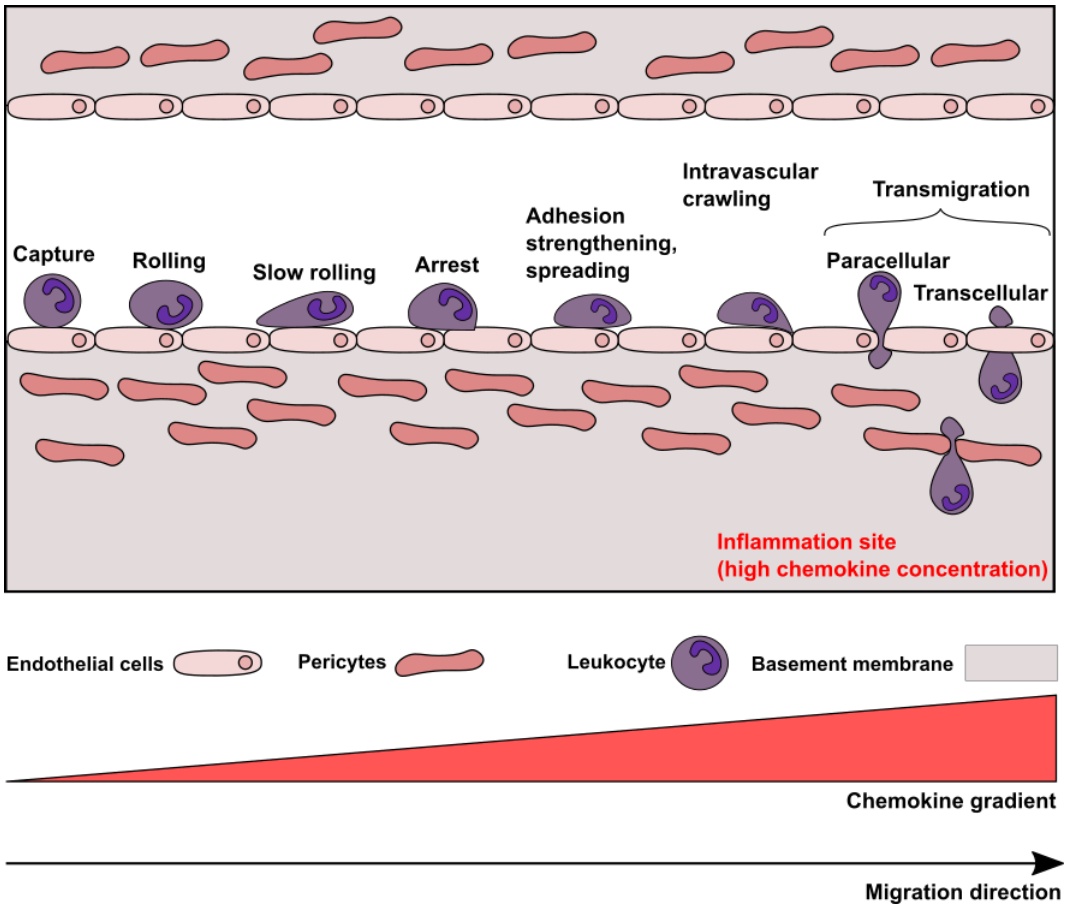

Figure 3.11.: Illustration of the different steps of cell migration as response to chemotactic stimuli, modified according to Ley *et al.* and Metzemaekers *et al.*[100, 104]

3.5. Microfluidic systems

Microfluidics are methods used to examine the flow of fluids in the scale of micrometers.[111] As microfluidics allow a controlled fluid flow, different applications have developed.[111] In terms of com-

mercial applications, microfluidics are used as microvalves for the dispersion of drugs, as microdevices for chemical reactions or as lab-on-chip systems for biochemical analysis, such as DNA amplification and sequencing.[111] Research applications include organ-on-chip systems, bioprinting and cell-based assays.[111] Microfluidic systems are a versatile platform for studying cell migration processes as they allow a spatial and temporal control of microenvironments [112], combined with low reagent consumption and sensitivity.[113] Moreover, only small cell numbers are needed [112] and a precise control of the flow rate is possible.[114] The flow rate influences the shear stress applied to the cells that can have an effect on cell behavior.[114] Due to the small dimensions of microfluidic devices, laminar flow rather than turbulent flow is dominant in microfluidic systems.[113] The dimensionless Reynolds number describes the relation of inertial and viscous forces and can be used to describe the flow in microfluidic devices.[113] If the Reynolds number reaches a value larger than 2300, inertial forces are dominant and turbulent flow takes place.[113] In contrast, a Reynolds number below 2000 describes laminar flow.[113] In planar microfluidic devices, the flow of a liquid is induced by externally-induced pressure differences at the inlets of a microfluidic channel.[113] In microfluidic systems, two types of transport mechanisms are distinguished from each other.[113] In directed transport the flow is either controlled electrically or mechanically, e.g. by a pump.[113] In statistical transport, transport is entropy-driven, e.g. the generation of gradients by diffusion of soluble molecules from one reservoir into another or from one partial flow into another.[113]

Microfluidic devices for studying cell migration are mostly fabricated from polydimethylsiloxane (PDMS) that has the advantage of being optical transparent, stable, biocompatible and permeable to gas.[112, 115] For example, mammalian cells require an adequate CO_2 supply for growth, which is maintained by appropriate incubators.[112] Since PDMS is hydrophobic and therefore only poorly adhesive to cells, the adhesion of cells has to be improved by modifying the surface of the microfluidic channel.[115] Protein coatings, such as direct coating of PDMS with collagen or (3-aminopropyl)triethoxysilane (APTES) as linker between PDMS and collagen can improve adhesion.[114, 115]

The migration of cells along soluble CXCL8 gradients in microfluidic devices has been studied by different research groups that used various channel designs and methods for gradient formation. Li Jeon *et al.* studied the chemotaxis of neutrophils along concentration profiles and showed that neutrophils directly migrate along linear gradients towards higher CXCL8 concentrations.[116] Halilovic *et al.* also analyzed the migration of neutrophils in soluble CXCL8 gradients of different steepness with microfluidic devices.[117] Besides soluble chemokine gradients, different methods have been published to generate surface-bound chemokine gradients in order to study haptotaxis. Rink *et al.* also showed that agarose stamps can be used to transfer diffusion-based CXCL8 gradients to surfaces.[118] Moreover, microfluidics in combination with laser-assisted protein adsorption by photobleaching (LAPAP) also allows the generation of immobilized gradients.[119] Schwarz *et al.* examined the migration of dendritic cells along immobilized CCL21 gradients with overlaid soluble CCL19 gradients and analyzed at which concentration the soluble gradient predominates the immobilized gradient.[119]

In previous works in our group, a method was developed to reversibly immobilize CXCL8 on a heparin-coated microfluidic device to study directed cell migration.[120] The method is based on the principle that polymerized dopamine has a strong adsorption onto a variety of substrates [121] and can therefore be used to modify the surface of PDMS. Chuah *et al.* showed that the proliferation of bone marrow stromal cells (BMScs) was improved if PDMS was functionalized with collagen by using polydopamine as bonding agent.[121] Furthermore, Leung *et al.* published a method to modify the surface of PDMS with an antithrombin-heparin complex (ATH) by using polydopamine.[122] The possible reaction mechanism

for the polymerization of dopamine and its reaction with heparin is displayed in figure 3.12. Based on the method of Leung *et al.*, CXCL8 was reversibly immobilized in a microfluidic channel coated with dopamine and heparin.[120]

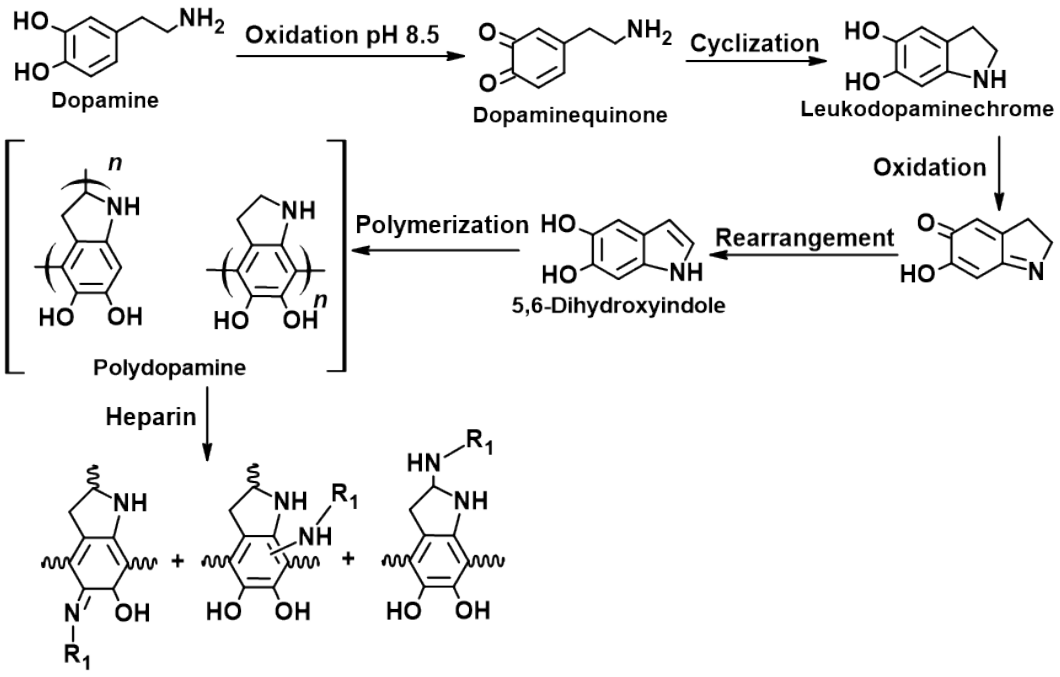

Figure 3.12.: Possible reaction mechanism for the polymerization of dopamine and its reaction with heparin, modified according to Lee *et al.*[123] and Sharma *et al.*[124]

4. Objective

Photodynamic modifications of biomaterials have a wide range of applications, ranging from the presentation of biologically active molecules for the study of cell migration to biomedical applications.

One field of application represents the prevention of surgical site infections, which can be achieved by directed and controlled antibiotic release. Rose bengal and green light cross-linking (RGX) enables the modification of collagen materials and has already been used in different clinical applications. In previous works in our group an RGX method for selected collagen materials was established and the assembly of these materials into laminates using RGX was demonstrated for the first time. In this work, multilayered collagen laminates for the prevention of surgical site infections should be developed and characterized. Different collagen laminates should be examined in terms of their swelling degree and whether they allow a controlled and directed release of the model antibiotic vancomycin under different conditions.

As described above, modified biomaterials can also be used for the presentation of biologically active molecules, for example to study chemokine-induced cell migration. Chemokines are small signaling proteins that are involved in homeostatic and inflammatory processes by influencing the communication and interaction of cells. Cell migration occurs along soluble or surface-bound chemokine gradients. Consequently, the analysis of cell migration along chemokine concentration gradients contributes to understand inflammatory and homeostatic processes. In previous works in our group, a method to non-covalently immobilize the chemokine CXCL8 in a microfluidic device, based on the interaction of chemokines with the glycosaminoglycan heparin, was developed. Here, the reversibly immobilized CXCL8 gradient, should be further characterized and tested in different migration studies. As the non-covalently immobilized gradients are not very stable, a method to covalently immobilize the chemokine CXCL8 in microfluidic devices is of interest. Here, the proven RGX method should be used for covalent immobilization, as collagen is also a frequently used substrate for migration experiments.

Biomaterials can not only be adapted to the respective biomedical application by photodynamic modifications, but can also be used to present biologically active molecules to understand cellular processes. The topic of this work represents a scientific contribution to the controlled and directed release of antibiotics and the development of methods to analyze chemokine-induced cell migration.

5. Materials and methods

5.1. General materials and chemicals

If not stated otherwise materials and chemicals were obtained from Carl Roth GmbH + Co.KG (Karlsruhe, Germany), Sigma-Aldrich (St. Louis, MO, USA), AppliChem GmbH (Darmstadt, Germany), Roche Holding AG (Basel, Switzerland), Alfa Aesar (Haverhill, MA, USA), Merck Millipore (Burlington, MA, USA), Thermo Fisher Scientific (Waltham, MA, USA), Corning Inc. (Corning, NY, USA), Sarstedt AG & Co. KG (Nümbrecht, Germany), Sartorius AG (Göttingen, Germany), Greiner Bio-One (Kremsmünster, Germany), VWR International (Radnor, PA, USA) and Biomol GmbH (Hamburg, Germany).

The following table 5.1 lists the frequently used buffers and their composition. Table 5.2 shows the used devices and table 5.3 the used software.

Table 5.1.: Frequently used buffers. Buffers were prepared with demineralized water. The pH was adjusted with sodium hydroxide or hydrochloric acid.

Buffer	**Composition**	
Microfluidic PBS (pH 7.4 or 8.5)	Disodium hydrogen phosphat	12.0 mM
	Sodium chloride	137.0 mM
	Potassium chloride	2.7 mM
PBS (pH 7.4)	Sodium chloride	137.0 mM
	Potassium chloride	2.7 mM
	Potassium dihydrogen phosphate	1.5 mM
	Disodium hydrogen phosphat	8.1 mM
MES (pH 5.5)	Sodium chloride	140.0 mM
	MES	9.6 mM
Tris (pH 8.5)	Sodium chloride	140.0 mM
	Tris base	9.6 mM

Table 5.2.: Overview of the devices used in this work.

Device	**Type**	**Manufacturer**
Analytical balance	R 180 D	Sartorius AG, Göttingen, Germany
Ultrasonic sensor	Sonoplus	BANDELIN electronic GmbH & Co. KG, Berlin, Germany
Power LED	M565L3 Mounted LED	Thorlabs GmbH, Newton, NJ, USA
HPLC system	SPD-M20A, CBM-20A, DGU-403, 2 x LC-20AD, SIL-20ACHT	Shimadzu, Kyoto, Kyoto, Japan
HPLC system	ÄKTApurifier 10	GE Healthcare, Chicago, IL, USA
Spectrophotometer	Genesys 10S UV-Vis	Thermo Fisher Scientific Inc., Waltham, MA, USA
Freeze-drying system	Alpha 2-4 LDplus	Martin Christ Gefriertrocknungsanalgen GmbH, Osterode am Harz, Germany
SLA printer	Formlabs Form 3	Formlabs, Somerville, MA, USA
Rotating shaker	Roto Shake Genie™	Scientific Industries Inc., Bohemia, NY, USA
Syringe pumps	LA-120	Landgraf Laborsysteme HLL GmbH, Langenhagen, Germany
Fluorescence microscope	Axio Observer. Z1 with HXP 120 C	Carl Zeiss AG, Oberkochen, Germany
Microplate reader	Infinite M®1000	Tecan Group AG, Männedorf, Switzerland
Incubator	B 5060 EK/CO_2	Heraeus, Hanau, Germany
Incubator	KS 4000 I control	IKA® Werke GmbH & Co. KG, Staufen, Germany
Incubator	BB 15 CO2	Thermo Fisher Scientific Inc., Waltham, MA, USA

Table 5.3.: Overview of the software used in this work.

Software	Device/Purpose	Manufacturer
Unicorn 5.20	ÄKTApurifier10	GE Healthcare, Chicago, IL, USA
AxioVision SE64 Rel. 4.8.3 and AxioVision Rel. 4.8.2 SP1	Axio Observer.Z1	Carl Zeiss AG, Oberkochen, Germany
OriginPro 2021b	Data analysis	OriginLab Corp., Northampton, MA, USA
FIJI	Image Processing	Johannes Schindelin *et al.*[125]
LabSolutions Release 5.42 SP5	HPLC (Shimadzu)	Shimadzu, Kyoto, Kyoto, Japan
FreeCAD version 0.19 Build 24276 (Git)	Design of the sample holder	Open-source software, available from: http://www.freecadweb.org
PreForm version 3.14.0	Additive manufacturing	Formlabs, Somerville, MA, USA
Inkscape 0.92.4	Illustration creation	Open-source software, available from: https://inkscape.org
ACD/ChemSketch (Freeware) 2021.2.1	Drawing chemical structures	Advanced Chemistry Development Inc., Toronto, ON, Canada

5.2. Characterization of collagen laminates and collagen sheets

In this work, the commercially available collagen types Atelocollagen sponge (CLS-01, Koken Co. Ltd., Tokyo, Japan) derived from bovine dermis type I collagen and a non-perforated collagen film (Collagen Solutions Ltd., Glasgow, UK) from bovine tendon type I collagen were used for the fabrication of collagen laminates.

5.2.1. Determination of the loading capacity

The loading capacity of single collagen sheets has to be determined in order to fabricate laminates from single sheets. The determination of the loading capacity has previously been described by Eckes *et al.*[67] In detail, collagen single sheets were cut to a size of 1 cm x 1 cm. Each collagen sheet was weighed three times (m_{dry}) and transferred to a well of a non-treated, flat bottom 24-well microplate (VWR International, Radnor, PA, USA). In the next step, 2 mL of PBS (pH 7.4, see table 5.1) were added and the samples were incubated for 2 h at room temperature (RT). The wet samples were carefully blotted with green paper towels to remove non-absorbed liquid and weighed three times (m_{wet}). The loading capacity per square centimeter was calculated according to equation 5.1 with the density of PBS (ρ=1.01 g/mL). The analysis of the loading capacity was performed in triplicates.

$$Loading\ capacity[mL] = \frac{m_{wet}\ [g] - m_{dry}\ [g]}{\rho_{PBS}\ [g/mL]} \tag{5.1}$$

5.2.2. Determination of the swelling degree

The procedure for experimentally determining the swelling degree of collagen samples has already been described by Eckes *et al.* and Braun *et al.*[67, 68] In detail, collagen samples were prepared and

freeze-dried overnight. Next, the dry weight of each sample was determined by weighing each sample three times (m_{dry}). Each collagen sheet was transferred to a well of a non-treated, flat bottom 24-well microplate (VWR International, Radnor, PA, USA). The samples were incubated for 2 h in 2 mL of PBS (pH 7.4, see table 5.1), MES buffer (pH 5.5, see table 5.1) or Tris buffer (pH 8.5, see table 5.1) at RT or at 37 °C. The wet samples were carefully blotted with green paper towels to remove non-absorbed liquid and weighed three times to obtain the wet weight (m_{wet}). Swelling degree analysis was performed in triplicates and calculated according to equation 5.2. A Kruskal-Wallis ANOVA was used to determine the significance level at which the experimental mean swelling degrees differed from each other.

$$Swelling\ degree\ [\%] = \frac{m_{wet}\ [g] - m_{dry}\ [g]}{m_{dry}\ [g]} * 100\ \% \tag{5.2}$$

The theoretical mean swelling degree of each laminate was calculated from the wet weight and dry weight of the single collagen sheets (triplicates). For this purpose, the mean value of each combination of single sheets was calculated. A Mann-Whitney-Test was used to analyze whether experimental and theoretical swelling degrees significantly differ from each other at $p = 0.05$.

5.2.3. Preparation of RGX-treated collagen single sheets

The preparation of collagen sheets treated with RGX has previously been described by Eckes *et al.*[67] Dry collagen single sheets with a size of 1 cm x 1 cm were placed on a droplet of 0.01 % (w/v) RB (Alfa Aesar, Ward Hill, MA, USA) in PBS (pH 7.4, see table 5.1) on a Petri dish (Sarstedt AG & Co. KG, Nümbrecht, Germany) and swollen for 2 h at RT in the dark. The volume of 0.01 % (w/v) RB in PBS used for swelling corresponded to the determined loading capacity. After incubation, each sheet was exposed to green light for 10 min using a M565L3 Mounted LED ($\lambda_{max.}$=569 nm [126], Thorlabs GmbH, Newton, NJ, USA) with a distance of 2 cm between the LED and the sample.

5.2.4. Preparation of collagen laminates

The preparation of collagen laminates has been published by Eckes *et al.*, Kilb *et al.* and Braun *et al.* [67, 68, 127] In detail, collagen sheets were cut to a size of 1 cm x 1 cm and placed on a droplet of 0.01 % (w/v) RB (Alfa Aesar, Ward Hill, MA, USA) in PBS (pH 7.4, see table 5.1) on a Petri dish (Sarstedt AG & Co. KG, Nümbrecht, Germany) and swollen for 2 h at RT in the dark. The volume of 0.01 % (w/v) RB in PBS used for swelling corresponded to the determined loading capacity. After 2 h, the sheets were placed onto each other with a layer of 20 µL of 0.01 % (w/v) RB in PBS between adjacent sheets. The piled sheets were exposed to green light for 10 min using a M565L3 Mounted LED (Thorlabs GmbH, Newton, NJ, USA) with a distance of 2 cm between the LED and the top sheet.

5.2.5. Fabrication of an additively manufactured sample holder

The fabrication of the sample holder has been published by Kilb *et al.*[127] The sample holder was constructed with the software FreeCAD (see table 5.3) with the support of Yannik Moos. The construction drawings are shown in figure A.1 and figure A.2. The following slicing and additive manufacturing of the sample holder were performed at the Staatliche Studienakademie Glauchau under the supervision of Prof. Dr. Ing. habil. Daniela Nickel. Both parts of the sample holder were sliced with the slicing software PreForm (see table 5.3) with a layer thickness of 50 µm, a full raft type, a density of 1.0 and a touch point size of 0.4 mm. The internal support structure was turned off and the support structure was

automatically generated. A Formlabs Form 3 with a construction volume of 14.5 x 14.5 x 18.5 cm, a layer thickness of 25–300 µm (vertical resolution), a XY-resolution of 25 µm and a laser spot size of 85 µm was used for additive manufacturing. A Formlabs Clear Resin (Formlabs, Somerville, MA, USA) or a Formlabs Standard White Resin (Formlabs, Somerville, MA, USA) was used for the fabrication of both parts of the sample holder. The additively manufactured parts of the sample holder were washed in isopropanol for 20 min and separated from the build plate. The supporting structures were removed from each part. Hardening of both parts was performed in a UV light chamber at 60 °C for 10 min.

5.2.6. Tightness analysis of the sample holder

The tightness analysis of the sample holder has been published by Kilb *et al.*[127] A calibration series of bromophenol blue sodium salt (Serva Electrophoresis GmbH, Heidelberg, Germany) in PBS (pH 7.4, see table 5.1) ranging from 500 x 10^{-5} % (w/v) to 1.95 x 10^{-5} % (w/v) (72.3 µM to 0.28 µM) was freshly prepared for each experiment and its absorption at 595 nm was recorded in triplicates (3 x 30 µL) in a clear polystyrene flat bottom non-sterile 384 well microplate (Corning Inc., Corning, NY, USA) with a microplate reader (Infinite M®1000, Tecan Group AG, Männedorf, Switzerland). For tightness analysis, an AC-laminate was prepared as described above. The laminate was inserted into the sample holder either supported with or without a single layer of parafilm (PARAFILM 'M' Laboratory Film, Bemis, Neenah, WI, USA) underneath the laminate. The upper part of the sample holder was then pushed into the lower part to fix the collagen laminate between both parts. The sample holder was then placed into a well of a non-treated, flat bottom 24-well microplate (VWR International, Radnor, PA, USA), containing 1 mL of PBS (pH 7.4, see table 5.1, lower chamber). The upper chamber was filled with 1 mL of 500 x 10^{-5} % (w/v) (72.3 µM) bromophenol blue sodium salt (Serva Electrophoresis GmbH, Heidelberg, Germany) in PBS. At the beginning and after 1 h, 2 h and 24 h of incubation at RT 120 µL samples were taken from both chambers. Next, the absorption of bromophenol blue at 595 nm was measured in triplicates of 30 µL each in a clear polystyrene flat bottom non-sterile 384 well microplate (Corning Inc., Corning, NY, USA) in a microplate reader (Infinite M®1000, Tecan Group AG, Männedorf, Switzerland). The calibration series was used to calculate the concentration of bromophenol blue in each sample.

5.2.7. Analysis of vancomycin release

The general method for analyzing the release of vancomycin from collagen samples has been described by Eckes *et al.* and Kilb *et al.*[67, 127] In detail, collagen laminates were prepared as described in the previous chapter, but with the supplement of 1 mg vancomycin hydrochloride (Carl Roth GmbH + Co. KG, Karlsruhe, Germany) dissolved in the RB solution used for loading the single sheets. After preparing the collagen laminates, the samples were positioned in the lower part of the sample holder using tweezers and fixed with the upper part of the sample holder. After placing the sample holder in the well of a non-treated, flat bottom 24-well microplate (VWR International, Radnor, PA, USA), 1 mL of buffer was added to the well (lower chamber) and 1 mL was filled into the upper part of the sample holder (upper chamber). The buffer was either PBS (pH 7.4, see table 5.1), MES (pH 5.5, see table 5.1) or Tris (pH 8.5, see table 5.1). The composition of the MES buffer and Tris buffer was calculated according to the molar amount of chloride and phosphate used for PBS. The tissue culture plate with the sample holder was incubated at 37 °C. At different time points, the liquid from the upper and lower chamber was completely withdrawn and analyzed. After taking the samples, 1 mL of fresh buffer was added to both chambers and the plate was further incubated at 37 °C. The samples were analyzed by reversed-phase HPLC. A C18 Synergi™4 µm Fusion-RP 80 Å 250 4.6 mm column (Phenomenex Inc.,

Torrance, CA, USA) was used for sample analysis. In detail, 100 µL of the sample were injected onto the column by the autosampler and the column was washed with 100 % of eluent A at a flow rate of 0.5 mL/min for 20 min. Then, the concentration of eluent B was increased from 0 % to 90 % over 50 min at a total flow rate of 0.5 mL/min. Next, the column was washed with 100 % of eluent A for 10 min at a flow rate of 0.5 mL/min. The absorption of vancomycin was monitored at 280 nm and the absorption of collagen at 220 nm. Vancomycin eluted after 40 min. To calculate the amount of released vancomycin from the peak area, a calibration curve of vancomycin from 0.001 mg/mL to 1 mg/mL was recorded in triplicates. The release values of the different time points were added up. A Kruskal-Wallis ANOVA was used to test if the difference of the mean total release values between vancomycin-loaded Atelocollagen or vancomycin-loaded Atelocollagen (AC-laminate) and vancomycin-loaded Collagen Solutions (AC-laminate) significantly differ from each other at a threshold value of $p = 0.05$. A Mann-Whitney-Test was used to analyze whether release values of samples with or without prior placement into the sample holder significantly differ from each other at a threshold value of $p = 0.05$.

5.3. Microbiological methods

5.3.1. Subcultivation of THP-1 cells

The suspension cell line THP-1, initially derived from a boy suffering from acute monocytic leukemia [128], was cultivated in RPMI-1640 medium supplemented with 10 % (v/v) fetal bovine serum (FBS), 2 mM L-glutamine, 100 µg/mL streptomycin and 100 U/mL penicillin. The cells were cultivated under sterile conditions at 37 °C and 5 % CO_2. For sub-cultivation, the cells were split 1:4 in 75 cm^2 cell culture flasks (Sarstedt AG & Co. KG, Nümbrecht, Germany) twice a week. Sub-cultivation was supported by Anke Imrich. The concentration of living cells was determined by trypan blue staining. Trypan blue diffuses through the porous membrane of dead cells and is enriched in their cytoplasm, resulting in a blue discoloration.[129] In contrast, living cells do not show a blue discoloration as trypan blue is not able to pass their intact membrane.[129] Staining was performed with 0.5 % (w/v) trypan blue in 0.9 % (w/v) sodium chloride solution. In detail, 50 µL of cell suspension were mixed with 50 µL trypan blue solution in a transparent 96 well microplate (Sarstedt AG & Co. KG, Nümbrecht, Germany). Next, 50 µL of the stained cell suspension were pipetted into a Neubauer chamber and the number of living cells was counted. For migration studies in microfluidic devices, a cell density of $3x10^6$ THP-1 cells per mL was used.

5.4. Protein biochemical methods

5.4.1. Protein expression and cell lysis

The expression of CXCL8 and CXCL8-S72C was performed similar to the method published by Rink *et al.*[118] For overnight cultures, four 50 mL conical centrifuge tubes each containing 20 mL of 2.5 % (w/v) lysogeny broth (LB) medium supplemented to a final concentration of 60 µg/mL ampicillin were inoculated with a pipette tip of the expression strain *Escherichia coli* BL21 (DE3) RIL. The expression strain harbored the plasmid pET-22b with the sequence for CXCL8 or CXCL8-S72C, inserted after the sequence for the pelB tag for transport to the periplasm. The cultures were incubated at 37 °C and 200 rpm overnight. Four 2 L Erlenmeyer flasks with 400 mL of 2.5 % (w/v) LB medium were supplemented to a final concentration of 60 µg/mL ampicillin and inoculated with one overnight culture per flask. The cell suspensions were incubated at 37 °C and 200 rpm until an optical density (OD_{600}) of 0.6 to 1.0 was reached. Then, the chemokine expression was induced by adding isopropyl β-D-1-thiogalactopyranoside

to each cell suspension to a final concentration of 0.1 mM. The expression was performed at 30 °C and 160 rpm for 3 h. The cell suspensions were centrifuged at 4 °C and 4739 x g for 45 min. The cell pellets were stored at -20 °C until further use.

Cell lysis was performed similar to the protocol published by Rink *et al.* [118] The four cell pellets from the protein expression were resuspended in 10 mL of lysis buffer (see table 5.4) and incubated on ice for 90 min. During incubation, the solution was inverted several times. After incubation, 50 µL of Triton X-100 were added to the solution and vortexed. In the next step, ultrasonic treatment was performed three times on ice for 30 s (1 s puls and 1 s pause in alternation with an amplitude of 28 %) with 30 s pause between each treatment. Next, 100 µL of 10 mg/mL DNase I were added to the cell suspension. Following incubation at RT for 30 min, the solution was incubated in a water bath at 70 °C for 10 min. The suspension was centrifuged at 4688 x g and 4 °C for 45 min.

Table 5.4.: Buffers used for the purification of CXCL8 and CXCL8-S72C. Buffers A, B and C were prepared with ultrapure water. The lysis buffer was prepared with buffer A. The pH value was adjusted with sodium hydroxide or hydrochloric acid.

Buffer	**Composition**	
Lysis buffer	EDTA	1 mM
	Lysozyme	0.2 mg/mL
	DNase I	0.1 mg/mL
	Protease inhibitor tablet (cOmplete Mini, Roche)	0.25 tablet
Buffer A (pH 7.4)	Disodium hydrogen phosphate	40 mM
	Sodium chloride	90 mM
Buffer B (pH 7.4)	Disodium hydrogen phosphate	40 mM
	Sodium chloride	1.5 M
Buffer C (pH 7.4)	Disodium hydrogen phosphate	40 mM
	Sodium chloride	35 mM

5.4.2. Purification of CXCL8 variants

The purification of CXCL8 and CXCL8-S72C was performed similar to the protocol published by Rink *et al.* [118] The supernatant from cell lysis was purified with an ÄKTApurifier 10 system (GE Healthcare, Chicago, IL, USA). In detail, purification was performed by cation exchange chromatography by using a 5 mL HiTrap SPFF column (GE Healthcare, Chicago, IL, USA). The column was equilibrated with 1 column volume (CV) buffer A and then loaded with the sample. After washing the column with 6 CV of buffer A, bound proteins were eluted by a linear gradient from 0 % to 35 % of buffer B (see table 5.4), which corresponds to a sodium chloride gradient of 90 mM to 583.5 mM. Protein was detected by measuring the absorption at 280 nm. The chemokine containing fractions were pooled. The buffer was changed to buffer C (see table 5.4) by using a centrifugal concentrator (Vivaspin® 20, Sartorius AG, Göttingen, Germany) and centrifuging the protein solution at 4 °C and 4688 x g for 45 min.

To determine the concentration of the purified chemokine solution, 18 µL of buffer C and 18 µL of the protein solution were pipetted in triplicates into wells of a UV-transparent 384 flat bottom microplate (Corning Inc., Corning, NY, USA). The absorption at 280 nm was measured and the protein concentration was calculated according to equation 5.3, which was established by a calibration series in a previous

work.[130]

$$c[mg/mL] = \frac{A_{280nm} - 0.079}{0.122} \tag{5.3}$$

The purified protein was aliquoted, freeze-dried and stored at -20 °C.

5.4.3. Labeling of CXCL8-S72C with fluorescein

To selectively label CXCL8 with the fluorescent dye fluorescein, a CXCL8 variant with a C-terminal cysteine instead of a serine at position 72 was used. In the first step, existing intermolecular disulfide bonds in the chemokine were reduced, resulting in free C-terminal thiols that are able to react with the maleimide-conjugated fluorophore at a pH between 6.5 and 7.5.[131]

In the first step, three to four equivalents of Immobilized TCEP Disulfide Reducing Resin (Thermo Fisher Scientific Inc., Waltham, MA, USA) with a loading capacity of 8 µmol/mL [132] were washed with 200 µL of washing buffer (20 mM EDTA in Microfluidic PBS pH 7.4 (see table 5.1)). The suspension was centrifuged at 1000 x g and RT for 1 min and the supernatant was discarded. The freeze-dried chemokine was resuspended in 1 mL of washing buffer, added to the resin and incubated for 60 min at RT while shaking. After centrifugation at 1000 x g and RT for 1 min, the supernatant was transferred into a new 1.5 mL conical tube. The resin was washed with 200 µL of washing buffer, centrifuged at 1000 x g and RT for 1 min and the supernatant was transferred to the previous supernatant. In the next step, four equivalents of fluorescein-5-maleimide (AAT Bioquest Inc., Pleasanton, CA, USA) in dimethylformamide (DMF) were added and the solution was incubated for 2 h at RT while shaking. The labeled chemokine was purified by size-exclusion chromatography with an ÄKTApurifier 10 system (GE Healthcare, Chicago, IL, USA) by using a 53 mL HiPrep 26/10 Desalting column (GE Healthcare, Chicago, IL, USA). The column was equilibrated with 2 CV of buffer C (see table 5.1). The labeled chemokine was purified by isocratic elution with 2 CV of buffer C. The protein was detected by measuring the absorption at 280 nm. The fractions containing the labeled chemokine were pooled by using a centrifugal concentrator (Vivaspin® 20, Sartorius AG, Göttingen, Germany) and centrifuging the protein solution at 4 °C and 4688 x g for 45 min. The labeled protein was freeze-dried and stored at -20 °C.

5.4.4. Labeling of bovine albumin fraction V (BSA) with fluorescein isothiocyanate

A 1 mL protein solution with 2 mg/mL of albumin fraction V (BSA, NZ-Origin, Carl Roth GmbH + Co. KG, Karlsruhe, Germany) in reaction buffer (50 mM sodium tetraborate in ultrapure water) was prepared in a 1.5 mL conical tube. In the next step, 20 equivalents of fluorescein isothiocyanate (FITC) in DMF were added to the protein solution and incubated for 2 h in the dark at RT. The reaction mixture was purified with a PD-10 column prepacked with sephadex G-25 resin (GE Healthcare, Chicago, IL, USA). In detail, the column was equilibrated four times with 5 mL of reaction buffer and the flow-through was discarded. After applying the reaction mixture to the column bed, 2 mL of Microfluidic PBS (pH 7.4, see table 5.1) were added. The column was rinsed with Microfluidic PBS pH 7.4 until the fluorescence band was removed and 250 µL fractions were collected. The column was regenerated by rinsing three times with 5 mL ultrapure water, followed by rinsing three times with 5 mL of buffer C (see table 5.4). The fractions containing FITC-labeled BSA were identified by absorption and fluorescence measurements.

For the absorption measurements, 40 µL of each fraction were filled into a well of a UV-transparent 384 flat bottom microplate (Corning Inc., Corning, NY, USA) and the absorption at 280 nm was measured. For the fluorescence measurements, 40 µL of each fraction were filled into a well of a black flat bottom 384 microplate (Corning Inc., Corning, NY, USA) and the relative fluorescence intensity at an excitation wavelength of 490 nm and an emission wavelength of 535 nm was measured. After identification of the FITC-labeled protein fractions, these fractions were pooled and the protein concentration as well as the degree of protein labeling were calculated using an Infinite M®1000 reader (Tecan Group, Männedorf, Switzerland).[133]

5.5. Microfluidics

5.5.1. Fabrication and handling of microfluidic devices

The microfluidic devices used in this work consisted of a 498 µm wide main channel with three 166 µm wide inlet channels and a total height of 55 µm (see figure 5.1).[120] The microfluidic devices were fabricated from PDMS by Dr. Asma Siddique (Institute of Materials Science, Physics of Surfaces) according to the method described by Siddique *et al.*[114] and Kilb *et al.*[120]

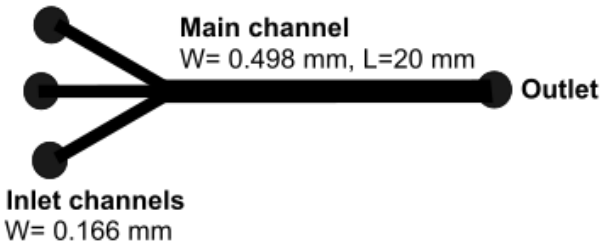

Figure 5.1.: Channel used for microfluidic experiments. The final device has a height of 55 µm. Three 166 µm wide inlet channels lead into a 498 µm wide main channel that has a length of 2 cm.

In order to rinse the channel, a single-use 1 mL fine dosage syringe (B. Braun SE, Melsungen, Germany) was connected to a standard dosing needle with an interior diameter of 0.33 mm (VIEWEG GmbH, Kranzberg, Germany). The dosing needle was connected to a flexible 0.51 x 1.52 mm Tygon ND100-80 Tubing (Darwin Microfluidics, Paris, France) and the latter was connected to a stainless straight PDMS coupler with a gauge size of 23G (Darwin Microfluidics, Paris, France), which allows a connection to the microfluidic device.

5.5.2. Coating of microfluidic devices with dopamine and heparin

For the coating with dopamine, Microfluidic PBS (pH 8.5, see table 5.1) was autoclaved and degassed in an ultrasonic cleaner for 10 min. The syringe and tubing used for the coating with dopamine were manually rinsed four times with 1 mL of degassed Microfluidic PBS pH 8.5. The microfluidic channel was manually rinsed from the outlet with 1 mL of 70 % (v/v) ethanol and then with 1 mL of degassed Microfluidic PBS pH 8.5, by using the previously rinsed syringe and tubing. In the next step, the channel was manually rinsed with 1 mL of a 1 mg/mL dopamine (Merck Millipore, Burlington, MA, USA) solution in Microfluidic PBS pH 8.5 from the outlet. The channel openings were sealed with parafilm. The

channel was then placed in a 50 mL conical centrifuge tube, which was rotated overnight at RT at step 2.5.

For the coating with heparin, the syringe and tubing used for the coating with heparin were manually rinsed four times with 1 mL of 70 % (v/v) ethanol. Autoclaved Microfluidic PBS (pH 7.4 and pH 8.5, see table 5.1) was degassed in an ultrasonic device for 10 min. The channel was then manually rinsed three times with 1 mL of Microfluidic PBS pH 7.4 from the outlet to remove non-bound dopamine. Next, the channel was manually flushed with 1 mL of 0.1 mg/mL heparin sodium salt (AppliChem GmbH, Darmstadt, Germany) in Microfluidic PBS (pH 8.5, see table 5.1) from the outlet and the channel openings were sealed with parafilm. The channel was placed in a 50 mL conical centrifuge tube that was rotated overnight at RT at step 2.5.

5.5.3. Preparation of reversibly immobilized chemokine gradients

In previous works in our group, an optimized procedure for the reversible immobilization of CXCL8 gradients in microfluidic devices had been developed.[120, 134] The syringes and tubings used for gradient formation were manually rinsed four times with 1 mL of 70 % (v/v) ethanol and once with 1 mL of loading buffer (0.4 % (w/v) skim milk powder in Microfluidic PBS (pH 8.5, see table 5.1)). The three inlet channels were rinsed for 20 min with loading buffer at a flow rate of 0.8 µL/min using syringe pumps. The syringe of the top inlet channel was then replaced against a syringe filled with 8 µM CXCL8- or CXCL8-S72C-fluorescein in loading buffer and the channel was rinsed with the syringe pumps for additional 240 min at a flow rate of 0.8 µL/min for all three inlet channels. The general setup is depicted in figure 5.2. The channel was then manually flushed from the outlet with 1 mL of loading buffer to remove non-bound chemokine. For stability and overlay analysis, the channel was then incubated at 37 °C and 5 % CO_2. To prevent the formation of air bubbles during incubation, the channel openings were sealed with adhesive seal tabs (diameter 7.62 mm, Grace Bio-Labs, Bend, OR, USA) and the channel was covered with buffer. Images of the channel were taken in 900 µm segments under the fluorescence microscope ($\lambda_{Ex.}$ = 450-490 nm, $\lambda_{Em.}$ = 500-550 nm) with a 10x total magnification .

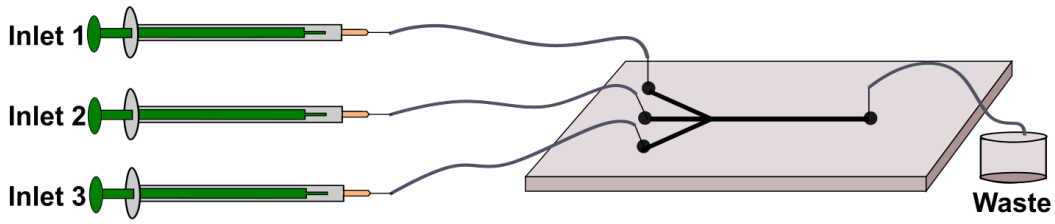

Figure 5.2.: General setup for gradient formation.

5.5.4. Coating of microfluidic devices with collagen

The microfluidic devices were fabricated and coated by Dr. Asma Siddique according to the method published by Siddique *et al.*[114] The surfaces of the microfluidic devices were either modified with oxygen plasma-collagen or with APTES-collagen.[114] For the coating with oxygen plasma-collagen, oxygen plasma treatment was performed without APTES self-assembled monolayers (SAMs) [114], followed by collagen coating with rat tail collagen type I (Thermo Fisher Scientific Inc., Waltham, MA, USA) dissolved in 0.1 M $NaHCO_3$ solution in PBS [114] or dissolved in 17.5 mM acetic acid in sterile

ultrapure water. Different concentrations of rat tail collagen type I were used. For the modification with APTES-collagen, oxygen plasma treatment was performed with APTES SAMs [114], followed by coating with 20 µg/cm^2 collagen in 17.5 mM acetic acid in sterile ultrapure water.

5.5.5. Covalent immobilization of CXCL8 variants on collagen

For the covalent immobilization of CXCL8 by RGX the parameters were varied during method development and based on the optimized procedure for reversible immobilization of CXCL8 [120] and the parameters used for RGX.[127] The general method was carried out with the following steps. In the first step the syringes and tubings were manually rinsed two to four times with 1 mL of PBS used for the RB solution. The channel was then flushed from the outlet with 8 µM CXCL8 in RB solution and the entire channel or only a half of the channel was exposed to green light for 10 min using a M565L3 Mounted LED (Thorlabs GmbH, Newton, NJ, USA) with a distance of 2 cm between the LED and the channel. To remove non-bound chemokine, the channel was flushed from the outlet with the respective buffer. The bound chemokine was either detected by fluorescent labeling or by antibody staining. The latter was carried out with 1 mL of 100 µg/mL anti-IL8-FITC (BioLegend, San Diego, CA, USA), diluted 1:100 in PBS (pH 7.4, see table 5.1). After 1 h of incubation at RT, excess antibody was removed by flushing the channel manually from the outlet with 1 mL of 0.4 % (w/v) skim milk powder in PBS (pH 7.4, see table 5.1). Images of the channel were taken under the fluorescence microscope ($\lambda_{\mathrm{Ex.}}$ = 450-490 nm, $\lambda_{\mathrm{Em.}}$ = 500-550 nm) with a 10x total magnification in 900 µm segments.

5.5.6. Analysis of chemokine gradients

Analysis of chemokine gradients (see figure 5.3) was performed with the software FIJI and OriginPro 2021b. In FIJI, the size of the channel section was defined as region of interest (ROI) and saved. The image of each channel section was then cropped to the size of the ROI and saved as text image, with each pixel as relative grey value according to the fluorescence intensity. Then the mean fluorescence intensity of each pixel row in x-direction ($\bar{X}_{\mathrm{RFU}}$) for each channel section was calculated. In the next step, the width of the channel section in y-direction was calculated from pixel into µm by using the factor 0.645 µm/pixel. In OriginPro 2021b, the mean fluorescence intensities of each pixel row in x-direction were plotted against the channel width in y-direction in µm, for each channel section. As the concentration gradient in each channel section refers to the mean fluorescence intensity per µm along the channel width in y-direction, a linear fit was performed by using the tool QuickFit. In detail, the linear fit was only performed for the area of the channel where the gradient is linear. The determined slope of the linear fit of each channel section was plotted against its position along the total channel length z, resulting in a concentration gradient along the entire main channel. The main channel outlet (channel section 23) was excluded from analysis. Furthermore, images of channel sections with bright rings of light were treated as outliers and excluded from analysis.

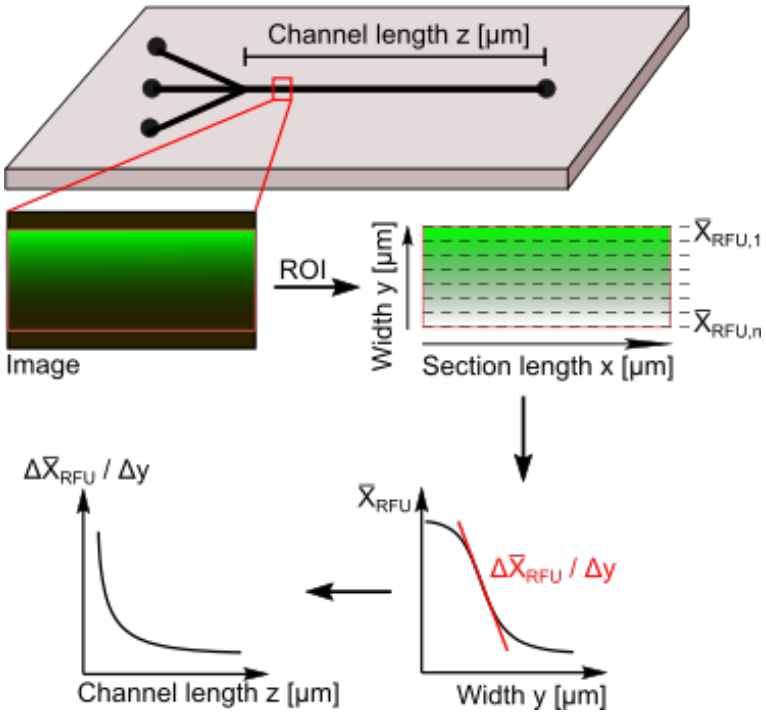

Figure 5.3.: Workflow for the analysis of chemokine gradients. The length of the entire main channel z is divided into 23 channel sections with a length of 900 µm each. The microscopic image of each channel section is cropped to the ROI. The mean fluorescence intensity of each pixel row for each channel section is calculated and plotted against the width of the channel section. The resulting slope is plotted against its position along the entire channel length z.

5.5.7. Migration studies

After preparing the microfluidic channel with a reversibly immobilized CXCL8 gradient or control solutions and removing non-bound chemokine by flushing the channel with 1 mL of loading buffer from the outlet, the channel was manually rinsed from the outlet with 1 mL of 3 x 10^6 THP-1 cells/mL in medium used for cell cultivation. The channel openings were sealed with adhesive seal tabs (diameter 7.62 mm, Grace Bio-Labs, Bend, OR, USA) and the channel was incubated at 37 °C and 5 % CO_2 for 20 h and 43 h. The formation of air bubbles in the channel was prevented by covering the channel with buffer.

Images of the channel were taken under the fluorescence microscope in phase contrast with a 10x total magnification in 900 µm segments. In order to determine the cell migration before, after 20 h and after 43 h of incubation, each channel section was divided into a lower half and an upper half. The relative number of cells in both channel halves was calculated and plotted against the incubation time. The distribution of the data was represented by a boxplot in which each box was composed of a lower end (0.25 quantile), an upper end (0.75 quantile), a median (horizontal line), a mean (black dot) and whiskers. Outliers were marked as red dots. Based on previous works [120, 134], cell migration was analyzed from channel section 15 to 21. Statistical analysis of cell migration was performed by a Friedman-ANOVA at $p = 0.05$.

5.6. Interaction studies

5.6.1. Determination of the appropriate concentration of fluorescent molecule

For the interaction studies of fluorescently labeled protein with collagen or interaction studies of RB with native protein the appropriate concentration of the fluorescent molecule had to be determined. For that purpose, 70 µL of fluorescently labeled protein (8 µM BSA-FITC, 2.82 µM CXCL8-S72C-fluorescein) or RB (1 mg/mL) in Microfluidic PBS (pH 7.4, see table 5.1) were filled into a well of a flat black 384 microplate (Corning Inc., Corning, NY, USA) and a serial dilution of 1:2 was performed in triplicate with a total volume of 35 µL of solution in each well. As blank, 35 µL of Microfluidic PBS pH 7.4 were used. The fluorescence intensity of the fluorescein-labeled protein was measured at an excitation wavelength of 490 nm and an emission wavelength at 525 nm with an optimal gain (149 (CXCL8-S72C-fluorescein) and 140 (BSA-FITC)). For RB, the fluorescence intensity at an excitation wavelength of 530 nm and an emission wavelength at 571 nm was measured with a gain of 120. For the interaction studies, a concentration of the fluorescently labeled protein or RB higher than the mean fluorescence intensity of the blank plus three times the standard deviation of the blank was used.

5.6.2. Interaction of fluorescently labeled protein with collagen

For interaction studies, 70 µL of rat tail collagen type I (3.83 mg/mL, Corning Inc., Corning, NY, USA) were filled into a well of a flat black 384 microplate (Corning Inc., Corning, NY, USA) and a serial dilution of 1:2 was performed with a total volume of 35 µL of solution in each well. As collagen was formulated in 0.02 M acetic acid, 35 µL of 0.02 M acetic acid were also included in the analysis. In the next step, 5 µL of the fluorescently labeled protein in 8-fold concentration of the previously determined, appropriate concentrations were added to the wells with the serial dilution and the 0.02 M acetic acid sample. For the blank, 40 µL of Microfluidic PBS (pH 7.4, see table 5.1) were used. The analysis was performed in triplicates. The microtiter plate was centrifuged at 2194 x g for 40 s. The fluorescence intensity was measured with an Infinite M®1000 reader (Tecan Group AG, Männedorf, Switzerland) at an excitation wavelength of 470 nm and an emission wavelength at 525 nm with a gain of 120 for CXCL8-S72C-fluorescein and a gain of 100 for BSA-FITC. The measurement was repeated after at least 1 h to ensure that an equilibrium was reached.

5.6.3. Interaction of RB with native proteins

For interaction studies with RB, 70 µL of 3.83 mg/mL native CXCL8 or BSA in Microfluidic PBS (pH 7.4, see table 5.1) were filled into a well of a flat black 384 microplate (Corning Inc., Corning, NY, USA) and a serial dilution of 1:2 was performed with a total volume of 35 µL of solution in each well. In the next step, 5 µL of RB diluted in Microfluidic PBS pH 7.4 in 8-fold concentration of the previously determined, appropriate concentration were added to the wells with the serial dilution. For the blank, 40 µL of Microfluidic PBS pH 7.4 were used. The analysis was performed in triplicates. The microtiter plate was centrifuged at 2194 x g for 40 s. The fluorescence intensity was measured Infinite M®1000 reader (Tecan Group AG, Männedorf, Switzerland) at an excitation wavelength of 530 nm and an emission wavelength at 571 nm with a gain of 160. The measurement was repeated after 2 h to ensure that an equilibrium was reached.

6. Results and discussion

6.1. Characterization of collagen laminates

Collagen laminates with different properties are of interest in tissue engineering and regenerative medicine, in particular for a controlled and directed antibiotic release to prevent SSIs.[67, 68, 127] In previous works the commercially available collagen materials Atelocollagen (A) and Collagen Solutions (C) were selected and characterized in terms of their swelling degree, microstructure, thickness, effect on cell viability and antibiotic release.[67] Eckes *et al.* showed that both collagen materials can be linked to each other by RGX.[67] The possible combinations of both collagen materials to bi- and triple-layered collagen laminates shall now be systematically characterized. In order to characterize collagen laminates and to find out which laminates composed of Atelocollagen (A) and Collagen Solutions (C) remain stable during incubation, the swelling behaviors of different bi-layer and triple-layer laminates were analyzed. In literature, Eckes *et al.* described that the swelling of collagen sheets at RT is completed within two hours.[67] Based on these findings, the swelling degrees of different collagen laminates at RT in PBS (pH 7.4) after two hours were determined. For a comparison, the swelling degrees of single sheets of RGX-treated Atelocollagen as well as RGX-treated Collagen Solutions were analyzed under the same conditions to calculate the theoretical swelling degrees of collagen laminates.

In figure 6.1 (a) the experimentally and theoretically determined mean swelling degrees of homogeneous Atelocollagen laminates and RGX-treated Atelocollagen single sheets are displayed. The experimental mean swelling degree decreased about 47 % from the single RGX-treated Atelocollagen sheet to the bi-layer Atelocollagen laminate, but did not further decrease with addition of a third Atelocollagen sheet ($A_{Exp.}$: 795±117 %, $AA_{Exp.}$: 418±103 % and $AAA_{Exp.}$: 422±53 %). A similar result has been described by Braun *et al.*[68], who analyzed the swelling degree after 10 min of incubation at RT. In literature, the effect of the cross-linking method on the swelling degree has been reported by different groups.[135, 136] For RGX, a decrease of the collagen swelling ratio with an increasing concentration of RB has been described.[137] The decreased mean swelling degree from a single sheet to a bi-layer Atelocollagen laminate might be explained by the additional RB at the interface between the piled sheets. As the amount of RB at the interfaces between the stapled sheets of bi-layer and triple-layer Atelocollagen laminates is the same, the experimentally determined swelling degrees do not differ from each other. Compared to the theoretical swelling degrees of bi-layer and triple-layer Atelocollagen laminates, the experimentally determined mean swelling degrees corresponded to 53 % of the theoretically determined swelling degrees ($AA_{Theo.}$: 795±81 % and $AAA_{Theo.}$: 796±70 %).

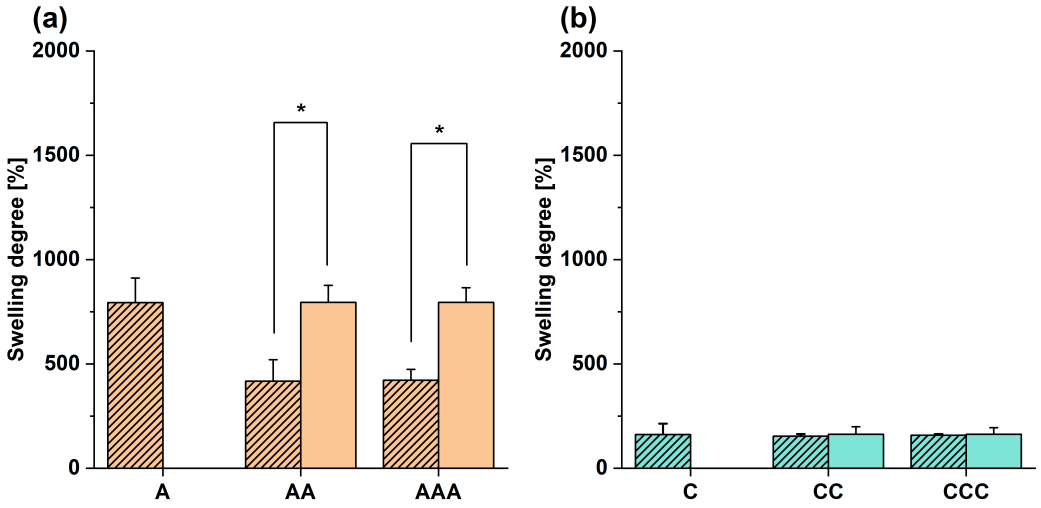

Figure 6.1.: Swelling degree of Atelocollagen and Collagen Solutions laminates. The experimental swelling degree (dashed bars, *n = 3*) was determined after 2 h of incubation at RT. The theoretical swelling degree (non-patterned bars) was calculated from single RGX-treated collagen sheets. Error bars represent the standard deviation. The significance (black asterisk) between the experimentally and theoretically determined mean swelling degrees was tested by a Mann-Whitney-Test at p = 0.05. (a) Atelocollagen laminates. (b) Collagen Solutions laminates.

The significant differences between the experimental and theoretical values might be explained by the swelling phenomenon described by Peppas *et al.*[25] If the buffer diffuses into a single collagen sheet, a swelling interface moves towards the center of the collagen sheet and the swelling takes place in the opposite direction at the polymer interface (see figure 3.2). Since buffer can diffuse from two directions into the single collagen sheet, two swelling interfaces per single collagen sheet are available. If a laminate is composed of two collagen sheets, four swelling interfaces are theoretically available. However, as the collagen sheets are cross-linked with each other only two swelling interfaces are experimentally available. It follows, that the amount of available swelling interfaces is two-fold higher for theoretical calculated swelling degrees compared to experimentally determined swelling degrees.

In figure 6.1 (b) the experimentally and theoretically determined mean swelling degrees of homogeneous Collagen Solutions laminates and RGX-treated Collagen Solutions single sheets are displayed. Compared to the results of the Atelocollagen laminates, bi-layer and triple-layer laminates composed of Collagen Solutions did not show any difference in their experimentally determined mean swelling degrees compared to single RGX-treated Collagen Solutions ($C_{Exp.}$: 162±52 %, $CC_{Exp.}$: 154±10 % and $CCC_{Exp.}$: 158±6 %). A similar result has been described by Braun *et al.*[68], for the swelling degree after 10 min of incubation at RT. This result might be explained by the more compact structure of Collagen Solutions compared to Atelocollagen.[67, 68] Therefore, the additional collagen layers only have a negligible effect and do not result in different swelling degrees. Furthermore, the theoretically ($CC_{Theo.}$: 163±37 % and $CCC_{Theo.}$: 163±32 %) and experimentally determined mean swelling degrees did not differ from each other in contrast to the results with Atelocollagen. This might also be explained by the more compact structure of Collagen Solutions compared to Atelocollagen.

In figure 6.2 the experimentally and theoretically determined mean swelling degrees of heterogeneous

bi-layer and triple-layer collagen laminates are displayed. The experimental swelling degree of the laminate ACA could not be determined as ACA did not remain stable during incubation. Bi-layer and triple-layer laminates composed of both, Atelocollagen and Collagen Solutions, showed almost identical experimental swelling degrees with values between the swelling degrees of homogeneous laminates containing either Atelocollagen or Collagen Solutions ($AC_{Exp.}$: 328±34 %, $CAC_{Exp.}$: 335±45 %, $AAC_{Exp.}$: 329±32 % and $ACC_{Exp.}$: 323±93 %). This result meets the expectations, as the heterogeneous collagen laminates are composed of both collagen types. Since Atelocollagen swells much more than Collagen Solutions in percentage terms, its behavior should dominate. The experimentally determined mean swelling degrees corresponded to 47-63 % of the theoretically determined swelling degrees ($AC_{Theo.}$: 626±77 %, $CAC_{Theo.}$: 527±60 %, $AAC_{Theo.}$: 698±66 % and $ACC_{Theo.}$: 527±60 %) and significantly differed from the theoretically determined mean swelling degrees. This result might be explained by the differing number of swelling interfaces between theoretically and experimentally determined swelling degrees, as described for homogeneous Atelocollagen laminates.

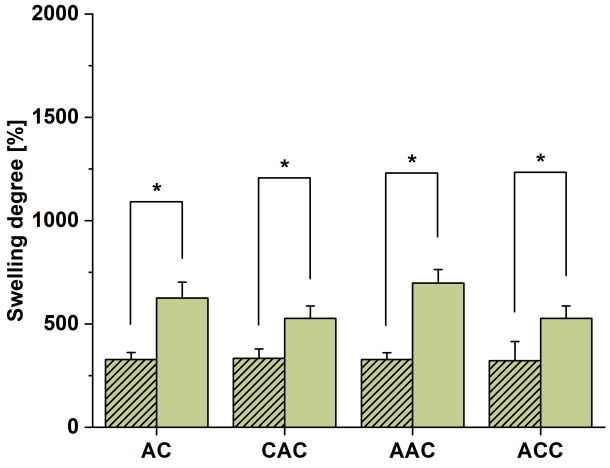

Figure 6.2.: Swelling degree of heterogeneous collagen laminates. The experimental swelling degree (dashed bars, *n = 3*) was determined after 2 h of incubation at RT. The theoretical swelling degree (non-patterned bars) was calculated from single RGX-treated sheets. Error bars represent the standard deviation. The significance (black asterisk) between the experimentally and theoretically determined mean swelling degrees was tested by a Mann-Whitney-Test at p = 0.05.

In summary, homogeneous collagen laminates composed of sponge-like Atelocollagen [67] showed a higher swelling degree than homogeneous laminates composed of the thinner Collagen Solutions. Heterogeneous collagen laminates composed of both types of collagen were characterized by swelling degrees with almost identical values between the homogeneous collagen laminates.

6.2. Release of vancomycin from collagen samples

6.2.1. Development of an additively manufactured sample holder

The release of the model antibiotic vancomycin from different collagen laminates should be analyzed, as theses laminates are to be used for drug release. The following results have been partly published in the journal ”Biomedicines” [127] and in the journal ”Polymers” [138].

In order to study the directional release of vancomycin from collagen samples across the main surfaces of the laminate, an appropriate sample holder was required. The sample holder was based on the principle of the Boyden chamber, where two chambers are separated from each other by a microporous membrane [139]. In this case, the collagen sample should separate two chambers from each other (see figure 6.3).

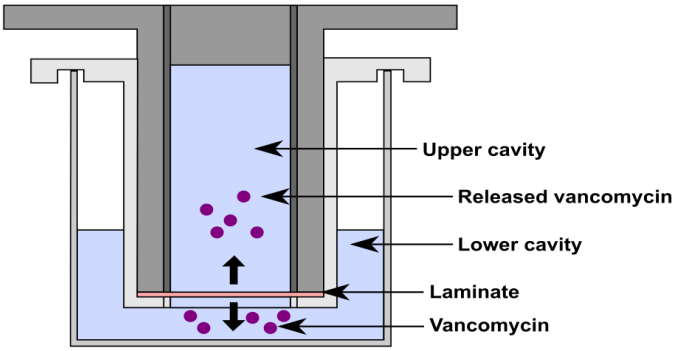

Figure 6.3.: Cross section of the sample holder consisting of an upper and a lower part. The laminate is placed between the upper and the lower part. After placing the sample holder into a cavity of a 24-well plate, the antibiotic release (thick arrows) into the lower and upper chamber can be quantified.

The prototype of the sample holder was designed according to the following requirements: It should form two chambers with a filling volume of 1 mL each and should have dimensions that allow a fitting of the sample holder into a well of a conventional 24-well tissue culture plate. Furthermore, the collagen sample should be tightly inserted into the sample holder so that the released compound could not diffuse to the opposite chamber.

Regarding the handling of the sample holder, different dimensions were tested and the parameters were adjusted in an iterative process. For example, the width of slot for the collagen sample was adjusted, the walls of the lower part and the outer walls of the upper part were tilted, the release area was adjusted, the edges of the release areas were phased and notches were added to the wings of the lower part to ensure a tight positioning of the collagen sample in the sample holder as well as an improved positioning of the sample holder in the well of a 24-well plate. The construction drawings and dimensions of both, the upper and the lower part of the sample holder, are shown in figure A.1 and figure A.2.

To test the tightness of the sample holder, which was fabricated from a transparent resin, the transport of bromophenol blue from the upper into the lower chamber was analyzed. For this purpose, the

tightness experiment was performed with two types of laminates, a bi-layer laminate consisting of Atelocollagen and Collagen Solutions (AC-laminate) and a ”non-permeable” laminate consisting of the AC-laminate with a layer of parafilm underneath the laminate, as the AC-laminate itself might be permeable to the transport of bromophenol blue. The results of both experiments are displayed in figure 6.4. For the AC-laminate without parafilm, the concentration of bromophenol blue decreased after 24 h of incubation in the upper part and increased after 24 h in the lower part. In contrast, the AC-laminate supported by a layer of parafilm showed a decrease of the bromophenol blue concentration in the upper part after 24 h but did not show any increase in the lower part after 24 h. Furthermore, the laminate supported by the layer of parafilm showed a blue discoloration. The fact that the permeable laminate showed a transport of bromophenol blue from the upper into the lower chamber while the non-permeable laminate only showed absorption of bromophenol blue but did not show any transport into the lower chamber indicates that the AC-laminate is permeable to bromophenol blue. Furthermore, as the supporting layer of parafilm prevented any leakage of bromophenol blue into the lower chamber, the tightness of the sample holder was considered as sufficient.

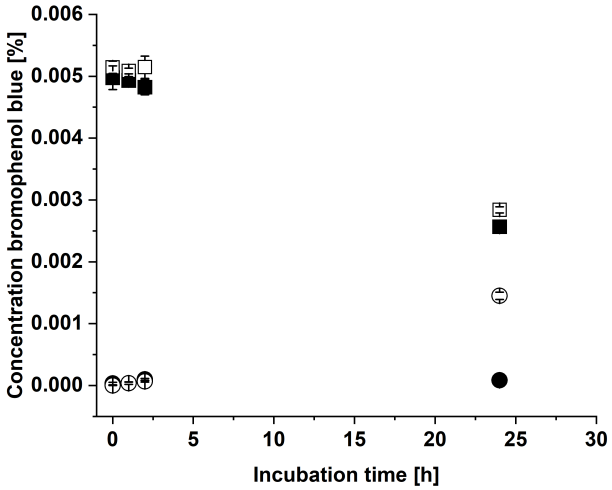

Figure 6.4.: Tightness analysis of the sample holder, which was fabricated from a transparent resin. The tightness was quantified by analyzing the concentration of bromophenol blue in the upper chamber (squares) and in the lower chamber (dots). The experiment was performed with a permeable AC-laminate (empty squares/dots) and an AC-laminate with a layer of parafilm (filled squares/dots). Error bars represent the standard deviation ($n = 3$).

After demonstrating the tightness of the sample holder, vancomycin release experiments with different collagen samples were performed. First, a calibration series of vancomycin was recorded with reversed-phase HPLC by measuring the absorption at 280 nm in order to calculate the amount of released vancomycin from the peak area at a retention time of 40 min. The calibration series is displayed in figure 6.5.

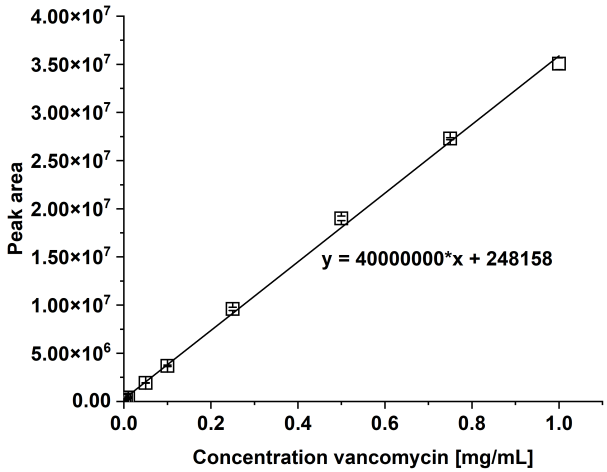

Figure 6.5.: Calibration series of vancomycin in the range of 0.001 - 1 mg/mL measured by reversed-phase HPLC. The adjusted R-square has a value of 0.9985, the intercept a value of 248158 and the slope a value of $4x10^7$. Error bars represent the standard deviation (*n = 3*).

The following release experiments were carried out at 37 °C according to physiological conditions. As asymmetrical bi-layer laminates were particular of interest, a first release experiment with the sample holder fabricated from a transparent resin and an AC-laminate with vancomycin-loaded Atelocollagen facing the upper chamber was exemplarily performed. The result is displayed in figure 6.6. In total, 71 % of the loaded vancomycin were released after 24 h. As this measurement was only performed with a single laminate to test the performance of the sample holder in general, the difference between the lower chamber and the upper chamber after 24 h of incubation could not be statistically evaluated (lower chamber: 31 %, upper chamber: 40 %). This experiment shows in general that the sample holder allows the quantification of the vancomycin release in opposite directions over time. As a white resin contributed to a more stable handling compared to the transparent resin, the following experiments were performed with a sample holder constructed from a standard white resin.

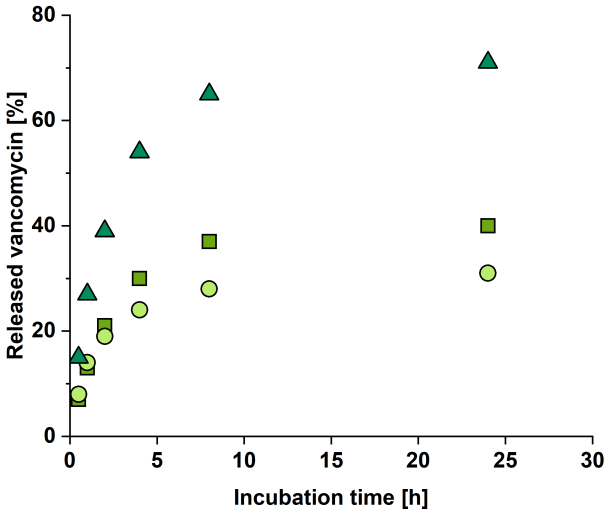

Figure 6.6.: Vancomycin-release from an AC-laminate consisting of Atelocollagen and Collagen Solutions. Vancomycin-loaded Atelocollagen was facing the upper chamber after positioning in a transparent sample holder. The release was analyzed in a single measurement in the upper chamber (squares), the lower chamber (dots) and in total (triangles).

6.2.2. Release at physiological conditions

The following results have been partly published in the journal "Biomedicines".[127]

In figure 6.7 the release of vancomycin from an RGX-treated Atelocollagen sheet is depicted. The release was analyzed over 72 h in the sample holder and an additional hour in PBS without the sample holder to quantify if the sample holder retains any amount of vancomycin. The total release was completed after 24 h (24 h: 68±8 %, 48 h: 69±8 %, 72 h: 69±8 %) and the half-maximal release was reached within 1 h of incubation (1 h: 32±6 %). Interestingly, the half-maximal release was reached 30 min later compared to release experiments performed with a free Atelocollagen sample immersed in PBS as described by Eckes *et al.*[67] This might be explained by the decreased release area of the sample positioned in the sample holder compared to the sample in solution, as the release area was reduced about 37 % from 1 cm^2 to 0.635 cm^2 for each main face. A similar value of the total release has been reported for RGX-treated Atelocollagen without the sample holder by Eckes *et al.*[67] It follows, that the sample holder does not decrease the amount of released vancomycin. The equal release into the upper and lower chamber meets the expectations as both release areas of a single sheet are structurally equal to each other. As the additional hour of incubation without the sample holder did not show any further release of vancomycin, the sample holder does not retain any amount of released vancomycin.

As a total release of 100 % could not be achieved and the sample holder did not retain any vancomycin during the release experiment, it was investigated whether the use of the sample holder was responsible for the loss of vancomycin. For this purpose, vancomycin-loaded, RGX-treated Atelocollagen was directly incubated in 1 mL of PBS for 24 h at 37 °C and compared to a sample that was placed into the sample holder, then removed and incubated under the same conditions. The amount of vancomycin released from both samples (directly incubated: 50±1 %, with sample holder: 53±1 %) did not differ significantly from each other according to a Mann-Whitney-Test. Consequently, the incomplete release

of vancomycin during the release experiment cannot be explained by the insertion of the sample into the sample holder. In summary, the positioning of the sample into the sample holder as well as the multiple sampling at different times has no effect on the total amount of released vancomycin. The incomplete vancomycin release from cross-linked collagen has already been observed in our group and by others.[17, 67] Hartinger *et al.* examined the release of vancomycin from EDC-NHS-cross-linked collagen sponges that were produced from collagen dispersions.[17] Although Hartinger *et al.* used a different method for the preparation and cross-linking of collagen materials, they reached a comparable maximum release *in vitro*.[17] Furthermore, Hartinger *et al.* describe that the largest amounts of vancomycin were released after 8 h, similar to the results in this work.[17]

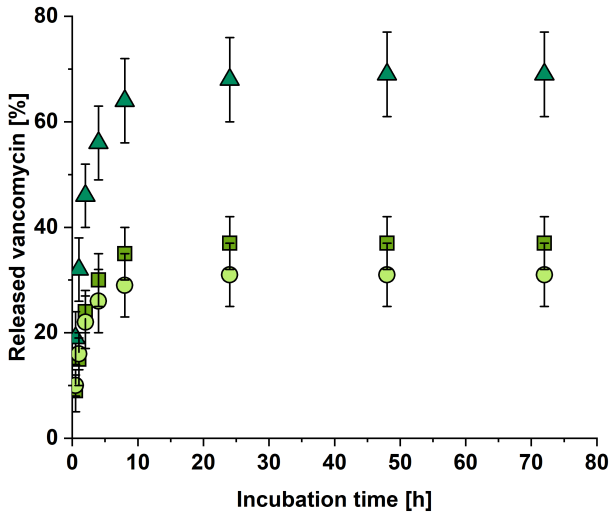

Figure 6.7.: Vancomycin-release from an RGX-treated Atelocollagen sheet in a white sample holder. The release was analyzed over 72 h in the upper chamber (squares), the lower chamber (dots) and in total (triangles). The error bars represent the standard deviation (*n = 3*).

After characterizing the vancomycin release from a single RGX-treated Atelocollagen sample, the release of vancomycin from heterogeneous bi-layer collagen laminates was analyzed (see figure 6.8). For this purpose, an AC-laminate consisting of Atelocollagen and Collagen Solutions with vancomycin-loaded Atelocollagen was placed in the sample holder with Atelocollagen either facing the upper or the lower chamber, and the release was analyzed over 72 h. Both samples showed a similar total release of vancomycin, which was completed within 24 h, as the total maximal release did not change after 48 h or 72 h of incubation (Atelocollagen facing the upper chamber: 69±4 % (24 h), 69±4 % (48 h) and 69±4 % (72 h)), Atelocollagen facing the lower chamber: 62±3 % (24 h), 64±3 % (48 h) and 64±3 % (72 h). The total half-maximal release for both samples was reached within 2 h of incubation (Atelocollagen facing the upper chamber: 38±5 %, Atelocollagen facing the lower chamber: 37±3 %), with one hour delay compared to the single sheet of RGX-treated Atelocollagen (see figure 6.7). Both samples showed an increased release of vancomycin into the chamber facing Collagen Solutions instead of the chamber facing the vancomycin-loaded Atelocollagen. Furthermore, both samples did not show any further release of vancomycin after an additional hour of incubation without the sample holder.

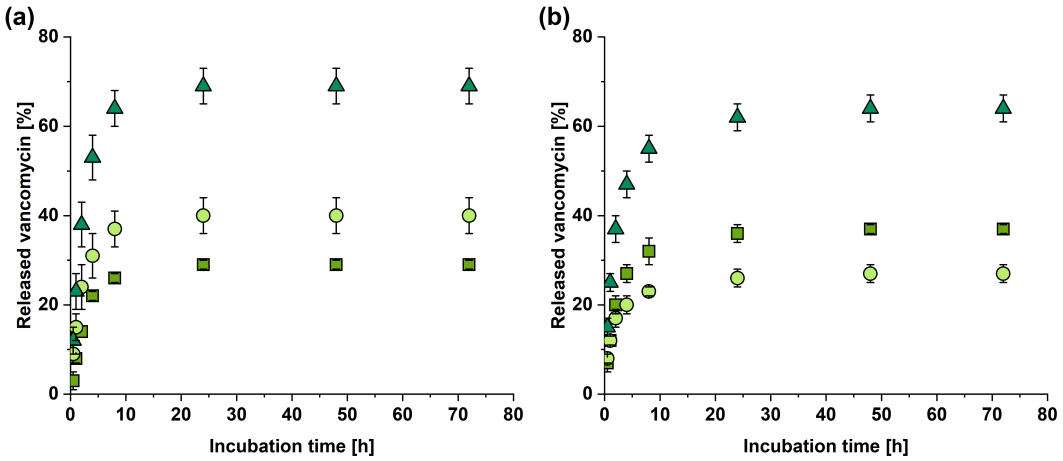

Figure 6.8.: Vancomycin release from heterogeneous bi-layer collagen laminates composed of Atelocollagen and Collagen Solutions with vancomycin loaded into Atelocollagen. The release was analyzed over 72 h in triplicates in the upper chamber (squares), the lower chamber (dots) and in total (triangles). The error bars represent the standard deviation (*n = 3*). (a) Atelocollagen facing the upper chamber. (b) Atelocollagen facing the lower chamber.

The preferred release of vancomycin at the side of Collagen Solutions might be explained by the structural properties of the laminate, since RGX-treated Atelocollagen and Collagen Solutions have different swelling degrees [67] (see figure 6.1) and different porosities as indicated by electron microscopy.[67] Furthermore, the effect of compression might influence the release of vancomycin. Leddy *et al.* described that the diffusivity decreases by compression [140] and Kihara *et al.* showed that the diffusion coefficient of biomolecules with a comparable size to vancomycin decreased in condensed collagen gels compared to non-condensed collagen gels or biomolecules in solution.[141] As compressed hydrogels re-swell in solution [142], the vancomycin release by diffusion might be decreased due to the fluid influx into the opposite direction of release. It follows, that the higher porosity of Atelocollagen results in a stronger swelling and stronger compression, leading to a larger fluid inflow. The release should be reduced at the surface of Atelocollagen, resulting in a preferential release at the side of Collagen Solutions. Consequently, loading of vancomycin into the Collagen Solutions layer, which has a more compact structure than Atelocollagen [67], should result in the same preferential release direction. To verify this assumption, further release experiments with the AC-laminate and vancomycin loaded in Collagen Solutions were performed (see figure 6.9). The release was only analyzed over 24 h instead of 72 h, as the previous measurements had revealed no further release level after 24 h. Both samples showed a similar total release of vancomycin after 24 h (Collagen Solutions facing the upper chamber: 13±1 %, Collagen Solutions facing the lower chamber: 16±2 %). The total mean release from the AC-laminate with vancomycin-loaded Collagen Solutions was significantly lower compared to RGX-treated Atelocollagen and the AC-laminates with vancomycin-loaded Atelocollagen, according to a Kruskal-Wallis ANOVA. This result might be explained by the different structures of both collagen types and the effect of RGX. The total half-maximal release for both samples was reached within 1 h of incubation (Collagen Solutions facing the upper chamber: 8±1 %, Collagen Solutions facing the lower chamber: 7±2 %), which is comparable to the time for half-maximal release from a single RGX-treated Atelocollagen sheet and 1 h earlier than the time for half-maximal release from vancomycin-loaded Atelocollagen in the AC-laminate. Since Collagen Solutions is thinner and more compact than Atelocollagen [67], shorter diffusion paths in Collagen Solutions should be accountable for the faster release. As Collagen Solutions has a compact structure, the compression and fluid uptake during re-swelling

opposed to the antibiotic release direction should have a negligible effect on the vancomycin release, leading to an earlier half-maximal release compared to the AC-laminate with vancomycin-loaded Atelocollagen. Both AC-laminate samples showed an increased release of vancomycin into the chamber facing Collagen Solutions, independent of the layer to which vancomycin was loaded. These results confirm the assumption that due to the structural properties of the Atelocollagen in the AC-laminate more vancomycin is released at the side of Collagen Solutions. The shorter diffusion paths through Collagen Solutions might also explain the almost complete release via the surface of Collagen Solutions.

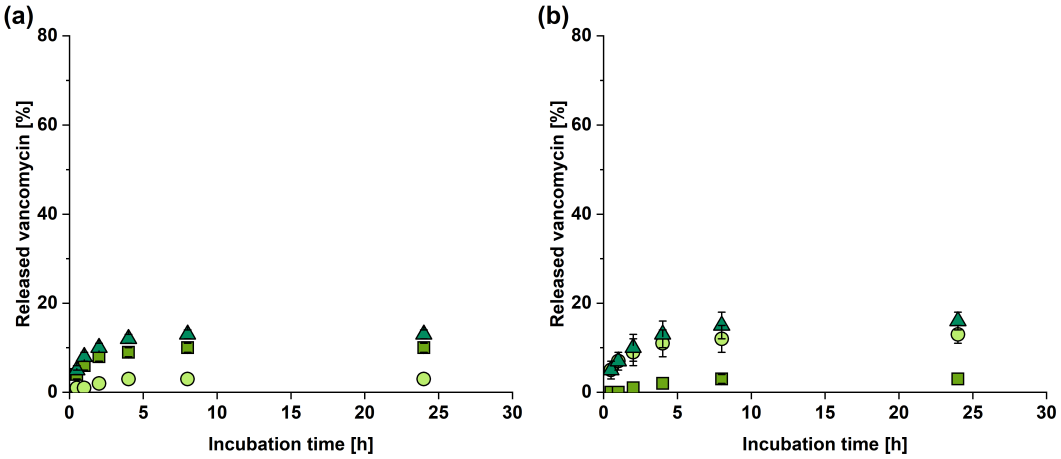

Figure 6.9.: Vancomycin-release from heterogeneous bi-layer collagen laminates composed of Atelocollagen and Collagen Solutions with vancomycin loaded into Collagen Solutions. The release was analyzed over 24 h in the upper chamber (squares), the lower chamber (dots) and in total (triangles). The error bars represent the standard deviation (*n = 3*). (a) Collagen Solutions facing the upper chamber. (b) Collagen Solutions facing the lower chamber.

In summary, the release experiments from heterogeneous two-layer collagen laminates showed that vancomycin was preferentially released to the side of Collagen Solutions, independent of the collagen type loaded with vancomycin and the orientation of the laminate in the sample holder.

In the next step, release experiments with different three-layered collagen laminates were performed. As AC-laminates with vancomycin-loaded Atelocollagen led to higher values of total released vancomycin, symmetrical and asymmetrical three-layered collagen laminates with vancomycin-loaded Atelocollagen as central layer were analyzed.

In figure 6.10 the vancomycin release of the symmetrical three-layered laminates Collagen Solutions-Atelocollagen-Collagen Solutions (CAC) and Atelocollagen-Atelocollagen-Atelocollagen (AAA) are displayed.

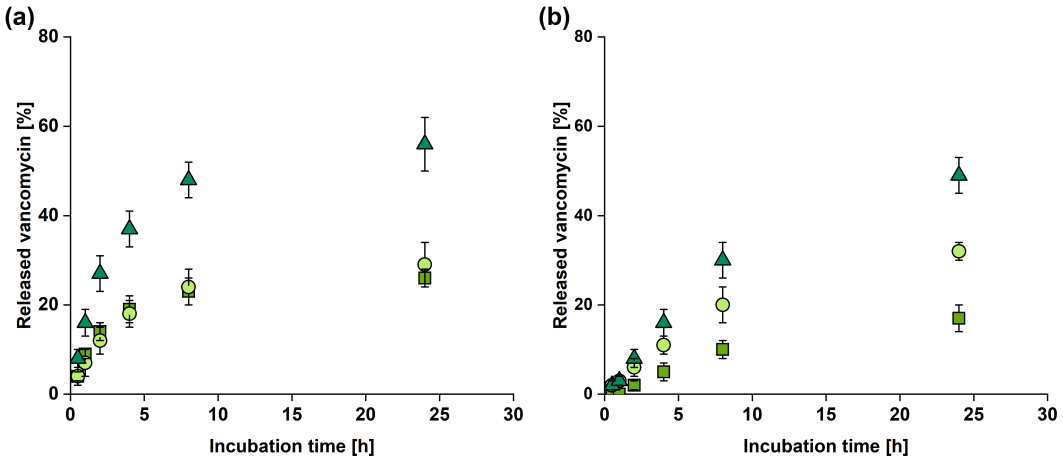

Figure 6.10.: Vancomycin-release from heterogeneous, symmetrical three-layer collagen laminates composed of Atelocollagen and Collagen Solutions. Vancomycin was loaded into the central collagen layer. The release was analyzed over 24 h in the upper chamber (squares), the lower chamber (dots) and in total (triangles). The error bars represent the standard deviation (*n = 3*). (a) Laminate CAC. (b) Laminate AAA.

Both, the laminate CAC as well as AAA reached similar values for the total maximal release after 24 h (CAC: 56±6 % and AAA: 49±4 %). The half-maximal release from both laminates differed, as the half-maximal release for CAC was reached within 2 h (27±4 %) and for AAA within 8 h (30±4 %). Compared to the AC-laminate with vancomycin-loaded Atelocollagen, the time for half-maximal release of CAC was similar to the AC-laminate, while the time for half-maximal release of AAA was at least four-times longer compared to the AC-laminate. Since Collagen Solutions is very thin [67] and diffusion paths across the material are correspondingly short, it should not have any additional effect on the time for half-maximal release, so that the latter should not differ between the AC-laminate with vancomycin-loaded Atelocollagen and the CAC laminate, as the data confirm. The elongated time for half-maximal release of AAA might be explained by the swelling degrees of the Atelocollagen layers. Interestingly, AAA showed a preferential release of vancomycin into the lower chamber while for CAC, vancomycin was equally released into both directions. This result does not meet the expectations as for symmetrical laminates an equal release into both directions is expected, since the release areas have identical surface areas and material properties. Upon inspection of the laminate after the experiment, AAA showed a swelling of the laminate's bottom side into the lower chamber (see figure A.3), which indicates that both sides of the laminate cannot be considered as equal. The increased swelling at the bottom side might lead to an increased release area, which would explain the preferred release to the lower chamber. The thickness of AAA, resulting in a force effect from top to bottom after fixing the sample in the sample holder, might explain the swelling of AAA at the bottom side. As the asymmetrical swelling was not visible for CAC, the central layer of Atelocollagen might be stabilized by Collagen Solutions.

After analyzing the release of vancomycin from symmetrical three-layer laminates, the asymmetrical triple-layer laminate Atelocollagen-Atelocollagen-Collagen Solutions (AAC) with vancomycin-loaded Atelocollagen as central layer was analyzed with Atelocollagen either facing the upper or the lower chamber (see figure 6.11).

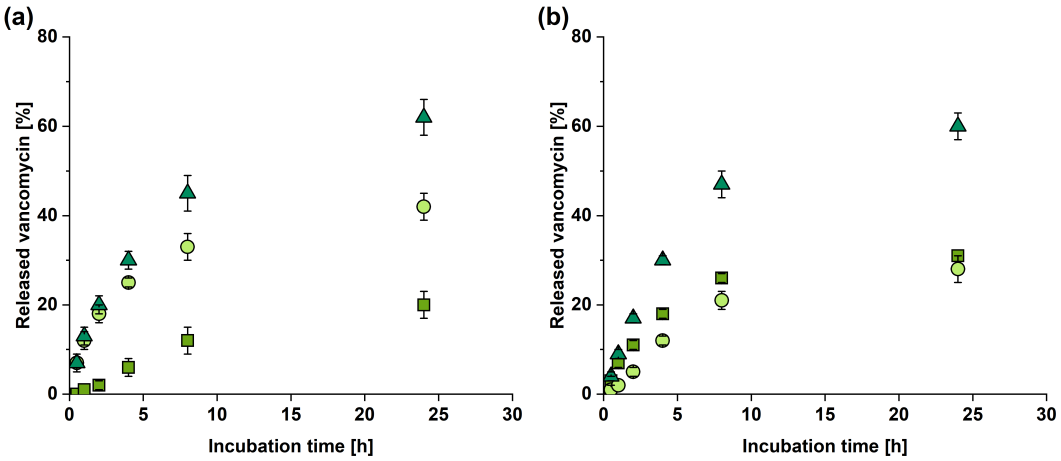

Figure 6.11.: Vancomycin-release from heterogeneous, asymmetrical three-layer collagen laminates composed of Atelocollagen and Collagen Solutions. Vancomycin was loaded into the central collagen layer. The release was analyzed over 24 h in the upper chamber (squares), the lower chamber (dots) and in total (triangles). The error bars represent the standard deviation. (a) Laminate AAC with Atelocollagen facing the upper chamber (*n = 3*). (b) Laminate AAC with Atelocollagen facing the lower chamber (*n = 3*).

As depicted in figure 6.11, both samples reached similar total release values after 24 h of incubation (Atelocollagen facing the upper chamber: 62±4 %, Atelocollagen facing the lower chamber: 60±3 %). Furthermore, the half-maximal release was reached within 4 h for both samples (Atelocollagen facing the upper chamber: 30±2 %, Atelocollagen facing the lower chamber: 30±1 %), which lies between the time for half-maximal release of CAC (2 h) and AAA (8 h). The elongated time for half-maximal release might be attributed to the additional layer of Atelocollagen. Interestingly, as already described for the AC-laminates, vancomycin was preferentially released at the side of Collagen Solutions (exception: Atelocollagen facing the lower chamber after 24 h). In contrast to the AC-laminates, the orientation of the AAC-laminate determines how large the proportion of vancomycin is that is released by the Collagen Solutions layer. Similar to the laminate AAA, AAC with Atelocollagen facing the laminate's bottom side showed a swelling into the lower chamber. If Atelocollagen faces the bottom side of the thick laminate and swells out of the sample holder, it increases the release area. This allows more vancomycin to diffuse out of the Atelocollagen surface and the difference between both sides becomes smaller. However, since diffusion through Collagen Solutions is faster, more vancomycin is still released on the side of Collagen Solutions in percentage terms.

In summary, the release experiments from triple-layer laminates showed that similar to bi-layer laminates, vancomycin is preferentially released at the side of Collagen Solutions in asymmetrical laminates. Furthermore, the time for half-maximal release increased with the number of Atelocollagen sheets in the laminate. Moreover, swelling and surface deformation showed an influence that can be attributed to a limitation of the sample holder. A lattice structure at the bottom side of each part of the sample holder might stabilize flexible biomaterials, allowing to tailor the sample holder to the properties of a given biomaterial, e.g. its swelling degree or flexibility. However, the effect of the sample holder is also of practical relevance, as compressive forces can also occur in the body.[143] In addition to the strength of the surrounding tissue (bone versus muscle/skin) [143], the availability of fluid for swelling also plays a role.

6.2.3. Release under acidic and alkaline conditions

During physiological cutaneous wound healing, pH values ranging from pH 9.0 to pH 5.5 can occur within 14 days after surgery.[144] Acidification is also reported for the first day of cultivation of *Staphylococcus aureus* on rat jawbones.[145] *Staphylococcus aureus* belongs to the predominant microorganisms causing SSIs [6], as it has the ability to form biofilms on implants.[146] Zmantar *et al.* showed that an increased biofilm formation of *Staphylococcus aureus* occurs at pH 5.[147] It follows that *Staphylococcus aureus* creates optimal living conditions for itself by acidifying the environment. Another example for acidification is reported for osteotomy hematomas.[148] The latter showed a decrease of the pH from physiological values to pH 6.62±0.33 within four hours after bone injury.[148] Consequently, the effect of the pH value on the release of vancomycin from collagen samples should be examined. The following results have been partly published in the journal "Polymers".[138] In the literature, a pH of 5.5 is commonly used to simulate the moderately acidic environment found at sites of bacterial infection [149, 150] and was therefore used to analyze the vancomycin release at acidic conditions. As a representative value for alkaline conditions, a pH of 8.5 was used, referring to the initial mean value reported for second degree burns.[151] All release experiments were carried out with the white sample holder at 37 °C and compared with the previous results at pH 7.4 and 37 °C. Besides a single sheet of RGX-modified Atelocollagen, analysis was performed with a heterogeneous AC-laminate that was positioned in the white sample holder with the vancomycin-loaded Atelocollagen facing the upper cavity. This AC-laminate was used for analysis since release experiments under physiological conditions showed a collagen-dependent vancomycin release independent of the orientation of the laminate in the sample holder. Furthermore, the orientation of the laminate with vancomycin-loaded Atelocollagen facing the upper cavity contributed to a better handling and a higher amount of totally released vancomycin. For RGX-modified Atelocollagen (see figure 6.12 (a)-(b)) no differences in totally released vancomycin amounts were observed after 24 h of incubation (pH 5.5: 71±2 %, pH 7.4: 68±8 % (see figure 6.7) and pH 8.5: 74±3 %). Comparable values were also obtained for the AC-laminate (see figure 6.12 (c)-(d)) with the vancomycin-loaded Atelocollagen facing the upper cavity (pH 5.5: 61±6 %, pH 7.4: 69±4 % (see figure 6.8) and pH 8.5: 67±3 %). These results indicate that the total amount of vancomycin released from a single sheet of RGX-modified Atelocollagen or an AC-laminate does not depend on the pH value of the environment. For RGX-modified Atelocollagen, the time for half-maximal release was two to four times longer than at pH 7.4 (pH 5.5: 41±1 % (4 h), pH 7.4: 32±6 % (1 h, see figure 6.7) and pH 8.5: 39±3 % (2 h)). The AC-laminate showed a similar result, as the time for half-maximal release was doubled compared to physiological pH (pH 5.5: 33±3 % (4 h), pH 7.4: 38±5 % (2 h, see figure 6.8) and pH 8.5: 45±2 % (4 h)).

In terms of the release direction, vancomycin was equally released into the upper and lower cavity from RGX-modified Atelocollagen at pH 5.5. Under alkaline conditions, only slightly more antibiotic was released into the upper cavity after 8 h of incubation. In contrast to the single sheet of RGX-modified Atelocollagen, vancomycin was preferentially released from the AC-laminate into the cavity facing Collagen Solutions, independent of the surrounding pH.

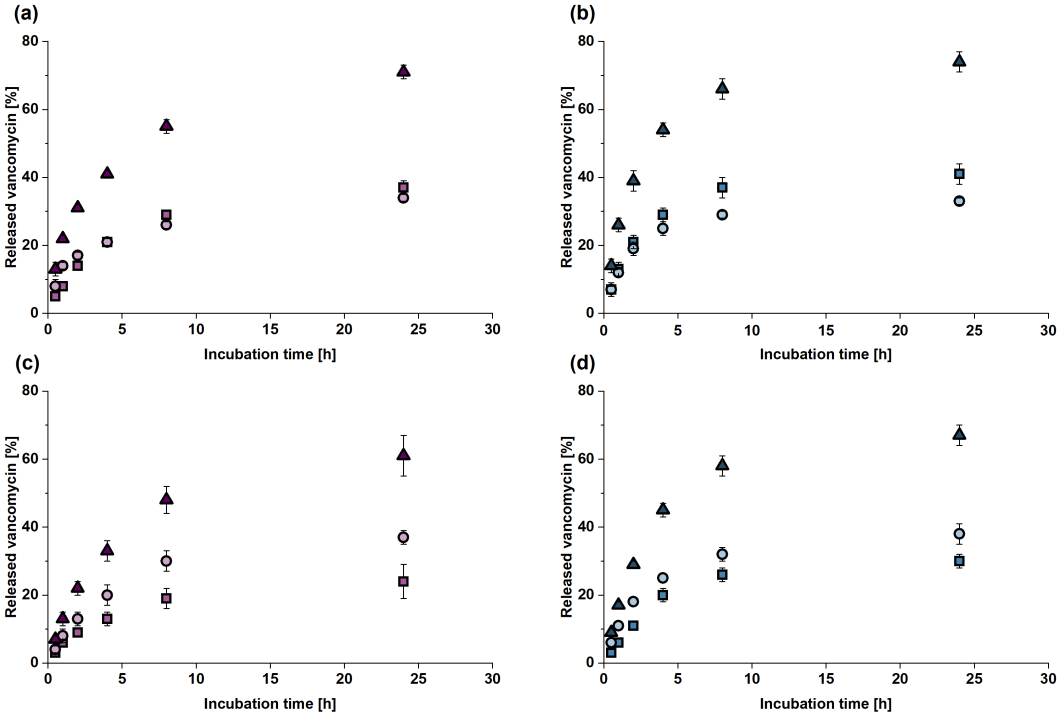

Figure 6.12.: Release profiles of vancomycin from RGX-modified Atelocollagen or an AC-laminate at pH 5.5 or pH 8.5. For the AC-laminate, vancomycin-loaded Atelocollagen was facing the upper cavity. The release was analyzed over 24 h at 37 °C in the upper chamber (squares), the lower chamber (dots) and in total (triangles). Error bars represent the standard deviation ($n = 3$). (a) Release at pH 5.5 from Atelocollagen. (b) Release at pH 8.5 from Atelocollagen. (c) Release at pH 5.5 from an AC-laminate. (d) Release at pH 8.5 from an AC-laminate.

The elongated times for half maximal release at acidic and alkaline conditions might be explained by differing swelling behaviors of both samples compared to physiological conditions. Therefore, the swelling degrees at different pH values were analyzed. The mean swelling degree of RGX-modified Atelocollagen (see figure 6.13(a)) reached a higher value at pH 5.5 and did not change at pH 8.5 compared to physiological pH (pH 5.5: 1562±283 %, pH 7.4: 539±20 % and pH 8.5: 541±64 %). The swelling degree at pH 5.5 differed significantly from the swelling degrees at both pH 7.4 and pH 8.5, according to a Kruskal-Wallis ANOVA at $p = 0.05$. Compared to the previous determination of the swelling degree of RGX-modified Atelocollagen at pH 7.4 at RT (see figure 6.1), the swelling degree at 37 °C was significantly reduced, indicating a temperature dependency (RT: 795±117 % and 37 °C: 539±20 %). A temperature dependency of RGX-modified Atelocollagen has already been described by Eckes *et al.*, who analyzed a loss of thickness from RT to 37 °C for RGX-modified Atelocollagen.[67] The swelling degree of Collagen Solutions did not change at pH 5.5 and significantly decreased at pH 8.5 compared to physiological pH (see figure 6.13 (a), pH 5.5: 144±16 %, pH 7.4: 214±73 % and pH 8.5: 112±18 %). Furthermore, the mean swelling degree of RGX-modified Atelocollagen was significantly higher than the mean swelling degree of RGX-modified Collagen Solutions.

For the AC-laminate, the mean swelling degree (see figure 6.13(b)) reached a higher value at acidic pH and did not change at alkaline pH compared to physiological pH (pH 5.5: 1053±114 %, pH 7.4: 643±69 % and pH 8.5: 568±73 %). Again, the mean swelling degrees significantly differed from pH 5.5 to pH 7.4 and from pH 5.5 to pH 8.5. At pH 7.4, the swelling degree at 37 °C was significantly

reduced compared to RT (see figure 6.2), indicating a temperature dependency (RT: 328±34 % and 37 °C: 643±69 %). As the temperature dependency was not observed for Collagen Solutions, the above described temperature dependence of Atelocollagen is reflected in the laminate.

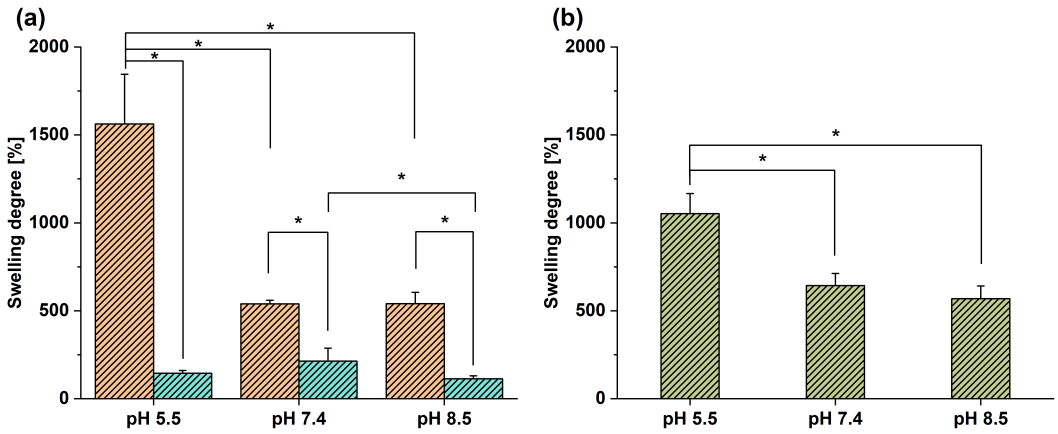

Figure 6.13.: Swelling degrees of RGX-modified Atelocollagen, RGX-modified Collagen Solutions and an AC-laminate at different pH conditions. The swelling degree was determined after 2 h of incubation at 37 °C. Error bars represent the standard deviation (*n = 3*). The significance (black asterisk) was tested by a Kruskal-Wallis ANOVA at p = 0.05. (a) Swelling degree of Atelocollagen (orange) and Collagen Solutions (blue) at pH 5.5, pH 7.4 and pH 8.5. (b) Swelling degree of an AC-laminate at pH 5.5, pH 7.4 and pH 8.5.

The increased mean swelling degrees of RGX-modified Atelocollagen and the AC-laminate at acidic conditions meet the expectations as a pH-dependent swelling of collagen has been previously reported.[71] During swelling, fluid is taken up by the polymer due to an osmotic pressure gradient across the interface of bulk polymer and surface.[152] Swelling is limited by the polymeric network structure [153], because as an equilibrium is reached, the elastic force of the network that contracts in the opposite direction of fluid inflow equals the osmotic force.[24] The isoelectric point (pI), where the swelling reaches the smallest extent [152], lies around pH 8.[38] At pH 5.5, the biopolymer has a positive net charge, leading to a repulsion of the positive electric charges and a stretching of the biopolymer fibers, resulting in an increase of the swelling degree at acidic conditions.[71] The similar swelling degrees at pH 7.4 and pH 8.5 of both samples also meet the expectations as both pH values lie about the same distance away from the isoelectric point of Atelocollagen and therefore the net charge of both samples is low, resulting in similar swelling degrees. The lower net charge at pH 8.5 and pH 7.4 suggests that the swelling degree should be lower than at pH 5.5, as the data confirm. For the AC-laminate, the swelling effect of Collagen Solutions can be neglected since the data showed that Collagen Solutions swells significantly less than Atelocollagen.

The described swelling behaviors of both samples only partly explain the release properties of both samples at different pH conditions. The two to four times longer duration for reaching the half-maximal release at pH 5.5 compared to physiological pH can be explained by the significantly increased swelling degrees of Atelocollagen at acidic pH. In detail, the fluid influx into the collagen sample might counteract the release of vancomycin in the opposite direction. As the swelling is increased and diffusion paths are longer at pH 5.5, the fluid influx might be increased resulting in a retarded release of vancomycin and consequently an elongated time for half-maximal release. As the swelling of Atelocollagen is significantly

higher than the swelling of Collagen Solutions, the time for half-maximal release is also elongated for the AC-laminate.

At a pH of 8.5 the swelling behaviors of both samples do not explain the release properties as the swelling degrees did not differ between pH 8.5 and pH 7.4. However, the times for half-maximal release were twice as long as at physiological pH. These results might be explained by electrostatic interactions, as negatively charged vancomycin (pI = 7.2) [154, 155] might interact with collagen chains that have remaining positively charged regions at pH 8.5. Likewise, electrostatic interactions between positively charged amino groups and guanidinium groups of arginine of collagen-like peptide and negatively charged rose bengal (pKa = 1.89 and 3.93 [56]) have been described in literature.[44] Since the times for half-maximal release at pH 8.5 were similar or shorter than at pH 5.5, the stronger effect of swelling at pH 5.5 might counteract the repulsion of positively charged vancomycin and the positive net charge of the polymer.

In summary, vancomycin release studies from RGX-modified Atelocollagen and a two-layer laminate composed of Atelocollagen and Collagen Solutions revealed that the total amount of released vancomycin was independent of the surrounding pH. Furthermore, a change of the pH from neutral to acidic conditions led to an elongated time for half-maximal release that can be explained by the increased swelling of Atelocollagen at pH 5.5. At alkaline conditions, the elongated time for half-maximal release, compared to physiological pH, might be explained by electrostatic interactions instead of swelling properties, as the swelling behavior did not differ between pH 7.4 and pH 8.5. These findings are of interest for the composition of collagen laminates to support wound healing, as both, the swelling of collagen as well as the electrostatic interactions between the collagen and the antibiotic need to be considered. In case of an inflammation, the fast release of antibiotics is preferred. Since the swelling of Atelocollagen is increased at pH 5.5 and leads to a delayed antibiotic release, Atelocollagen should not be used for antibiotic delivery if signs of an infection occur. Instead, a more stable collagen with less swelling degree at pH 5.5 and a pI in the acidic range would be preferable. In contrast to a fast release, Atelocollagen might rather be used for the retarded release of growth factors that support cell proliferation and angiogenesis, leading to tissue regeneration.[156] Furthermore, in addition to the composition of the laminate, the biodegradability of the polymer should also be considered, as degradation processes could also affect the release of the antibiotic.[18]

6.3. Reversible immobilization of CXCL8 in microfluidic devices

Glycosaminoglycans, such as heparan sulfate, act as natural binding partners of chemokines and are therefore involved in the generation of chemokine gradients on the surface of endothelial cells, leading to the directed migration of immune cells to the site of inflammation.[70, 92] To study the migration of cells along heparin-bound chemokine concentration gradients, a method was previously developed for microfluidic channels made of PDMS. Theses channels were coated with polydopamine and heparin and CXCL8 gradients generated by microfluidics were immobilized by binding to the heparin surface.[120, 134] We were able to show that a rotating incubation of dopamine and heparin along the channel's roll axis improved the homogeneous distribution of heparin as well as CXCL8.[120] Furthermore, a spatially continuously decreasing concentration gradient was established with an initial concentration of 8 µM of CXCL8 at a flow rate of 0.8 µL/min (see figure 5.2 and figure 5.3).[120] The general form of the gradient is characterized by an approximately linear decrease of the gradient along the channel length in x-direction, with the flattest gradients in the rear channel sections.[134] Stability analysis at RT revealed that the gradient decreases to half of its initial slope after 12 h.[120] Additionally, a single cell migration experiment with THP-1 cells confirmed the recognition of the CXCL8 gradient by THP-1 cells, which migrated towards higher chemokine concentrations. In the work presented here, the reversibly immobilized CXCL8 gradient should be further examined and the migration of THP-1 cells along the heparin-bound CXCL8 gradient should be further quantified under different conditions. The following results have been partly published in the journal "Colloids and Surfaces B: Biointerfaces".[120]

6.3.1. Homogeneity of the dopamine-heparin coating

To further characterize the reversible immobilization of a CXCL8 gradient in a microfluidic device coated with dopamine and heparin, the homogeneity of the coating was analyzed. For this purpose, one channel was coated with dopamine and heparin and another channel was just rinsed with 1 mL of 70 % (v/v) ethanol and then with 1 mL of degassed Microfluidic PBS (pH 8.5). In the next step, both channels were rinsed with 0.8 µL/min loading buffer from the outlet for 20 min, followed by 0.8 µL/min of 8 µM CXCL8-S72C-fluorescein from the outlet for 240 min (see figure 6.14). As described in the method, the channels were manually washed with 1 mL of loading buffer to remove non-bound chemokine. The mean relative fluorescence intensities between both channels were compared to each other after 0 h of incubation. As displayed in figure 6.15, higher mean relative fluorescence intensities were obtained for the channel without coating in the front region (0 - 12500 µm) than in the rear channel region (12500 - 20000 µm). Consequently, there is a decreasing trend of the mean relative fluorescence intensities over the total length of the channel, with a difference of ΔRFU: 899 between the minimum (448 RFU) and maximal (1347 RFU) values. In contrast, the mean relative fluorescence intensities for the channel with coating ranged from 623 RFU to 872 RFU, resulting in a smaller difference between minimum and maximum values (ΔRFU: 249). Since the chemokine solution was added to the channels from the outlet under flow and therefore should be evenly distributed over the entire channel, a uniform fluorescence intensity over the length of the channel was expected. As the differences between the respective minimal and maximal fluorescence intensities were larger for the non-coated channel compared to the coated channel, the dopamine-heparin coating enabled a more even distribution of fluorescently labeled chemokine in the microfluidic channel. Furthermore, the high fluorescence intensities for the channel without coating indicated that the fluorescently labeled chemokine interacted with the PDMS surface. However, as PDMS is hydrophobic, a modification of its surface is required to enhance cellular adhesion.[114, 124] The coating of PDMS with dopamine and heparin therefore not only enables a more even distribution of the chemokine in the channel, it also

provides a natural environment for cells.[92]

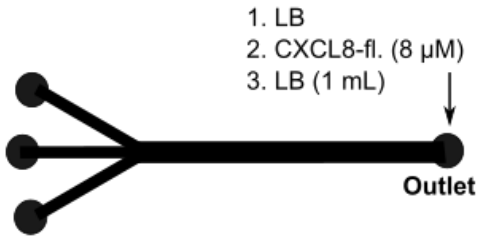

Figure 6.14.: Setup used for homogeneity analysis. Both channels were rinsed with 0.8 µL/min loading buffer (LB) from the outlet for 20 min, followed by 0.8 µL/min of 8 µM CXCL8-S72C-fluorescein (CXCL8-fl.) in loading buffer from the outlet for 240 min. The channels were then manually washed with 1 mL loading buffer from the outlet to remove non-bound chemokine.

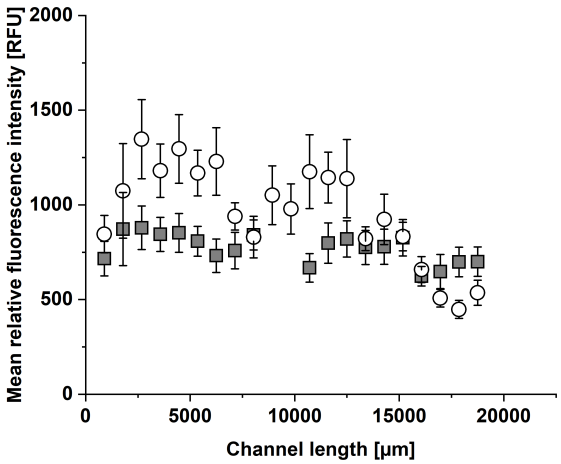

Figure 6.15.: Homogeneity analysis of the dopamine-heparin coating. The microfluidic channel was either coated (grey squares) or not coated (white squares) with dopamine-heparin. The channels were rinsed from the outlet at a flow rate of 0.8 µL/min with loading buffer for 20 min, followed by 8 µM CXCL8-S72C-fluorescein in loading buffer for 240 min. After immobilization, non-bound chemokine was removed by a manual washing step. Images of the channel (900 µm-sections) were taken under the fluorescence microscope ($\lambda_{Ex.}$ = 450-490 nm and $\lambda_{Em.}$ = 500-550 nm) with 10x magnification at an exposure time of 300 ms. The mean relative fluorescence intensity of each channel section was analyzed. Outliers were eliminated.

6.3.2. Stability analysis of the chemokine concentration gradient at 37 °C

In previous experiments the stability of the gradient at RT had been examined [120], however, the normal body temperature of a human adult is 37 °C and migration studies were performed at this temperature.[157] For this purpose, the stability of the reversibly immobilized chemokine concentration gradient was analyzed at 37 °C over 43 h, since cell migration was examined over this period. The setup

is shown in figure 6.16. Since many outliers were present in the first channel half and no continuous evaluation was possible, only the second channel half (channel sections 13 to 21) was used for analysis. As displayed in figure 6.17, the concentration profile was detectable in the second half of the channel length with values ranging between 3.8 RFU/µm (11635 µm, section 13) and 1.3 RFU/µm (18795 µm, section 21). After 20 h of incubation the values of the concentration profile had decreased about 50 % in the second half of the channel length (1.7 RFU/µm (15215 µm, section 17) and 0.6 RFU/µm (17900 µm, section 20)). After total of 43 h of incubation the values of the concentration profile did not show any further decrease (1.7 RFU/µm (12530 µm, section 14) and 0.5 RFU/µm (15215 µm, section 17)). The decrease of the steepness of the reversibly immobilized CXCL8 gradient about 50 % within incubation equals the previous result of the stability analysis at RT.[120] It follows that no larger decrease of the gradient is to be expected in the experiments at 37 °C than already verified at RT. As cell migration experiments were carried out over 43 h [120], the stability of the concentration gradient should be sufficient to sustain cell migration towards higher CXCL8 concentrations. As Yang *et al.* analyzed that polydopamine coatings are stable under slightly alkaline conditions (pH 8 – 10), which even supports the polymerization reaction, and the stability is only slightly decreased at a physiological pH, a decrease of the concentration gradient due to the instability of the polydopamine coating can be neglected.[158] Furthermore, polydopamine improved the stability of an ATH on PDMS and Leung *et al.* were able to show that 75 % of an initial ATH-coating on a polydopamine-modified PDMS surface remained stable after 24 h of incubation in blood.[122] Consequently, the decrease of the concentration gradient due to the instability of the heparin-coating on the polydopamine-modified PDMS surface can also be neglected. The decrease of the concentration gradient within the first 20 h of incubation can be explained by dissociation of reversibly bound CXCL8 from heparin, followed by diffusion, re-binding and consequently a redistribution of the chemokine in the channel.[120] The change of the gradient over time corresponds to natural conditions as chemokine concentration gradients naturally occur as a mixture of soluble and immobilized gradients.[159]

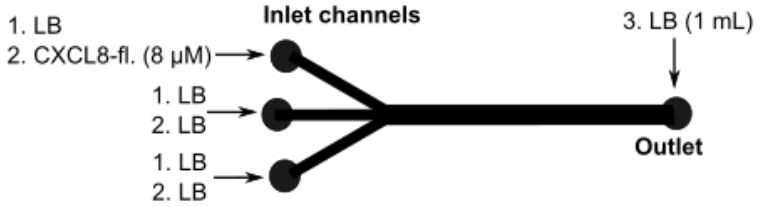

Figure 6.16.: Setup used for stability analysis. In the first step the channel was rinsed from the inlet channels with loading buffer (LB) with 0.8 µL/min for 20 min. In the second step the channel was rinsed from the top inlet channel with 8 µM CXCL8-S72C-fluorescein (CXCL8-fl.) in loading buffer and from the middle and bottom inlet channel with loading buffer with 0.8 µL/min for 240 min. The channel was manually washed with 1 mL of loading buffer from the outlet to remove non-bound chemokine. After incubation at 37 °C and 5 % CO_2 in the dark, analysis was performed after different time points.

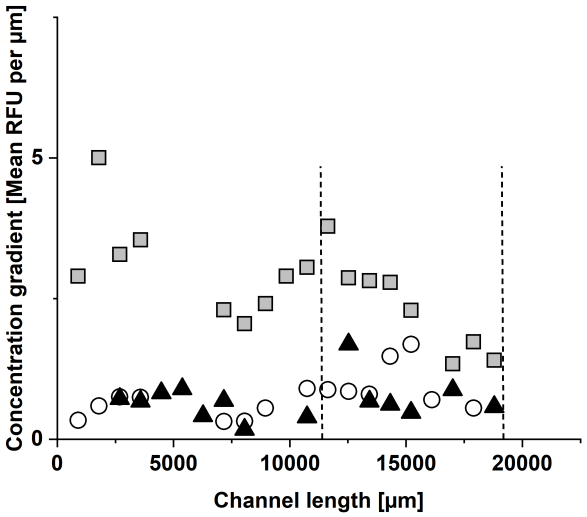

Figure 6.17.: Stability analysis of the CXCL8-S72C-fluorescein concentration gradient. The microfluidic channel was coated by rotating incubation with 1 mg/mL dopamine and 0.1 mg/mL heparin. The channel was rinsed from the inlet channels with loading buffer for 20 min at a flow rate of 0.8 µL/min. The top inlet channel was then rinsed with 8 µM CXCL8-S72C-fluorescein in loading buffer, while the middle and lower inlet channel were rinsed with loading buffer for 240 min at a flow rate of 0.8 µL/min. Non-bound chemokine was removed by a manual washing step. The gradient was incubated at 37 °C and 5 % CO_2 in the dark for 20 h and additional 23 h (43 h in total). Images of the channel (900 µm-sections) were taken under the fluorescence microscope ($\lambda_{Ex.}$ = 450-490 nm and $\lambda_{Em.}$ = 500-550 nm) with 10x magnification at an exposure time of 1145 ms. The mean relative fluorescence intensity of each channel section was analyzed. Analysis was performed before (grey squares), 20 h (empty dots) and 43 h (black triangles) after incubation. The dashed lines show the second half of the channel that was used for analysis of the gradient. Outliers were eliminated.

6.3.3. Overlay of 10 µM soluble CXCL8

As chemokine concentration gradients are naturally present as a mixture of both, immobilized and soluble gradients [159], the change of the reversibly immobilized concentration gradient by an overlay with soluble chemokine is of interest. For this purpose, a reversibly immobilized chemokine concentration gradient was formed in the dopamine-heparin-coated device and non-bound chemokine was removed after immobilization. Next, a 10 µM CXCL8-S72C-fluorescein solution was added to the channel and after a resting incubation at 37 °C and 5 % CO_2 in the dark, non-bound chemokine was removed by a washing step after different time points. One channel was used for each analysis time point. The used setup is shown in figure 6.18. A concentration of 10 µM of soluble CXCL8-S72C-fluorescein was used, as cell migration experiments showed a delayed cell migration after addition of 10 µM of soluble CXCL8.[120] The change of the concentration gradient across the channel width was exemplarily analyzed for channel section 11 and channel section 21 in the range of 201 µm to 401 µm across the channel width in y-direction, where the linear part of the concentration profile was located.

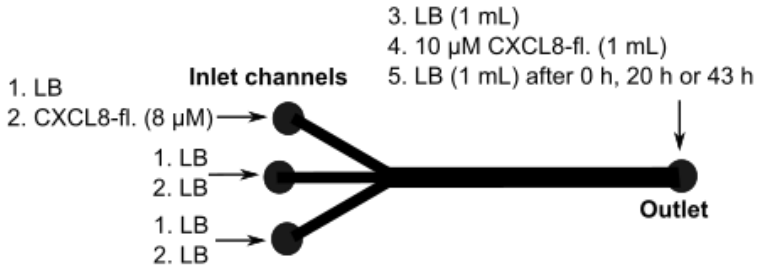

Figure 6.18.: Setup used for the overlay with 10 µM CXCL8. In the first step the channel was rinsed from the inlet channels with loading buffer (LB) with 0.8 µL/min for 20 min. In the second step the channel was rinsed from the top inlet channel with 8 µM CXCL8-S72C-fluorescein (CXCL8-fl.) in loading buffer and from the middle and bottom inlet channel with loading buffer with 0.8 µL/min for 240 min. The channel was then manually washed with 1 mL of loading buffer from the outlet to remove non-bound chemokine. In the fourth step, 1 mL of 10 µM CXCL8-S72C-fluorescein (CXCL8-fl.) in loading buffer were added to the channel from the outlet. After incubation at 37 °C and 5 % CO_2 in the dark, the channel was then manually washed with 1 mL of loading buffer from the outlet after different time points to remove non-bound chemokine. One channel was used for each time point.

As displayed in figure 6.19, channel sections 11 and 21 showed similar values for the mean relative fluorescence intensities before and directly after addition of the soluble, fluorescently labeled chemokine. After 20 h of incubation with an overlay of 10 µM soluble chemokine, the relative mean fluorescence intensities had increased about 189-231 % for channel section 11 and 403-613 % for channel section 21. As CXCL8 has a dissociation constant of 0.1 - 16 µM for dimerization, the soluble chemokine with a concentration in the same order of magnitude as the initial concentration used for gradient formation is predominantly present as a dimer.[160] The soluble chemokine might interact with the equilibrium between soluble and heparin-bound chemokine of the reversibly immobilized chemokine concentration gradient. First, soluble chemokine that is predominantly present as a dimer should occupy free binding sites and already bound chemokine should bind free monomers by dimerization [85], leading to increased mean relative fluorescence intensities after 20 h of incubation.[120] After 43 h of incubation, the relative mean fluorescence intensities decreased around 17-27 % for channel section 11 and 15-43 % for channel section 21 compared to 20 h of incubation, but still remained higher than directly after addition of the soluble chemokine. The decrease of the relative mean fluorescence intensities after 43 h of incubation compared to 20 h of incubation might be explained by the reversible bonding of the gradient, as more chemokines detach from the surface during incubation time.

In terms of the slope of the linear concentration profile, both channel sections showed similar values before addition of the 10 µM soluble chemokine solution (0.069±0.002 RFU/µm (section 11) and 0.079±0.001 RFU/µm (section 21)). The slopes of the concentration profiles in both channel sections only slightly changed after addition of a 10 µM CXCL8-S72C-fluorescein solution (0.060±0.001 RFU/µm (section 11) and 0.053±0.001 RFU/µm (section 21)). Similar to the relative mean fluorescence intensities, the slopes of the concentration profiles increased after 20 h of incubation (0.351±0.003 RFU/µm (section 11) and 0.306±0.007 RFU/µm (section 21)) in both sections. This result shows that the overlaid CXCL8 has an influence on both, the mean relative fluorescence intensity as well as the slope of the concentration profile. The steepening of the concentration gradients in both channel sections after 20 h of incubation might be attributed to the dimerization of CXCL8, as soluble CXCL8 is predominantly present as a dimer at a concentration of 10 µM.[160] Since CXCL8 dimers bind with

higher affinity to GAGs than CXCL8 monomers, it is likely that CXCL8 dimers preferentially exist in the surface-bound form, while monomers rather exist in the soluble form.[161] The binding of free monomers from solution by surface-bound CXCL8 would lead to an equilibrium shift, so that dimers in solution dissociate in compensation and even more monomers are able to bind to surface-bound CXCL8. Consequently, an increased recruitment of soluble CXCL8 to the surface where already a high amount of CXCL8 has reversibly bound, would take place.[120] For channel section 11, the slope of the concentration profile further increased from 20 h to 43 h of incubation (0.494±0.010 RFU/µm), while for channel section 21 the slope decreased from 20 h to 43 h of incubation (0.209±0.010 RFU/µm).

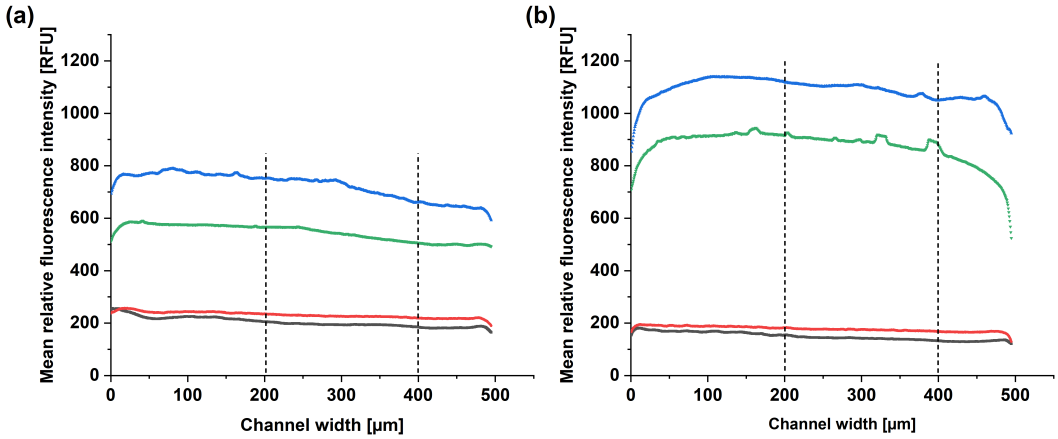

Figure 6.19.: Analysis of the overlay of 10 µM soluble CXCL8-S72C-fluorescein after gradient establishment in channel section 11 and 21. The microfluidic channel was coated with dopamine-heparin. The gradient was formed with 8 µM of CXCL8-S72C-fluorescein in loading buffer at a flow rate of 0.8 µL/min over 240 min. After gradient formation, 10 µM of soluble CXCL8-S72C-fluorescein in loading buffer was added to the channel. The channel was rinsed from the outlet before addition (grey) of the soluble chemokine as well as 0 h (red), 20 h (blue) and 43 h (green) after incubation at 37 °C and 5 % CO_2 in the dark. Images of the channel (900 µm-sections) were taken under the fluorescence microscope ($\lambda_{Ex.}$= 450-490 nm and $\lambda_{Em.}$= 500-550 nm) with 10x magnification at an exposure time of 100 ms. The mean relative fluorescence intensity as well as the slope of the mean relative fluorescence intensities across the channel width from 201 to 401 µm in y-direction were analyzed. Dashed lines show the analyzed linear region.(a) Channel section 11. (b) Channel section 21.

6.3.4. Reproducibility of THP-1 cell migration

Since the cell migration had only been analyzed once in a previous work in our group, the reproducibility of THP-1 cell migration in the microfluidic setup was tested. THP-1 cells naturally express the CXCL8 receptors CXCR1 and CXCR2 [162] and have been used in previous studies in our group for migration experiments with CXCL8.[130, 134] For this purpose, the migration experiment was repeated twice. Since the rear sections of the microfluidic channel were characterized by a shallow concentration gradient with small differences between adjoining sections, channel sections 15 to 21 were used for the analysis of cell migration.[120] Migration studies were performed with THP-1 cells incubated in the microfluidic device with an reversibly immobilized CXCL8 wildtype-gradient over 43 h. Graham *et al.* proposed

that the interaction of chemokines with glycosaminoglycans is based on a chemokine cloud model, in which soluble and reversibly bound chemokines are present.[163] This implies that the migration of THP-1 cells along the reversibly immobilized chemokine gradient is composed of both, chemotaxis and haptotaxis. The microscopic images of channel section 18 are exemplarily shown in figure A.4. In both experiments, THP-1 cells were evenly distributed along the channel width before incubation (0 h). After 20 h of incubation, a few cells aligned at the upper wall of the microfluidic device, where the highest concentration of CXCL8 was present. Further incubation led to even more cells aligning at the upper wall of the microfluidic channel (43 h). As CXCL8 is a chemoattractant, the migration of the THP-1 cells along the channel width towards the highest chemokine concentration meets the expectations.

The relative cell number in both channel halves was calculated for both experiments for each time point from channel section 15 to channel section 21. The result is shown in figure 6.20. In both experiments, the mean relative cell number in the lower channel half significantly decreased from 0 h to 43 h of incubation according to a Friedman-ANOVA at $p = 0.05$ (mean first/second experiment: 57 %/59 % (0 h), 42 %/71 % (20 h) and 29 %/15 % (43 h)). In the upper half of the channel, the mean relative number of cells was significantly higher after 43 h of incubation compared to 0 h of incubation (mean first/second experiment: 42 %/ 39 % (0 h), 56 %/28 % (20 h) and 69 %/85 % (43 h)). These results of both independently performed experiments show that the recognition of the chemokine concentration gradient by the THP-1 cells and resulting cell migration towards higher CXCL8 concentrations can be reproducibly verified.

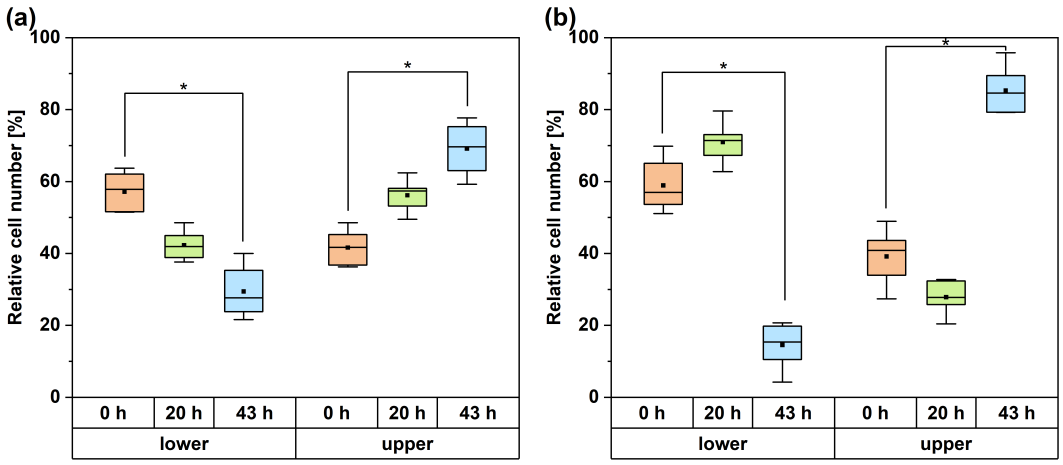

Figure 6.20.: Relative number of THP-1 cells in the upper and lower channel half of channel sections 15 to 21 before incubation (0 h), after 20 h of incubation and after 43 h of incubation at 37 °C and 5 % CO_2. Channels were coated by rotating incubation with dopamine and heparin. The gradient was formed with 8 µM of CXCL8 at a flow rate of 0.8 µL/min for 240 min. After gradient formation, the channel was rinsed from the outlet with loading buffer and $3x10^6$ THP-1 cells were flushed into the channel from the outlet. Images of the channel (900 µm-sections) were taken under the fluorescence microscope with 10x magnification in phase contrast. Statistical analysis was performed by Friedman-ANOVA and significance at $p \leq 0.05$ is indicated as black asterisk *(n = 7)*. (a) First experiment. (b) Second experiment.

After verifying the migration of THP-1 cells along the reversibly immobilized chemokine concentration

gradient, control experiments with microfluidic channels containing only loading buffer or only homogeneously distributed CXCL8 in solution were performed. As shown in figure A.5 (a) and figure 6.21 (a), the relative number of THP-1 cells in a dopamine-heparin-coated channel only filled with buffer did not change during 43 h of incubation in the upper or lower half of the channel (mean upper/lower channel half: 49 %/49 % (0 h), 49 %/48 % (20 h) and 49 %/48 % (43 h)). A similar result was obtained for THP-1 cells that were incubated in the dopamine-heparin-coated channel only filled with homogeneously distributed CXCL8 in solution (see figure A.5 (b) and figure 6.21 (b)), as the relative cell number in both channel halves did not change during incubation (mean upper/lower channel half: 55 %/44 % (0 h), 55 %/44 % (20 h) and 58 %/41 % (43 h)). Interestingly, higher standard deviations were visible for the control with homogeneously distributed CXCL8 in solution than for the control with buffer. This might be explained by an activation of the receptors after CXCL8 stimulation, leading to the random movement of cells as no chemoattractant gradient is present (chemokinesis).[164] Small inhomogeneities then might lead to a clustering of cells, resulting in larger standard deviations.

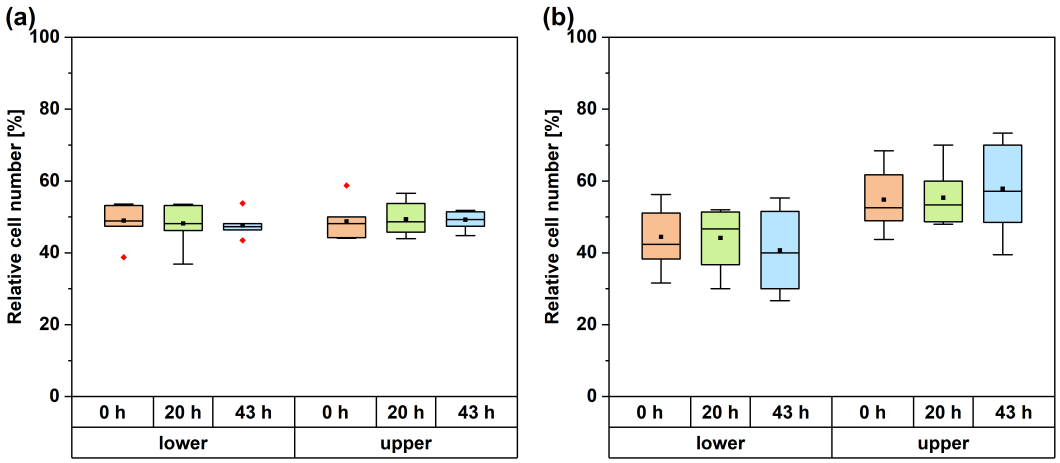

Figure 6.21.: Relative number of THP-1 cells in the upper and lower channel half of channel sections 15 to 21 before incubation (0 h), after 20 h of incubation and after 43 h of incubation at 37 °C and 5 % CO_2. Channels were coated by rotating incubation with dopamine and heparin. Loading buffer or 8 µM CXCL8 without gradient formation was flushed into the channel at a flow rate of 0.8 µL/min for 240 min. The channel was rinsed from the outlet with loading buffer and $3x10^6$ THP-1 cells were flushed into the channel from the outlet. Images of the channel (900 µm-sections) were taken under the fluorescence microscope with 10x magnification in phase contrast. Statistical analysis was performed by Friedman-ANOVA at p = 0.05 *(n = 7)*. (a) Only loading buffer. (b) Only 8 µM CXCL8 in loading buffer without gradient.

6.3.5. THP-1 cell migration: Overlay experiments with soluble CXCL8

Chemokine concentration gradients are naturally present as a mixture of both, immobilized and soluble gradients [159]. Since overlay experiments showed that the reversibly immobilized chemokine gradient is altered by the addition of soluble chemokine, the effect of the additional soluble chemokine on the migration of THP-1 cells was examined. For this purpose, soluble chemokine was added to the cell suspension immediately before infusing the cells into the microfluidic channel, which contained the

reversibly immobilized gradient. The experiment was performed with a concentration of the soluble chemokine significantly smaller (10 nM) or in the same order of magnitude (10 µM) as the initial concentration of CXCL8 used for gradient formation. For the overlay with 10 nM of soluble CXCL8 (see figure A.6 (a) and figure 6.22 (a)), THP-1 cells migrated from the lower half to the upper half of the channel within the first 20 h of incubation, followed by further cell migration within additional 23 h of incubation. Consequently, the mean relative cell number significantly decreased in the lower half of the channel between 0 h and 43 h of incubation and significantly increased in the upper half of the channel in the same time (mean upper/lower channel half: 50 %/48 % (0 h), 75 %/24 % (20 h) and 84 %/16 % (43 h)). In contrast, upon overlay with 10 µM of soluble CXCL8 (see figure A.6 (b) and figure 6.22 (b)), no cell migration was seen over the first 20 h of incubation. The mean relative number of THP-1 cells only changed after 43 h of incubation and significantly differed before and after 43 h of incubation in both channel halves (mean upper/lower channel half: 41 %/58 % (0 h), 44 %/54 % (20 h), 79 %/21 % (43 h)). Furthermore, the mean relative cell number significantly differed between 20 h and 43 h of incubation in the upper channel half. These results can be explained by the concentration difference between the added, soluble CXCL8 and the concentration of CXCL8 used for gradient immobilization. Since the 10 nM of soluble CXCL8 lie under the concentration of CXCL8 used for gradient immobilization (8 µM), the amount of immobilized chemokine should not significantly change after addition of the soluble chemokine. It follows that an overlay with the soluble chemokine across the channel width should not have any additional effect on the migration of the THP-1 cells. Consequently, the THP-1 cells showed cell migration within the first 20 h of incubation towards higher chemokine concentrations, comparable to the experiments with an CXCL8 gradient without an additional overlay of soluble chemokine. If 10 µM of soluble CXCL8 are added to the cells before incubation, soluble CXCL8 in the same order of magnitude as initial CXCL8 used for gradient formation might interfere with the equilibrium between soluble and heparin-bound chemokine, resulting in binding to free sites and an interference with the directed THP-1 migration. This implies that the cells are not able to directly sense the concentration gradient anymore and stimulation of the cells without a chemoattractant gradient leads to chemokinesis.[164] If the chemokine binds to the surface or is internalized and degraded by the cells, the concentration in solution decreases and the immobilized gradient with an altered slope prevails, leading to a retarded THP-1 migration. Consequently, the retarded cell migration after 43 h instead of 20 h is consistent with the previous result that the concentration profile of the reversibly immobilized CXCL8 gradient is altered by the addition of 10 µM, soluble CXCL8. In summary, it can be assumed that with soluble chemokine concentrations significantly lower than the initial concentration used for gradient formation, the immobilized gradient dominates and probably also the gradient of the dissociated chemokine. In contrast, at soluble chemokine concentrations in the same order of magnitude as the initial concentration used for gradient formation, the homogeneously distributed soluble chemokine dominates.

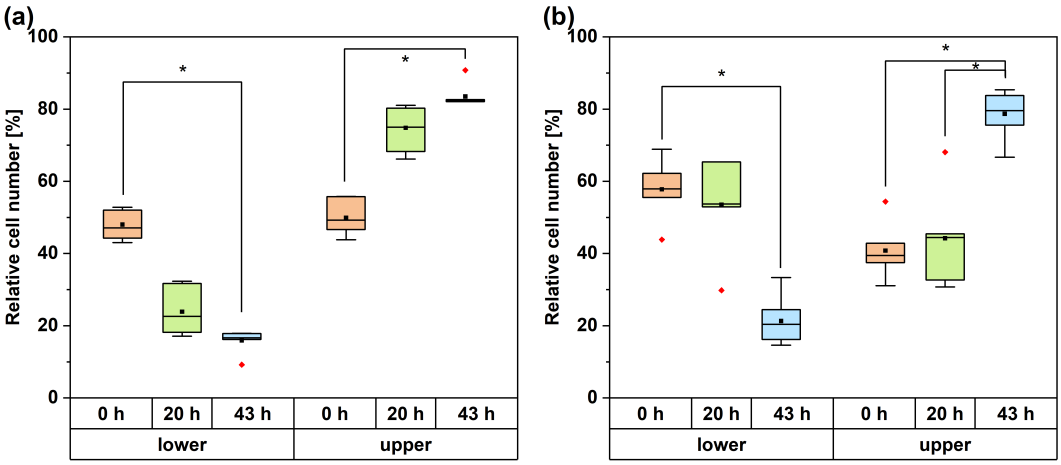

Figure 6.22.: Relative number of THP-1 cells in the upper and lower channel half of channel sections 15 to 21 before incubation (0 h), after 20 h of incubation and after 43 h of incubation at 37 °C and 5 % CO_2. Channels were coated by rotating incubation with dopamine and heparin. The gradient was formed with 8 µM of CXCL8 at a flow rate of 0.8 µL/min for 240 min. After gradient formation, the channel was rinsed from the outlet with loading buffer and $3x10^6$ THP-1 cells were flushed into the channel from the outlet. The cell suspension was supplemented with 10 nM or 10 µM of soluble CXCL8 directly before flushing the cells into the channel. Images of the channel (900 µm-sections) were taken under the fluorescence microscope with 10x magnification in phase contrast. Statistical analysis was performed by Friedman-ANOVA and significance at $p \leq 0.05$ is indicated as black asterisk *(n = 7)*. (a) Overlay with 10 nM chemokine. (b) Overlay with 10 µM chemokine.

In summary, the further characterization of the reversibly immobilized CXCL8 gradient showed that the coating of the PDMS-microfluidic channel with dopamine and heparin by rotating incubation not only enabled a natural environment for cell migration [92], it also allowed a more even distribution of CXCL8 within the channel compared to an non-coated device. Stability analysis showed a decrease of the steepness of the reversibly immobilized gradient about 50 % within incubation at 37 °C that equals the previous result of the stability analysis at RT.[120] Furthermore, overlay experiments showed that the reversibly immobilized chemokine gradient is altered by the addition of soluble chemokine. Cell migration experiments verified that THP-1 cells recognized the reversibly immobilized CXCL8 gradient and migrated along the gradient towards higher chemokine concentrations. Cell migration was reproducible and did not occur only in the presence of buffer or homogeneously distributed chemokine. By an overlay with soluble chemokine solution that is in the same order of magnitude as the initial chemokine solution used for gradient formation, the cell migration was retarded due to the interaction of the additional CXCL8 with the gradient.

6.4. Covalent immobilization of CXCL8 in microfluidic devices by RGX

Although the overlay of soluble and immobilized chemokine gradients corresponds to the natural conditions [70, 72], the interpretation of overlay experiments is difficult because chemokines can dissociate from the surface. Therefore, the immobilized gradient must be stable in order to vary the concentration of the chemokine in solution in a defined way. Schwarz *et al.* were able to generate immobilized chemokine gradients in microfluidic devices by LAPAP, using fluorescently labeled CCL21.[119] Compared to LAPAP, RGX would represent a simple method to immobilize native chemokines on collagen without modification. The covalent immobilization of native chemokines on collagen-coated surfaces is of interest since collagen, as a part of the ECM, supports cell migration.[165] For this reason, the RGX method used in the first part of this work should be used for the immobilization of CXCL8 gradients.

In order to covalently immobilize CXCL8 by RGX in collagen-coated microfluidic devices, collagen coating methods, CXCL8 detection methods and parameters for RGX were varied. The immobilization procedure was first carried out by manually rinsing the channel and later on by using syringe pumps to rinse the channel with constant flow rates. Overviews of the varied parameters for the setup are displayed in table 6.1 for manual rinsing and table 6.2 for the use of syringe pumps.

Table 6.1.: Overview of different parameters that were varied from setup to setup for manually rinsed collagen-coated channels. In setup 1 and 2 PBS (pH 7.4) was used for preparation of the RB solution. In setup 3 and 4 Microfluidic PBS (pH 7.4) was used for preparation of the RB solution. All channels were coated with oxygen plasma-collagen over their full length and totally exposed to green light after addition of the chemokine.

Setup	Collagen	Chemokine	Washing	Detection
1	200 µg/mL in 0.1 M $NaHCO_3$	8 µM CXCL8 in 0.01 % (w/v) RB (1 mL)	0.4 % (w/v) skim milk powder in PBS (pH 7.4, 1 mL)	Fluorescently labeled anti-CXCL8
2	200 µg/mL in 0.1 M $NaHCO_3$	8 µM CXCL8 in 0.1 % (w/v) RB (1 mL)	0.4 % (w/v) skim milk powder in PBS (pH 7.4, 1 mL)	Fluorescently labeled anti-CXCL8
3	25 µg/cm^2 or 50 µg/cm^2 in 0.1 M $NaHCO_3$	8 µM CXCL8-fluorescein in 0.1 % (w/v) RB (0.3 mL)	Microfluidic PBS (pH 7.4, 0.9 mL)	Fluorescently labeled CXCL8
4	25 µg/cm^2, 50 µg/cm^2 or 100 µg/cm^2 in 17.5 mM acetic acid	8 µM CXCL8-fluorescein in 0.1 % (w/v) RB (0.3 mL)	Microfluidic PBS (pH 7.4, 0.9 mL)	Fluorescently labeled CXCL8

In the first setup the chosen parameters were based on the optimized parameters to reversibly immobilize CXCL8 and to modify collagen samples with RGX. The channel was coated with 200 µg/mL collagen in 0.1 M $NaHCO_3$ solution and the immobilization procedure was carried out with CXCL8 in 0.01 % (w/v) RB-PBS (pH 7.4, see table 5.1). 0.4 % (w/v) skim milk powder in PBS (pH 7.4) was used for the washing step after exposure. The detection of immobilized CXCL8 was performed by staining with a fluorescently labeled CXCL8-antibody. The channels did not show any difference in

their fluorescence intensity compared to control channels, e.g. samples only containing RB or samples without exposure to green light (data not shown).

Since the concentration of RB might be too low for the immobilization of CXCL8 by RGX, the procedure was repeated with the modification that the concentration of RB was increased from 0.01 % (w/v) to 0.1 % (w/v) in the second setup. Even though the concentration of RB was increased, immobilization of CXCL8 could not be detected (data not shown).

As the first two setups did not enable a covalent immobilization of CXCL8 on collagen-coated microfluidic devices by RGX, different parameters were varied. As the detection with fluorescently labeled chemokine is faster than with fluorescently labeled anti-CXCL8, fluorescently labeled CXCL8 was used in further experiments. Furthermore, different concentrations of collagen in combination with different solvents were used. Since $NaHCO_3$ solution has already been used for the collagen coating of PDMS [114] and acetic acid has been described for a homogeneous collagen coating [166] on PDMS substrates in literature, both solvents were tested. In detail, the channel was coated with 25-100 µg/cm^2 collagen in 0.1 M $NaHCO_3$ solution or in 17.5 mM acetic acid (setup 3 and 4). The immobilization procedure was carried out with CXCL8-S72C-fluorescein in 0.1 % (w/v) RB-PBS solution (Microfluidic PBS pH 7.4, see table 5.1). Since the absorption spectrum of fluorescein ($\lambda_{max.}$ = 485 nm [167]) and the spectrum of the LED ($\lambda_{max.}$ =569 nm [126]) overlap in the range of approximately 475 nm to 500 nm, fluorescein might be excited during exposure with green light. To prevent the excitation of fluorescein, the channel was covered with a Y52 filter (Hoya K.K., Tokyo, Japan) that has a shortwave edge at 520 nm.[168] Microfluidic PBS (pH 7.4) was used for the washing step after exposure. Only the channel coated with 25 µg/cm^2 of collagen in 17.5 mM acetic acid showed a higher fluorescence intensity after exposure of the chemokine solution in the channel compared to the control sample with fluorescein exposed in the collagen-coated channel (see figure 6.23). At this collagen concentration, the mean relative fluorescence intensity ranged from 1547 RFU to 1754 RFU for the fluorescein control and from 1730 RFU to 2911 RFU for the chemokine sample. Interestingly, standard deviations were larger for the chemokine sample (160 - 557 RFU) than for the fluorescein control (70 - 172 RFU).

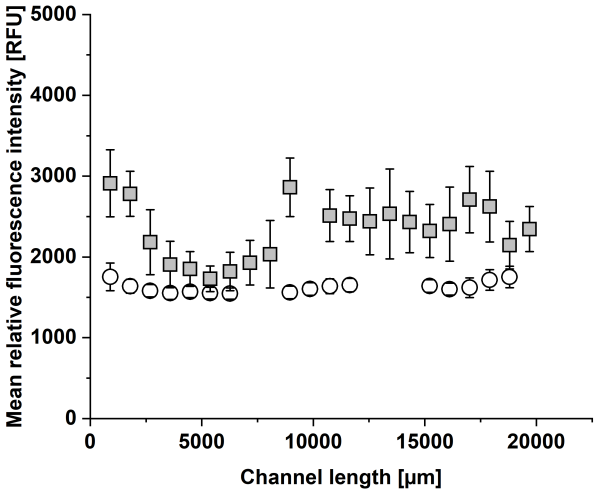

Figure 6.23.: Immobilization of fluorescently labeled CXCL8 and fluorescein in a microfluidic channel coated with 25 µg/cm^2 collagen. The microfluidic channel was rinsed from the outlet with 8 µM of CXCL8-S72C-fluorescein in 0.1 % (w/v) RB (grey squares) or 8 µM fluorescein in 0.1 % RB (control, white dots) and exposed to green light for 10 min. Microfluidic PBS (pH 7.4) was used to prepare the RB solutions. The channel was rinsed with Microfluidic PBS (pH 7.4) to remove non-bound chemokine/fluorophore. Images of the channel (900 µm-sections) were taken under the fluorescence microscope ($\lambda_{Ex.}$ = 450-490 nm and $\lambda_{Em.}$ = 500-550 nm) with 10x magnification at an exposure time of 2.56 s. The mean relative fluorescence intensity of each channel section was analyzed. Outliers were eliminated.

Based on the result that the fluorescently labeled chemokine exposed in the channel coated with 25 µg/cm^2 collagen in 17.5 mM acetic acid showed a higher fluorescence intensity than the control, the method for covalent immobilization was further developed. To prevent variations due to variable flow rates during manual flushing, the latter was replaced by rinsing the channel with syringe pumps. Furthermore, only half of the channel was exposed to green light to directly compare the exposed with the non-exposed area in the same channel. The non-exposed area was covered with black cardboard during exposure.

Table 6.2.: Overview of different parameters that were varied from setup to setup for collagen-coated channels rinsed with syringe pumps. All channels were rinsed for 5 min with 0.8 µL/min from the outlet with chemokine-RB-solution. The RB solution was prepared with Microfluidic PBS (pH 7.4). Only the second half of each channel was exposed to green light. The washing step was carried out from the outlet with 0.8 µL/min.

Setup	Collagen	Chemokine	Washing	Detection
5	2.5-55 µg/cm^2 in 17.5 mM acetic acid	8 µM CXCL8-fluorescein in 0.1 % (w/v) RB	Microfluidic PBS (pH 7.4, 5 min)	Fluorescently labeled CXCL8
6	20 µg/cm^2 in 17.5 mM acetic acid	8 µM CXCL8-fluorescein in 0.1 % (w/v) RB	Microfluidic PBS (pH 7.4, 30 min)	Fluorescently labeled CXCL8
7	20 µg/cm^2 in 17.5 mM acetic acid + APTES	8 µM CXCL8-fluorescein in 0.1 % (w/v) RB	Microfluidic PBS (pH 7.4, 30 min)	Fluorescently labeled CXCL8

In the fifth setup the channel was coated with 2.5-55 µg/cm^2 collagen in 17.5 mM acetic acid to check whether the result of the fourth setup was reproducible when syringe pumps were used. Furthermore, it should be tested if concentrations above or below 25 µg/cm^2 of collagen might lead to similar results. For this purpose, the channel was rinsed from the outlet with 0.8 µL/min of fluorescently labeled chemokine or fluorescein in 0.1 % (w/v) RB-PBS (Microfluidic PBS pH 7.4, see table 5.1) for 5 min. Only the second half of each channel was covered with a Y52 filter and exposed to green light to enable a comparison with the non-exposed, first half of the channel that was covered with black cardboard. Removal of non-bound fluorophore/chemokine was carried out with 0.8 µL/min of Microfluidic PBS (pH 7.4, see table 5.1) for 5 min. The result of two samples is exemplarily shown in figure 6.24 (a). For the favored concentration of 25 µg/cm^2 collagen, the fluorescein control and the fluorescently labeled CXCL8 showed equal fluorescence intensities in the channel sections that were exposed or not exposed to green light. For the fluorescein control, this result meets the expectations as fluorescein should not be immobilized by RGX and therefore show similar fluorescence intensities in both areas. However, the chemokine sample should have a higher fluorescence intensity in the area of exposure if the immobilization by RGX was successful. The similar fluorescence intensities of exposed chemokine and exposed fluorescein indicate that fluorescently labeled CXCL8 was not immobilized by RGX in the channel coated with 25 µg/cm^2. Interestingly, of all tested concentrations, only for the sample coated with 20 µg/cm^2 collagen, the mean fluorescence intensity of the chemokine sample was slightly higher in the RGX-treated area than in the non-treated area. Furthermore, the RGX-treated area of the chemokine sample (181±13 RFU) showed a higher fluorescence intensity than the RGX-treated area of the fluorescein control (123±11 RFU). These findings suggest that CXCL8-fluorescein might be immobilized in the channel coated with 20 µg/cm^2 collagen by RGX.

As the RGX-treated and non-treated area for the chemokine sample with 20 µg/cm^2 collagen only differed from each other by about 16 RFU and rinsing with buffer was only carried out for 5 min, the experiment was repeated in setup six with an extended time for washing. This might remove more non-covalently bound chemokine and therefore increase the difference between the RGX-treated and non-treated area in the collagen-coated channel. For this purpose the channel was coated with collagen and loaded with chemokine/RB as described in setup 5. As before, only the second half of each channel was covered with a Y52 filter and exposed to green light to enable a comparison with

the non-exposed, first half of the channel. Removal of non-bound chemokine was carried out with 0.8 µL/min of Microfluidic PBS (pH 7.4) for 30 min. Evaluation of the fluorescence intensity (see figure 6.24 (b)) showed that the RGX-treated area of the channel with fluorescently labeled chemokine did not show any increased mean fluorescence intensity compared to the non-exposed area. Thus, an immobilization of CXCL8-S72C-fluorescein on a 20 µg/cm^2 coated collagen channel by RGX could not be confirmed and the earlier result is an outlier.

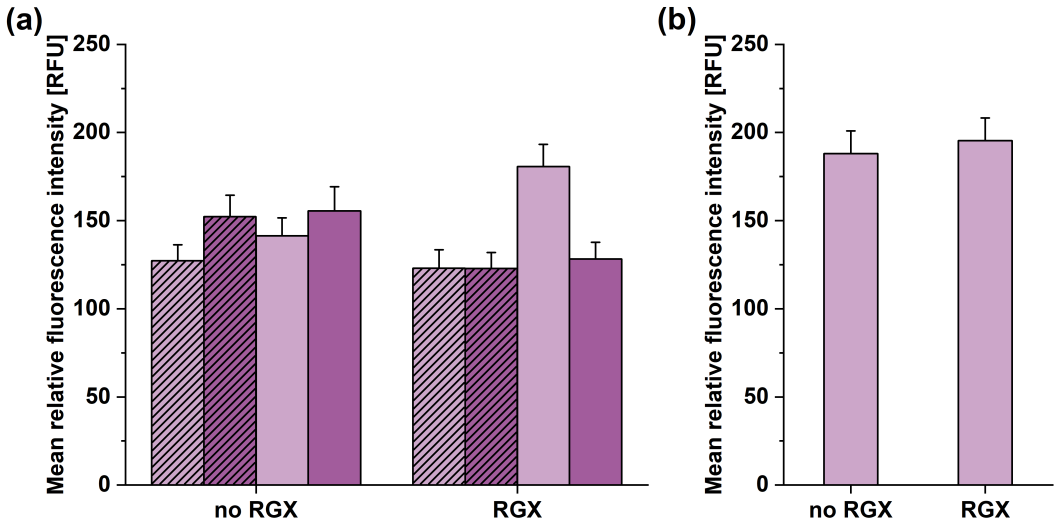

Figure 6.24.: Immobilization of CXCL8-S72C-fluorescein and fluorescein in a collagen-coated microfluidic channel. The channels were rinsed from the outlet with 8 µM of CXCL8-S72C-fluorescein or 8 µM fluorescein in 0.1 % (w/v) RB with 0.8 µL/min for 5 min. Microfluidic PBS (pH 7.4) was used to prepare the RB solutions. Half of each channel was covered with a Y52 filter and exposed to green light for 10 min and the other half was covered with black cardboard. The channels were rinsed with Microfluidic PBS (pH 7.4) with 0.8 µL/min to remove non-bound chemokine/fluorophore (5 min (a) or 30 min (b)). Images of the channel (900 µm-sections) in the exposed and non-exposed region were taken under the fluorescence microscope ($\lambda_{Ex.}$ = 450-490 nm and $\lambda_{Em.}$ = 500-550 nm) with 10x magnification at an exposure time of 300 ms. (a) Mean relative fluorescence intensities of one channel section with RGX/without RGX of 20 µg/cm^2 collagen with fluorescein (light violet, dashed lines), 25 µg/cm^2 collagen with fluorescein (dark violet, dashed lines), 20 µg/cm^2 collagen with CXCL8-S72C-fluorescein (light violet) and 25 µg/cm^2 collagen with CXCL8-S72C-fluorescein (dark violet). (b) Mean relative fluorescence intensities of one channel section with RGX/without RGX of 20 µg/cm^2 collagen with CXCL8-S72C-fluorescein.

One possible reason for the non-detectable immobilization could be that the collagen layer was not stable over the many loading and washing steps. Therefore, setup six was modified. Following plasma treatment, the channel was treated with APTES to obtain a SAM with amino groups (see table 6.2). According to Siddique *et al.* the linkage of APTES between the PDMS and collagen increased the stability of the collagen coating[114] and therefore might contribute to a better immobilization of CXCL8 by RGX. The results obtained with setup seven did not show any difference between the RGX-treated and non-treated area of the APTES-collagen-coated channel (data not shown). Even after stabilization of the collagen layer by APTES, no immobilization of CXCL8 by RGX was detected.

In literature, studies reported that tryptophan, tyrosine, histidine and lysin undergo cross-linking by RGX.[169–172] Since the sequence of CXCL8 only contains a single tyrosine, a single tryptophan, two histidines and nine lysins, the photo-cross-linking between collagen molecules might be more likely than the cross-linking of CXCL8 with collagen. With the assumption that a native protein larger than CXCL8, containing a greater proportion of activatable amino acids that can be reached by activated RB, might be more suitable for an immobilization by RGX on collagen, setup seven was repeated with 8 µM of fluorescently labeled BSA. Similar to the experiment with setup seven with fluorescently labeled CXCL8, the RGX-treated and non-treated area of the APTES-collagen-coated channel did not show any difference in the mean relative fluorescence intensity (data not shown).

As the underlying mechanism of RGX is based on the formation of radicals [52] in the proximity of the protein to be immobilized, the average spatial distance between the collagen coating and the dissolved CXCL8 might be too large for an immobilization reaction. Non-covalent bonds - even relatively non-specific ones - could increase the probability of a reaction with the light-activated species. Therefore, the interaction of RB with CXCL8 or BSA and the interaction of collagen with CXCL8 or BSA in solution was analyzed. As changes of fluorescence intensities or spectral properties can occur by binding of small molecules to proteins, fluorescence measurements are suitable to determine binding properties.[173]

To analyze the interaction of collagen with fluorescein-labeled BSA or CXCL8, the fluorescence intensities of serial dilutions of collagen supplemented with a constant concentration of fluorescently labeled protein were measured (see figure 6.25). For CXCL8-fluorescein (see figure 6.25 (a)) the data showed a change in fluorescence intensity with increasing collagen concentrations. As collagen was formulated in 0.02 M acetic acid, a control with 0.02 M acetic acid supplemented with CXCL8-fluorescein was included. The mean relative fluorescence intensity of the 0.02 M acetic acid control equaled that of the sample with the highest collagen concentration (0.02 M acetic acid: 76±2 RFU and 11.2 µM collagen: 73±3 RFU). Consequently, the increase of the fluorescence intensity from 11.2 µM collagen to 1.4 µM collagen might be attributed to the decreasing amount of acetic acid due to dilution of the stock solution and not to an interaction of collagen with fluorescently labeled CXCL8. A control experiment with a serial dilution of 0.02 M acetic acid supplemented with 125 nM of fluorescein confirmed this assumption (see figure A.7), as a decrease of the mean relative fluorescence intensity was observed for acetic acid concentrations higher than 1.25 mM. Likewise, fluorescently labeled BSA (see figure 6.25 (b)) did not show any change of the fluorescence intensity with increasing collagen concentration and the sample with the highest concentration of collagen reached an equal mean relative fluorescence intensity as the 0.02 M acetic acid control (0.02 M acetic acid: 23±1 RFU and 11.2 µM collagen: 24±1 RFU).

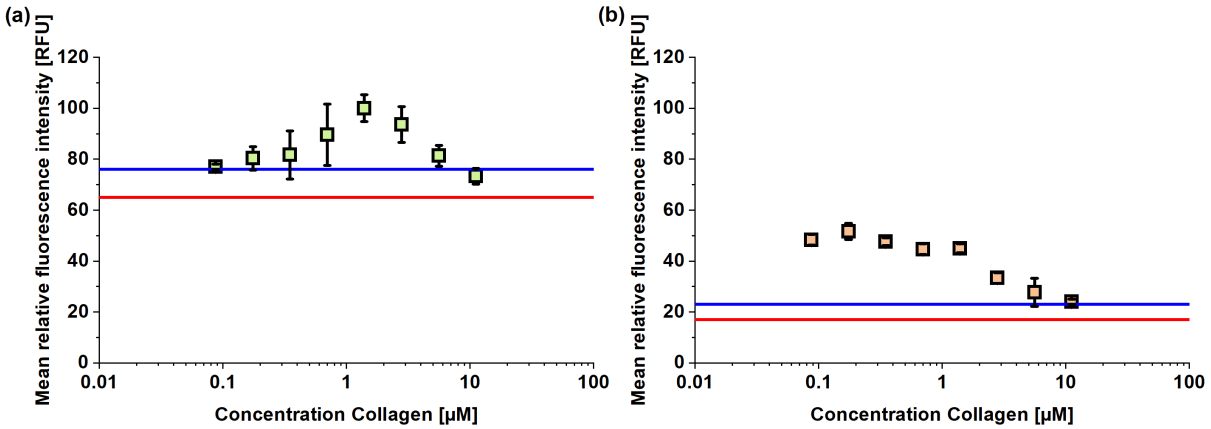

Figure 6.25.: Binding isotherms of proteins to be immobilized with collagen. Relative fluorescence intensities of fluorescently labeled proteins ($\lambda_{Ex.}$ = 470 nm and $\lambda_{Em.}$ = 525 nm) were measured. Error bars represent the standard deviation (*n = 3*). Controls are displayed as blue lines (0.02 M acetic acid) and red lines (only PBS). (a) Mean relative fluorescence intensity of CXCL8-S72C-fluorescein (39.3 nM) depending on the concentration of collagen (0-11.2 µM) at a gain of 120 after 80 min. (b) Mean relative fluorescence intensity of BSA-FITC (125 nM) depending on the concentration of collagen (0-11.2 µM) at a gain of 100 after 60 min.

For the interaction of native CXCL8 with RB (see figure 6.26 (a)) the data showed a slight increase of the mean relative fluorescence intensities from 3 µM (337±4 RFU) to 400 µM (615±8 RFU). As a CXCL8 concentration-dependent change of the mean relative fluorescence intensity would be expected for an interaction with RB, the data suggest very weak, non-specific interactions of CXCL8 with RB in the upper micromolar to millimolar range. For native BSA (see figure 6.26 (b)), the mean relative fluorescence intensities of RB increased with higher concentrations of BSA (350±26 RFU (0.2 µM) and 513±12 RFU (51 µM)). As described for native CXCL8, BSA might non-specifically interact with RB. The interaction can be found in the low micromolar range, which is also to be expected based on the non-specific binding properties of BSA.[174] However, if there are no activatable residues near the binding site or if the native protein with the activated site does not come close enough to the collagen, the binding of RB to the respective protein is not sufficient for an immobilization by RGX. This represents a difference from LAPAP, in which the fluorophore is already bound to the protein to be immobilized.[119] Moreover, the particular protein concentrations that indicated an interaction with RB were beyond the concentrations used in the above described microfluidic experiments. This makes an immobilization of CXCL8 by RGX rather unlikely and means that in the case of a gradient, immobilization could only occur in areas where very high concentrations of CXCL8 are present.

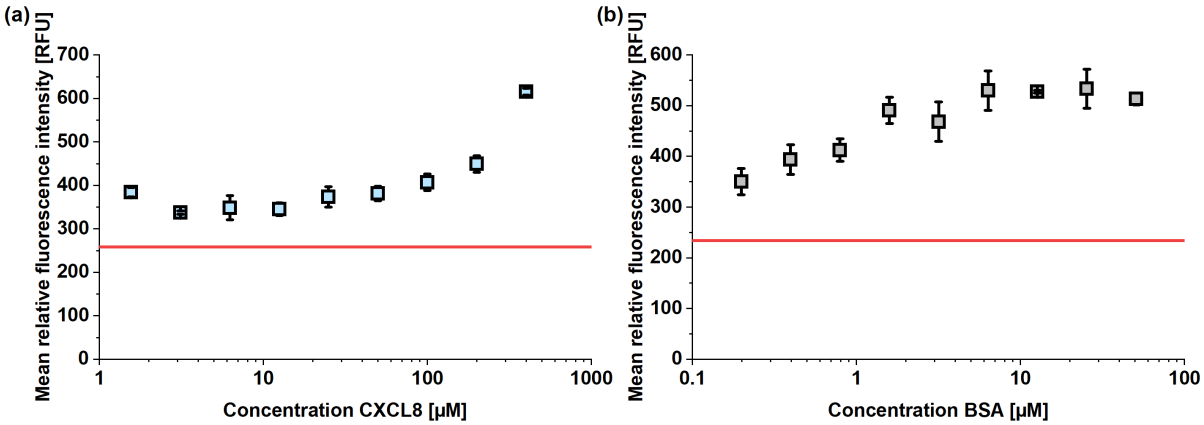

Figure 6.26.: Binding isotherms of proteins to be immobilized with RB. Relative fluorescence intensities of RB ($\lambda_{Ex.}$ = 530 nm and $\lambda_{Em.}$ = 571 nm) were measured. Error bars represent the standard deviation (*n = 3*). Controls are displayed as red lines (only PBS). (a) Mean relative fluorescence intensity of RB (100 nM) depending on the concentration of CXCL8 (0-400 µM) at a gain of 160 after 120 min. (b) Mean relative fluorescence intensity of RB (100 nM) depending on the concentration of BSA (0-51 µM) at a gain of 160 after 120 min.

In summary, under the tested conditions, covalent immobilization of CXCL8 on collagen was not possible. These findings agree with the results of the interaction studies as CXCL8 only showed weak, non-specific interactions with RB with concentrations that are outside the range of concentrations used for microfluidic experiments. In addition, no interaction of collagen with CXCL8 could be detected. Similarly, BSA as a larger model protein that is known for non-specific binding and binds RB could also not be immobilized by RGX on collagen.

7. Conclusions and outlook

7.1. Characterization of collagen laminates

The first aim of this work was the characterization of different collagen laminates in terms of their swelling behavior and release of vancomycin as a model antibiotic for the prevention of surgical site infections. Based on previous works, bi-layer and triple-layer collagen laminates composed of the collagen materials Atelocollagen and Collagen Solutions were bonded by RGX and analyzed. Homogeneous collagen laminates only composed of thick and sponge-like Atelocollagen showed a lower experimentally determined swelling degree than a single layer of RGX-modified Atelocollagen. This was explained by the additional rose bengal at the interface between the piled sheets. A comparison between theoretically and experimentally determined swelling degrees showed that for homogeneous Atelocollagen laminates, the experimental swelling degrees were significantly smaller than the theoretical ones. These results were explained by the differing number of available swelling interfaces considered by the theoretical (two interfaces for every sheeet) and experimental values (two interfaces for the entire laminate). In contrast, homogeneous laminates only composed of the thinner collagen material Collagen Solutions did not display any change of the experimentally determined swelling degree independent of the number of collagen layers. Furthermore, Collagen Solutions did not show any differences between experimental and theoretical swelling degrees. These results were explained by the compact structure of the material and the resulting low swelling degrees. The combination of both materials to heterogeneous laminates resulted in experimentally determined swelling degrees with values that lay between the homogeneous laminates made from either material, as expected. Since sponge-like Atelocollagen showed a relatively stronger swelling than Collagen Solutions, its behavior should dominate in the heterogeneous laminates. A comparison between theoretically and experimentally determined swelling degrees showed that for heterogeneous laminates, the experimental swelling degrees were significantly smaller than the theoretical ones. These results might be explained by the differing number of available swelling interfaces in laminates compared to individual sheets, as described above. The analysis of the swelling degrees of different laminates is necessary to determine the volume available for drug loading and the expected increase in volume inside the body. Consequently, swelling properties can be used for the loading of biomaterials with therapeutic substances.[175] In addition, the swelling properties of a hydrogel can also be used in orthopedics to relieve pressure on a weakened vertebrate disc so that it can be supported in its function.[176, 177] For example, the composition of collagen laminates could be adapted to stabilize the respective disc height.[176, 177] It follows, that the composition of multilayered collagen laminates can be adjusted to a given medical application. Collagen is commonly used for the controlled release of drugs to avoid antibiotic resistance or toxic effects by too high, local antibiotic concentrations. Laminates theoretically open up the possibility of promoting release through one of the two main surfaces by arranging the layers asymmetrically. In order to test, whether this idea is feasible and which material promotes release, a suitable sample holder is needed. Within this work, an additively manufactured sample holder that is compatible with a commercially available 24-well tissue plate was successfully developed to quantify the directed release of vancomycin from different collagen samples. Release experiments with a single sheet of RGX-modified Atelocollagen

showed that the total release was completed after 24 h. The positioning of the sample into the sample holder as well as the multiple sampling at different times had no effect on the total amount of released vancomycin. However, the sample holder elongated the time until half-maximal release was reached, due to the reduced size of the release areas compared to release from a free-floating sample of the same size. Under physiological conditions (pH 7.4, 37 °C), the direction and time of vancomycin release from heterogeneous, bi-layer collagen laminates depended on their structural properties, as vancomycin was always preferentially released at the side of the dense Collagen Solutions layer and loading the antibiotic into the sponge-like Atelocollagen increased the time until a half-maximal release was reached. As RGX-modified Atelocollagen and Collagen Solutions have different porosities and different swelling degrees, the compression in the sample holder and following re-swelling should have a stronger effect on the sponge-like Atelocollagen compared to the compact Collagen Solutions. The resulting larger fluid influx into the opposite direction of release during re-swelling should reduce the release at the surface of Atelocollagen. Furthermore, as Collagen Solutions is thinner and more compact than Atelocollagen, shorter diffusion paths would also explain the preferred release at the surface of Collagen Solutions. Heterogeneous, triple-layer collagen laminates showed an increased time of half-maximal release with an increasing number of thick Atelocollagen layers and vancomycin was again preferentially released at the side of the Collagen Solutions layer. In contrast to the heterogeneous, bi-layer laminates, the orientation of the triple-layer, heterogeneous laminate determined how large the proportion of vancomycin was that was released across the Collagen Solutions layer. This result can be attributed to the swelling of Atelocollagen at the bottom side of the laminate, leading to an increased release area that counteracts the faster release on the side of Collagen Solutions. Similarly, a triple-layer, homogeneous Atelocollagen laminate also showed an increased swelling and release at the bottom side that can be attributed to the thickness of the laminate, resulting in a force effect from top to down after fixing the sample in the sample holder. The effect of the sample holder is of practical relevance, as compressive forces can also occur in the body.[143] In addition to the strength of the surrounding tissue (bone versus muscle/skin) [143], the availability of fluid for swelling also plays a role. A lattice structure at the bottom side of each part of the sample holder might stabilize flexible biomaterials, allowing to tailor the sample holder to the conditions expected in a particular application and the properties of a given biomaterial, e.g. its swelling degree or flexibility. The fact that the side on which the antibiotic is preferentially released can be controlled by the design of the laminate makes collagen laminates an attractive tool for regenerative medicine. As vancomycin can impair the viability of cells that are involved in bone regeneration [4], vancomycin should be released to a lesser extent and more slowly in the direction of bone that can be controlled by the composition of the laminate.

As changes of the pH value can occur during wound healing or infections, the release of vancomycin from collagen samples at acidic (pH 5.5, 37 °C) and alkaline (pH 8.5, 37 °C) conditions should be examined in this work. The pH did not have any effect on the total amount of released vancomycin from single sheets of RGX-modified Atelocollagen or heterogeneous, bi-layer laminates. The time for half-maximal release was increased under acidic and alkaline conditions and, similar to previous results, vancomycin was preferentially released at the side of the Collagen Solutions layer in heterogeneous, bi-layer laminates. The elongated times for half-maximal release under acidic conditions were attributed to increasing swelling degrees of Atelocollagen compared to physiological conditions. At pH 5.5, Atelocollagen has a positive net charge that leads to a repulsion of positive electric charges and a stretching of the biopolymer fibers, resulting in an increased swelling degree. The longer diffusion paths and fluid influx in the opposite direction of release might elongate the release of vancomycin. Since Atelocollagen showed a significantly higher swelling than Collagen Solutions, the swelling of the sponge-like collagen should have a dominating effect. In contrast, swelling did not reach higher values

by increasing the pH to 8.5. As pH 8.5 lies around the isoelectric point of Atelocollagen, the net charge is low, leading to a lower swelling degree than at pH 5.5. Since swelling could not be accounted for the retarded vancomycin release at pH 8.5, the elongated times for half-maximal release at alkaline conditions were explained by electrostatic interactions between negatively charged vancomycin and remaining positively charged regions of collagen. These findings demonstrate that the swelling of collagen as well as the electrostatic interactions between the collagen and the antibiotic need to be considered for the biomedical application of laminates. As the swelling of sponge-like Atelocollagen is increased at pH 5.5 and leads to a delayed antibiotic release, Atelocollagen should not be used if signs of an infection are present and a fast antibiotic delivery is preferred. Instead, a more stable collagen with a lower swelling degree at pH 5.5 and a pI in the acidic range would be preferable. In contrast, Atelocollagen would be more suitable for a retarded release of growth factors that are essential for tissue regeneration.[156] Further studies might evaluate to which extent the release of vancomycin changes if the pH is varied over time with the intention of replicating the pH progression in certain healing processes. Future studies might also include the mathematical modeling of vancomycin release. The prediction of drug release based on mathematical models can improve the application accuracy and pharmacological safety.[178] A variety of models depending on different parameters, e.g. drug type and delivery geometry, exist.[178] Natural processes, such as diffusion and swelling, are included by mechanistic realistic mathematical theories.[178] One example for a mechanistic realistic mathematical theory that is based on polymer swelling for the determination of drug release is the Korsmeyer-Peppas model.[178] This model describes the time-dependent release of a drug, taking into account the simultaneous diffusion of the drug out of the system and the diffusion of water into the system, combined with the swelling of the polymer.[178] Based on the modeling data, instructions for physicians could be provided how which laminate composition affects the release. As metronidazole or cefuroxime belong to the most commonly used prophylactic antibiotics according to a study from 2022 [179], release studies with these antibiotics would also be of interest. In addition, the extent to which the release of various compounds is controlled only by diffusion and whether interaction with collagen play a role, could be examined. Besides antibiotics, the release of active substances that support wound healing, such as growth factors [156], should be examined. Examples for other commercially available collagen materials are the transparent collagen biomatrix RESODURA® or GENTA-COLL® *resorb*, a collagen sponge that is already loaded with the antibiotic gentamycin. Since various materials are commercially available and laminate production by RGX is relative simple, materials with different drug loadings could be combined as needed. In this case, it should be verified that the combination of materials does not result in undesirable properties, such as cell toxicity. Besides the release of active substances, the above mentioned materials should also be characterized in terms of mechanical stability, cell compatibility and biodegradability as the latter can also have an influence on the release of active substances.

7.2. Reversible immobilization of CXCL8 in microfluidic devices

Based on the result of a previous work, the aim of the second project was to further characterize a reversibly immobilized CXCL8 gradient in a microfluidic system and to perform different migration studies. The microfluidic system in combination with the coating for non-covalent chemokine capture allows a simultaneous work with different concentration profiles of soluble and immobilized chemokine. Systematic experiments indicated that the dopamine-heparin-coating not only allowed a reversible immobilization of CXCL8 from a homogeneous solution in a microfluidic channel, it also enabled a more homogeneous distribution of the chemokine in the microfluidic device. Furthermore, the results showed that the fluorescently labeled chemokine interacts with the PDMS surface. However, a coating

of PDMS is required to enhance cellular adhesion and provide a natural environment for cells. [92, 114, 124] Stability measurements at 37 °C showed a decrease of the steepness of the gradient about 50 % over time that equals the previous result of the stability analysis at RT. The decrease can be attributed to the dissociation of reversibly bound CXCL8 from heparin, resulting in a redistribution of the chemokine in the channel. The change of the gradient over time corresponds to natural conditions as chemokine concentration gradients naturally occur as mixture of soluble and immobilized gradients. For this purpose, the variation of the gradient by an overlay with soluble chemokine was analyzed in a further experiment. The results indicated that the overlay with soluble chemokine in the same order of magnitude as the initial concentration used for gradient formation first led to an increase and then to a decrease of the mean relative fluorescence intensity in the channel. The result was explained by the interaction of soluble chemokine with the equilibrium between soluble and heparin-bound chemokine. First, soluble chemokine that is predominantly present as dimer should occupy free binding sites and already immobilized chemokines should bind free monomers by dimerization. As more chemokines detach from the surface during incubation time, the mean relative fluorescence intensities then decrease. Similarly, the steepness of the gradient was increased by the overlay with soluble chemokine within the first 20 h of incubation. The binding of free monomers from solution by surface-bound CXCL8 would lead to an equilibrium shift, so that dimers in solution dissociate in compensation and even more monomers are able to bind to surface-bound CXCL8. After 43 h of incubation, the slope of the concentration profile either increased or decreased, depending on the channel section. It was also shown that THP-1 cells that express receptors for CXCL8 reproducibly recognize a CXCL8 gradient and migrate towards higher concentrations of CXCL8. Furthermore, control experiments confirmed that directed cell migration did not take place only in the presence of buffer or homogeneously distributed chemokine. Larger standard deviations in the presence of chemokine without an gradient might be explained by receptor activation after CXCL8 stimulation, resulting in random cell movement (chemokinesis). An overlay with soluble CXCL8 that has a concentration in the same range as initial CXCL8 used for gradient formation delayed the migration of THP-1 cells towards higher chemokine concentrations of the immobilized gradient. This result can be attributed to the interference with the equilibrium between soluble and heparin-bound chemokine, so that cells undergo chemokinesis rather than directed migration and the homogeneously distributed soluble chemokine dominates. If the chemokine binds to the surface or is internalized and degraded by the cells, the concentration in solution decreases and the immobilized gradient with an altered slope prevails, so that cells migrate. The decreasing concentration in solution will be part of future studies. Very low concentrations of soluble CXCL8 overlaid over the immobilized gradient had no impact on the directed cell migration, so that it can be assumed that the immobilized gradient dominates. The fact that from the immobilized gradient, chemokine dissociates and forms a soluble gradient contributes to this. These findings showed that the method to generate reversibly immobilized chemokine gradients enabled the analysis to which extent non-covalently immobilized chemokine gradients are influenced by soluble chemokine as well as a reproducible analysis of cell migration along these gradients. Further studies might include single-cell analysis to study the migration pathways of single cells in detail. Moreover, the influence of opposed soluble gradients and other chemokines in solutions should be examined. Future studies might also include the impact of chemokine inhibitors or chemokine receptor inhibitors on cell migration along reversibly immobilized CXCL8 gradients.

7.3. Covalent immobilization of CXCL8 in microfluidic devices

For some of the planned studies it would be advantageous if the immobilized gradients were stable and did not release any chemokine into solution. This would allow a precise adjustment of the chemokine concentration in solution. Therefore, the successfully used RGX-method from the first project should be

applied to covalently immobilize the chemokine. In detail, a method for the covalent immobilization of unmodified CXCL8 on a collagen-coated microfluidic device by RGX should be developed, as collagen is a commonly used substrate for migration studies. During method development different parameters such as the concentration of collagen and RB, the method used for collagen coating, the type of CXCL8 and the washing conditions were varied. A method that allowed a reproducible and clearly detectable covalent immobilization of native CXCL8 could not be developed with the tested parameters. Interaction studies could not confirm an interaction of CXCL8 with collagen, while weak, non-specific interactions of RB with CXCL8 and BSA were observed. In detail, the interaction of BSA with RB can be found in the low micromolar range, which is also to be expected based on the properties of BSA, whereas the interaction of the chemokine with RB is more likely to be in the upper micromolar to millimolar range. However, if there are no activatable residues near the binding site or if the native protein with the activated site does not come close enough to the collagen, immobilization by RGX will not occur. Moreover, the particular protein concentrations that indicated an interaction with RB were beyond the concentrations used in microfluidic experiments. It follows, that only areas of the gradient with high concentrations of CXCL8 could be immobilized by RGX. If high concentrations of chemokine and RB in combination with laser exposure for RGX would be used, the exposure time might control the amount of immobilized chemokine and could be used for the formation of a gradient. This method would still allow the immobilization of native proteins and the generation of soluble gradients by microfluidics [119], though significantly more expensive equipment compared to power LEDs would be needed.

References

[1] T. C. Horan, R. P. Gaynes, W. J. Martone, W. R. Jarvis, T. Grace Emori, *American Journal of Infection Control* **1992**, *20*, 271–274.

[2] T. G. Emori, R. P. Gaynes, *Clinical microbiology reviews* **1993**, *6*, 428–442.

[3] A. F. Chen, A. Fleischman, M. S. Austin, *The Journal of the American Academy of Orthopaedic Surgeons* **2018**, *26*, e371–e378.

[4] J. Braun, S. Eckes, P. M. Rommens, K. Schmitz, D. Nickel, U. Ritz, *Antibiotics* **2020**, *9*, 238.

[5] K. Yuan, H.-L. Chen, *International Journal of Surgery* **2013**, *11*, 383–388.

[6] V. Negi, S. Pal, D. Juyal, M. K. Sharma, N. Sharma, *Journal of Clinical and Diagnostic Research* **2015**, *9*, DC17–20.

[7] D. C. Classen, R. S. Evans, S. L. Pestotnik, S. D. Horn, R. L. Menlove, J. P. Burke, *The New England journal of medicine* **1992**, *326*, 281–286.

[8] T. Abdullah, K. Gauthaman, A. Mostafavi, A. Alshahrie, N. Salah, P. Morganti, A. Chianese, A. Tamayol, A. Memic, *Scientific reports* **2020**, *10*, 20428.

[9] H. Lu, Y. Liu, J. Guo, H. Wu, J. Wang, G. Wu, *International journal of molecular sciences* **2016**, *17*, 334.

[10] S. Harbarth, M. H. Samore, D. Lichtenberg, Y. Carmeli, *Circulation* **2000**, *101*, 2916–2921.

[11] N. A. Lopez, C. V. Luengo, M. J. Avena, *Adsorption* **2019**, *25*, 1349–1360.

[12] B. Snoddy, A. C. Jayasuriya, *Materials science & engineering. C Materials for biological applications* **2016**, *67*, 822–833.

[13] H.-Y. Chiang, L. A. Herwaldt, A. E. Blevins, E. Cho, M. L. Schweizer, *The Spine Journal* **2014**, *14*, 397–407.

[14] I. Chopra, M. Roberts, *Microbiology and molecular biology reviews* **2001**, *65*, 232–260.

[15] K. Anagnostakos, J. Kelm, *Journal of biomedical materials research. Part B Applied biomaterials* **2009**, *90*, 467–475.

[16] M. L. Edin, T. Miclau, G. E. Lester, R. W. Lindsey, L. E. Dahners, *Clinical orthopaedics and related research* **1996**, 245–251.

[17] J. M. Hartinger, P. Lukáč, P. Mitáš, M. Mlček, M. Popková, T. Suchý, M. Šupová, J. Závora, V. Adámková, H. Benáková, O. Slanař, M. Šíma, M. Bartoš, H. Chlup, T. Grus, *Bosnian journal of basic medical sciences* **2021**, *21*, 61–70.

[18] D. Tigani, C. Zolezzi, F. Trentani, A. Ragaini, M. Iafisco, S. Manara, B. Palazzo, N. Roveri, *Journal of Materials Science: Materials in Medicine* **2008**, *19*, 1325–1334.

[19] N. Hassani Besheli, F. Mottaghitalab, M. Eslami, M. Gholami, S. C. Kundu, D. L. Kaplan, M. Farokhi, *ACS applied materials & interfaces* **2017**, *9*, 5128–5138.

[20] Sigma-Aldrich, Product Specification Tetracycline, **2022**.

[21] Sigma-Aldrich, Product Specification Tobramycin, **2022**.

[22] Sigma-Aldrich, Product Specification Vancomycin-hydrochlorid, **2022**.

[23] J. Li, D. J. Mooney, *Nature reviews. Materials* **2016**, *1*, 16071.

[24] F. Ganji, S. Vasheghani-Farahani, E. Vasheghani-Farahani, *Iranian Polymer Journal* **2010**, *19*, 375–398.

[25] N. A. Peppas, N. M. Franson, *Journal of Polymer Science: Polymer Physics Edition* **1983**, *21*, 983–997.

[26] L. Zhao, X. Li, J. Zhao, S. Ma, X. Ma, D. Fan, C. Zhu, Y. Liu, *Materials science & engineering. C Materials for biological applications* **2016**, *68*, 317–326.

[27] S. Khan, N. M. Ranjha, *Polymer Bulletin* **2014**, *71*, 2133–2158.

[28] B. D. Ratner, *Regenerative biomaterials* **2016**, *3*, 107–110.

[29] S. Naahidi, M. Jafari, M. Logan, Y. Wang, Y. Yuan, H. Bae, B. Dixon, P. Chen, *Biotechnology advances* **2017**, *35*, 530–544.

[30] B. V. Slaughter, S. S. Khurshid, O. Z. Fisher, A. Khademhosseini, N. A. Peppas, *Advanced materials* **2009**, *21*, 3307–3329.

[31] S. R. Caliari, J. A. Burdick, *Nature methods* **2016**, *13*, 405–414.

[32] K. Gelse, E. Pöschl, T. Aigner, *Advanced Drug Delivery Reviews* **2003**, *55*, 1531–1546.

[33] E. Davison-Kotler, W. S. Marshall, E. García-Gareta, *Bioengineering* **2019**, *6*, 56.

[34] R. Parenteau-Bareil, R. Gauvin, F. Berthod, *Materials* **2010**, *3*, 1863–1887.

[35] M. D. Shoulders, R. T. Raines, *Annual review of biochemistry* **2009**, *78*, 929–958.

[36] K. Hanai, T. Kojima, M. Ota, J. Onodera, N. Sawada, *Journal of drug delivery* **2012**, *2012*, 245835.

[37] T. Miyata, T. Taira, Y. Noishiki, *Clinical Materials* **1992**, *9*, 139–148.

[38] C.-M. Lefter, S. S. Maier, V. Maier, M. Popa, J. Desbrieres, *Materials science & engineering. C Materials for biological applications* **2013**, *33*, 2323–2331.

[39] R. Holmes, S. Kirk, G. Tronci, X. Yang, D. Wood, *Materials science & engineering. C Materials for biological applications* **2017**, *77*, 823–827.

[40] M. Nair, S. M. Best, R. E. Cameron, *Applied Sciences* **2020**, *10*, 6911.

[41] L. H. H. Olde Damink, P. J. Dijkstra, M. J. A. van Luyn, P. B. van Wachem, P. Nieuwenhuis, J. Feijen, *Journal of Materials Science: Materials in Medicine* **1995**, *6*, 460–472.

[42] J. W. Keillor, C. M. Clouthier, K. Y. P. Apperley, A. Akbar, A. Mulani, *Bioorganic chemistry* **2014**, *57*, 186–197.

[43] B. P. Chan, K.-F. So, *Journal of biomedical materials research. Part A* **2005**, *75*, 689–701.

[44] E. I. Alarcon, H. Poblete, H. Roh, J.-F. Couture, J. Comer, I. E. Kochevar, *ACS omega* **2017**, *2*, 6646–6657.

[45] A. Alqerban, *Pharmaceuticals* **2021**, *14*, 48.

[46] A. S. McCall, S. Kraft, H. F. Edelhauser, G. W. Kidder, R. R. Lundquist, H. E. Bradshaw, Z. Dedeic, M. J. C. Dionne, E. M. Clement, G. W. Conrad, *Investigative ophthalmology & visual science* **2010**, *51*, 129–138.

[47] D. Hamidi Alamdari, A. Bagheri Moghaddam, S. Amini, A. Hamidi Alamdari, M. Damsaz, A. Yarahmadi, *The archives of bone and joint surgery* **2020**, *8*, 291–294.

[48] B. Wang, J.-H. Wang, Q. Liu, H. Huang, M. Chen, K. Li, C. Li, X.-F. Yu, P. K. Chu, *Biomaterials* **2014**, *35*, 1954–1966.

[49] X. Huang, M. A. El-Sayed, *Alexandria Journal of Medicine* **2011**, *47*, 1–9.

[50] B. J. Blackburn, A. M. Rollins, W. J. Dupps, *Translational vision science & technology* **2021**, *10*, 8.

[51] R. W. Redmond, I. E. Kochevar, *Photochemistry and photobiology* **2019**, *95*, 1097–1115.

[52] C. M. Wertheimer, C. Elhardt, S. M. Kaminsky, L. Pham, Q. Pei, B. Mendes, S. Afshar, I. E. Kochevar, *Investigative ophthalmology & visual science* **2019**, *60*, 1845–1852.

[53] S. M. Bachilo, R. B. Weisman, *The Journal of Physical Chemistry A* **2000**, *104*, 7711–7714.

[54] D. C. Neckers, *Journal of Photochemistry and Photobiology A: Chemistry* **1989**, *47*, 1–29.

[55] L. Ludvíková, P. Friš, D. Heger, P. Šebej, J. Wirz, P. Klán, *Physical Chemistry Chemical Physics* **2016**, *18*, 16266–16273.

[56] V. R. Batistela, D. S. Pellosi, F. D. de Souza, W. F. da Costa, S. M. de Oliveira Santin, V. R. de Souza, W. Caetano, H. P. M. de Oliveira, I. S. Scarminio, N. Hioka, *Spectrochimica acta. Part A Molecular and biomolecular spectroscopy* **2011**, *79*, 889–897.

[57] G. R. Fleming, A. W. E. Knight, J. M. Morris, R. J. S. Morrison, G. W. Robinson, *Journal of the American Chemical Society* **1977**, *99*, 4306–4311.

[58] C. Würth, M. Grabolle, J. Pauli, M. Spieles, U. Resch-Genger, *Nature protocols* **2013**, *8*, 1535–1550.

[59] E. Alarcón, A. M. Edwards, A. Aspee, F. E. Moran, C. D. Borsarelli, E. A. Lissi, D. Gonzalez-Nilo, H. Poblete, J. C. Scaiano, *Photochemical & photobiological sciences* **2010**, *9*, 93–102.

[60] C. M. Wertheimer, B. Mendes, Q. Pei, K. Brandt, I. E. Kochevar, *Translational vision science & technology* **2020**, *9*, 24.

[61] N. Vanerio, M. Stijnen, B. A. J. M. de Mol, L. M. Kock, *Photobiomodulation photomedicine and laser surgery* **2019**, *37*, 383–394.

[62] S. Tsao, M. Yao, H. Tsao, F. P. Henry, Y. Zhao, J. J. Kochevar, R. W. Redmond, I. E. Kochevar, *The British journal of dermatology* **2012**, *166*, 555–563.

[63] H. Zhu, C. Alt, R. H. Webb, S. Melki, I. E. Kochevar, *Cornea* **2016**, *35*, 1234–1241.

[64] T. Mazaki, Y. Shiozaki, K. Yamane, A. Yoshida, M. Nakamura, Y. Yoshida, Di Zhou, T. Kitajima, M. Tanaka, Y. Ito, T. Ozaki, A. Matsukawa, *Scientific reports* **2014**, *4*, 4457.

[65] J. R. Fernandes, H. M. Salinas, G. F. Broelsch, M. C. McCormack, A. M. Meppelink, M. A. Randolph, R. W. Redmond, W. G. Austen, *Plastic and reconstructive surgery* **2014**, *133*, 571–577.

[66] H. M. Salinas, S. I. Khan, M. C. McCormack, J. R. Fernandes, L. Gfrerer, M. T. Watkins, R. W. Redmond, W. G. Austen, *Journal of vascular surgery* **2017**, *65*, 190–196.

[67] S. Eckes, J. Braun, J. S. Wack, U. Ritz, D. Nickel, K. Schmitz, *International journal of molecular sciences* **2020**, *21*, 7408.

[68] J. Braun, S. Eckes, M. F. Kilb, D. Fischer, C. Eßbach, P. M. Rommens, P. Drees, K. Schmitz, D. Nickel, U. Ritz, *Regenerative biomaterials* **2021**, *8*, rbab059.

[69] S. Berkamp, S. H. Park, A. A. de Angelis, F. M. Marassi, S. J. Opella, *Journal of biomolecular NMR* **2017**, *69*, 111–121.

[70] C. L. Sokol, A. D. Luster, *Cold Spring Harbor perspectives in biology* **2015**, *7*, a016303.

[71] J.-M. Zhang, J. An, *International anesthesiology clinics* **2007**, *45*, 27–37.

[72] S. L. Deshmane, S. Kremlev, S. Amini, B. E. Sawaya, *Journal of interferon & cytokine research* **2009**, *29*, 313–326.

[73] S. P. Alexander, A. P. Davenport, E. Kelly, N. Marrion, J. A. Peters, H. E. Benson, E. Faccenda, A. J. Pawson, J. L. Sharman, C. Southan, J. A. Davies, *British journal of pharmacology* **2015**, *172*, 5744–5869.

[74] F. Bachelerie, A. Ben-Baruch, A. M. Burkhardt, C. Combadiere, J. M. Farber, G. J. Graham, R. Horuk, A. H. Sparre-Ulrich, M. Locati, A. D. Luster, A. Mantovani, K. Matsushima, P. M. Murphy, R. Nibbs, H. Nomiyama, C. A. Power, A. E. I. Proudfoot, M. M. Rosenkilde, A. Rot, S. Sozzani, M. Thelen, O. Yoshie, A. Zlotnik, *Pharmacological reviews* **2014**, *66*, 1–79.

[75] M. Arimont, S.-L. Sun, R. Leurs, M. Smit, I. J. P. de Esch, C. de Graaf, *Journal of medicinal chemistry* **2017**, *60*, 4735–4779.

[76] B. J. Rollins, *Blood* **1997**, *90*, 909–928.

[77] C. A. Hébert, R. V. Vitangcol, J. B. Baker, *The Journal of biological chemistry* **1991**, *266*, 18989–18994.

[78] I. Clark-Lewis, C. Schumacher, M. Baggiolini, B. Moser, *The Journal of biological chemistry* **1991**, *266*, 23128–23134.

[79] R. M. Strieter, P. J. Polverini, S. L. Kunkel, D. A. Arenberg, M. D. Burdick, J. Kasper, J. Dzuiba, J. van Damme, A. Walz, D. Marriott, *The Journal of biological chemistry* **1995**, *270*, 27348–27357.

[80] M. Baggiolini, A. Walz, S. L. Kunkel, *The Journal of clinical investigation* **1989**, *84*, 1045–1049.

[81] K. Matsushima, K. Morishita, T. Yoshimura, S. Lavu, Y. Kobayashi, W. Lew, E. Appella, H. F. Kung, E. J. Leonard, J. J. Oppenheim, *The Journal of experimental medicine* **1988**, *167*, 1883–1893.

[82] H. Ha, B. Debnath, N. Neamati, *Theranostics* **2017**, *7*, 1543–1588.

[83] M. Baggiolini, I. Clark-Lewis, *FEBS Letters* **1992**, *307*, 97–101.

[84] I. Lindley, H. Aschauer, J. M. Seifert, C. Lam, W. Brunowsky, E. Kownatzki, M. Thelen, P. Peveri, B. Dewald, V. von Tscharner, *Proceedings of the National Academy of Sciences of the United States of America* **1988**, *85*, 9199–9203.

[85] G. M. Clore, E. Appella, M. Yamada, K. Matsushima, A. M. Gronenborn, *The Journal of biological chemistry* **1989**, *264*, 18907–18911.

[86] D. J. J. Waugh, C. Wilson, *Clinical cancer research* **2008**, *14*, 6735–6741.

[87] P. M. Murphy, H. L. Tiffany, *Science* **1991**, *253*, 1280–1283.

[88] N. J. Skelton, C. Quan, D. Reilly, H. Lowman, *Structure* **1999**, *7*, 157–168.

[89] E. F. Barter, M. J. Stone, *Biochemistry* **2012**, *51*, 1322–1331.

[90] S. R. Leong, R. C. Kabakoff, C. A. Hébert, *The Journal of biological chemistry* **1994**, *269*, 19343–19348.

[91] P. R. B. Joseph, J. M. Sarmiento, A. K. Mishra, S. T. Das, R. P. Garofalo, J. Navarro, K. Rajarathnam, *The Journal of biological chemistry* **2010**, *285*, 29262–29269.

[92] J. Middleton, S. Neil, J. Wintle, I. Clark-Lewis, H. Moore, C. Lam, M. Auer, E. Hub, A. Rot, *Cell* **1997**, *91*, 385–395.

[93] G. M. Clore, E. Appella, M. Yamada, K. Matsushima, A. M. Gronenborn, *Biochemistry* **1990**, *29*, 1689–1696.

[94] R. C. Russo, C. C. Garcia, M. M. Teixeira, F. A. Amaral, *Expert review of clinical immunology* **2014**, *10*, 593–619.

[95] L. Li, J. Li, M. Gao, H. Fan, Y. Wang, X. Xu, C. Chen, J. Liu, J. Kim, R. Aliyari, J. Zhang, Y. Jin, X. Li, F. Ma, M. Shi, G. Cheng, H. Yang, *Frontiers in immunology* **2020**, *11*, 602395.

[96] U. Häcker, K. Nybakken, N. Perrimon, *Nature reviews. Molecular cell biology* **2005**, *6*, 530–541.

[97] S. Morla, *International journal of molecular sciences* **2019**, *20*, 1963.

[98] S. Sarrazin, W. C. Lamanna, J. D. Esko, *Cold Spring Harbor perspectives in biology* **2011**, *3*, a004952.

[99] C. Lanzi, G. Cassinelli, *Molecules* **2018**, *23*, 2915.

[100] K. Ley, C. Laudanna, M. I. Cybulsky, S. Nourshargh, *Nature reviews. Immunology* **2007**, *7*, 678–689.

[101] T. M. Handel, Z. Johnson, S. E. Crown, E. K. Lau, A. E. Proudfoot, *Annual review of biochemistry* **2005**, *74*, 385–410.

[102] L. M. Webb, M. U. Ehrengruber, I. Clark-Lewis, M. Baggiolini, A. Rot, *Proceedings of the National Academy of Sciences of the United States of America* **1993**, *90*, 7158–7162.

[103] G. S. Kuschert, A. J. Hoogewerf, A. E. Proudfoot, C. W. Chung, R. M. Cooke, R. E. Hubbard, T. N. Wells, P. N. Sanderson, *Biochemistry* **1998**, *37*, 11193–11201.

[104] M. Metzemaekers, M. Gouwy, P. Proost, *Cellular & molecular immunology* **2020**, *17*, 433–450.

[105] X. Xiong, X. Liao, S. Qiu, H. Xu, S. Zhang, S. Wang, J. Ai, L. Yang, *Frontiers in molecular biosciences* **2022**, *9*, 723846.

[106] K. Liu, L. Wu, S. Yuan, M. Wu, Y. Xu, Q. Sun, S. Li, S. Zhao, T. Hua, Z.-J. Liu, *Nature* **2020**, *585*, 135–140.

[107] S. de Oliveira, E. E. Rosowski, A. Huttenlocher, *Nature reviews. Immunology* **2016**, *16*, 378–391.

[108] R. Horwitz, D. Webb, *Current biology* **2003**, *13*, R756–9.

[109] S. SenGupta, C. A. Parent, J. E. Bear, *Nature reviews. Molecular cell biology* **2021**, *22*, 529–547.

[110] S. Nourshargh, R. Alon, *Immunity* **2014**, *41*, 694–707.

[111] B. Bhushan, *Springer Handbook of Nanotechnology*, Springer Berlin Heidelberg, Berlin, Heidelberg, **2017**.

[112] H.-M. Wu, T.-A. Lee, P.-L. Ko, H.-J. Chiang, C.-C. Peng, Y.-C. Tung, *Journal of Micromechanics and Microengineering* **2018**, *28*, 043001.

[113] S.-E. Ong, S. Zhang, H. Du, Y. Fu, *Frontiers in bioscience : a journal and virtual library* **2008**, *13*, 2757–2773.

[114] A. Siddique, T. Meckel, R. W. Stark, S. Narayan, *Colloids and surfaces. B Biointerfaces* **2017**, *150*, 456–464.

[115] Z. Qian, D. Ross, W. Jia, Q. Xing, F. Zhao, *Bioactive materials* **2018**, *3*, 167–173.

[116] N. Li Jeon, H. Baskaran, S. K. W. Dertinger, G. M. Whitesides, L. van de Water, M. Toner, *Nature biotechnology* **2002**, *20*, 826–830.

[117] I. Halilovic, J. Wu, M. Alexander, F. Lin, *Biomedical microdevices* **2015**, *17*, 9963.

[118] I. Rink, J. Rink, D. Helmer, D. Sachs, K. Schmitz, *The Journal of Immunology* **2015**, *194*, 5549–5558.

[119] J. Schwarz, V. Bierbaum, J. Merrin, T. Frank, R. Hauschild, T. Bollenbach, S. Tay, M. Sixt, M. Mehling, *Scientific reports* **2016**, *6*, 36440.

[120] M. F. Kilb, V. I. Engemann, A. Siddique, R. W. Stark, K. Schmitz, *Colloids and surfaces. B Biointerfaces* **2021**, *198*, 111498.

[121] Y. J. Chuah, Y. T. Koh, K. Lim, N. V. Menon, Y. Wu, Y. Kang, *Scientific reports* **2015**, *5*, 18162.

[122] J. M. Leung, L. R. Berry, H. M. Atkinson, R. M. Cornelius, D. Sandejas, N. Rochow, P. R. Selvaganapathy, C. Fusch, A. K. C. Chan, J. L. Brash, *Journal of materials chemistry. B* **2015**, *3*, 6032–6036.

[123] H. Lee, S. M. Dellatore, W. M. Miller, P. B. Messersmith, *Science* **2007**, *318*, 426–430.

[124] D. Sharma, W. Jia, F. Long, S. Pati, Q. Chen, Y. Qyang, B. Lee, C. K. Choi, F. Zhao, *Bioactive materials* **2019**, *4*, 142–150.

[125] J. Schindelin, I. Arganda-Carreras, E. Frise, V. Kaynig, M. Longair, T. Pietzsch, S. Preibisch, C. Rueden, S. Saalfeld, B. Schmid, J.-Y. Tinevez, D. J. White, V. Hartenstein, K. Eliceiri, P. Tomancak, A. Cardona, *Nature methods* **2012**, *9*, 676–682.

[126] Thorlabs GmbH, M565L3 Specification Sheet, **2019**.

[127] M. F. Kilb, Y. Moos, S. Eckes, J. Braun, U. Ritz, D. Nickel, K. Schmitz, *Biomedicines* **2021**, *9*, 1668.

[128] S. Tsuchiya, M. Yamabe, Y. Yamaguchi, Y. Kobayashi, T. Konno, K. Tada, *International journal of cancer* **1980**, *26*, 171–176.

[129] I.-J. Fang, B. G. Trewyn, *Methods in enzymology* **2012**, *508*, 41–59.

[130] I. Rink, Dissertation, Universitäts- und Landesbibliothek Darmstadt, Darmstadt, **2016**.

[131] Thermo Fisher Scientific Inc., Crosslinking Technical Handbook, **2012**.

[132] Thermo Fisher Scientific Inc., Immobilized TCEP Disulfide Reducing Gel, Instructions, **2013**.

[133] Thermo Fisher Scientific Inc., Calculate dye:protein (F/P) molar ratios, TECH TIP #31, **2011**.

[134] V. I. Engemann, Dissertation, Technische Universität Darmstadt, Darmstadt, **2021**.

[135] V. Charulatha, *Biomaterials* **2003**, *24*, 759–767.

[136] P. Angele, J. Abke, R. Kujat, H. Faltermeier, D. Schumann, M. Nerlich, B. Kinner, C. Englert, Z. Ruszczak, R. Mehrl, R. Mueller, *Biomaterials* **2004**, *25*, 2831–2841.

[137] B. P. Chan, T. Y. Hui, O. C. M. Chan, K.-F. So, W. Lu, K. M. C. Cheung, E. Salomatina, A. Yaroslavsky, *Tissue engineering* **2007**, *13*, 73–85.

[138] M. F. Kilb, U. Ritz, D. Nickel, K. Schmitz, *Polymers* **2022**, *14*, 5227.

[139] H.-C. Chen, *Methods in molecular biology* **2005**, *294*, 15–22.

[140] H. A. Leddy, M. A. Haider, F. Guilak, *Biophysical journal* **2006**, *91*, 311–316.

[141] T. Kihara, J. Ito, J. Miyake, *PloS one* **2013**, *8*, e82382.

[142] M. Tsintou, K. Dalamagkas, A. Seifalian, *International journal of biomaterials* **2018**, *2018*, 3514019.

[143] R. G. Wells, *Biochimica et biophysica acta* **2013**, *1832*, 884–890.

[144] S. Schreml, R. J. Meier, O. S. Wolfbeis, T. Maisch, R.-M. Szeimies, M. Landthaler, J. Regensburger, F. Santarelli, I. Klimant, P. Babilas, *Experimental dermatology* **2011**, *20*, 550–554.

[145] A. Junka, P. Szymczyk, G. Ziółkowski, E. Karuga-Kuzniewska, D. Smutnicka, I. Bil-Lula, M. Bartoszewicz, S. Mahabady, P. P. Sedghizadeh, *PloS one* **2017**, *12*, e0169565.

[146] J. L. Lister, A. R. Horswill, *Frontiers in cellular and infection microbiology* **2014**, *4*, 178.

[147] T. Zmantar, B. Kouidhi, H. Miladi, K. Mahdouani, A. Bakhrouf, *The new microbiologica* **2010**, *33*, 137–145.

[148] J. C. Berkmann, A. X. Herrera Martin, A. Ellinghaus, C. Schlundt, H. Schell, E. Lippens, G. N. Duda, S. Tsitsilonis, K. Schmidt-Bleek, *International journal of molecular sciences* **2020**, *21*, 2513.

[149] B. Onat, V. Bütün, S. Banerjee, I. Erel-Goktepe, *Acta biomaterialia* **2016**, *40*, 293–309.

[150] M. Cicuéndez, J. C. Doadrio, A. Hernández, M. T. Portolés, I. Izquierdo-Barba, M. Vallet-Regí, *Acta biomaterialia* **2018**, *65*, 450–461.

[151] S. Ono, R. Imai, Y. Ida, D. Shibata, T. Komiya, H. Matsumura, *Burns* **2015**, *41*, 820–824.

[152] H. R. Elden, *Science* **1958**, *128*, 1624–1625.

[153] P. J. Flory, J. Rehner, *The Journal of Chemical Physics* **1943**, *11*, 521–526.

[154] R. R. Pfeiffer, *Reviews of Infectious Diseases* **1981**, *3*, S205–S209.

[155] *Chiral recognition in separation methods, Mechanisms and applications*, (Ed.: A. Berthod), Springer, Heidelberg and Dordrecht, **2010**, 337 pp.

[156] S. Barrientos, O. Stojadinovic, M. S. Golinko, H. Brem, M. Tomic-Canic, *Wound repair and regeneration* **2008**, *16*, 585–601.

[157] M. Bommadevara, L. Zhu, *Biomechanics and modeling in mechanobiology* **2002**, *1*, 137–149.

[158] W. Yang, C. Liu, Y. Chen, *Langmuir* **2018**, *34*, 3565–3571.

[159] J. Wu, Z. Mao, H. Tan, L. Han, T. Ren, C. Gao, *Interface focus* **2012**, *2*, 337–355.

[160] H. Fernando, C. Chin, J. Rösgen, K. Rajarathnam, *The Journal of biological chemistry* **2004**, *279*, 36175–36178.

[161] P. R. B. Joseph, K. V. Sawant, K. Rajarathnam, *Open biology* **2017**, *7*, 170168.

[162] K. Vogiatzi, S. Apostolakis, Z. Vlata, E. Krabovitis, D. A. Spandidos, *Experimental and therapeutic medicine* **2013**, *5*, 987–991.

[163] G. J. Graham, T. M. Handel, A. E. I. Proudfoot, *Trends in immunology* **2019**, *40*, 472–481.

[164] Z. Liu, J. Klominek, *Anticancer research* **2004**, *24*, 1625–1630.

[165] G. A. Monteiro, H. G. Sundararaghavan, A. V. Fernandes, D. I. Shreiber in *ASME 2008 Summer Bioengineering Conference, Parts A and B*, **2008**, pp. 537–538.

[166] A. E. Stanton, X. Tong, F. Yang, *APL bioengineering* **2019**, *3*, 036108.

[167] J. Panchompoo, L. Aldous, M. Baker, M. I. Wallace, R. G. Compton, *The Analyst* **2012**, *137*, 2054–2062.

[168] Hoya Corporation, Data sheet Y52 filter, **2020**.

[169] L. Ludvíková, P. Štacko, J. Sperry, P. Klán, *The Journal of organic chemistry* **2018**, *83*, 10835–10844.

[170] H. R. Shen, J. D. Spikes, P. Kopeceková, J. Kopecek, *Journal of photochemistry and photobiology. B Biology* **1996**, *34*, 203–210.

[171] H. R. Shen, J. D. Spikes, P. Kopecková, J. Kopecek, *Journal of photochemistry and photobiology. B Biology* **1996**, *35*, 213–219.

[172] H.-R. Shen, J. D. Spikes, C. J. Smith, J. Kopeček, *Journal of Photochemistry and Photobiology A: Chemistry* **2000**, *130*, 1–6.

[173] L. Zhao, J. Liu, R. Guo, Q. Sun, H. Yang, H. Li, *RSC Advances* **2017**, *7*, 27796–27806.

[174] M. B. E. Turbay, V. Rey, N. M. Argañaraz, F. E. Morán Vieyra, A. Aspée, E. A. Lissi, C. D. Borsarelli, *Journal of photochemistry and photobiology. B Biology* **2014**, *141*, 275–282.

[175] A. Chyzy, M. E. Plonska-Brzezinska, *Molecules (Basel Switzerland)* **2020**, *25*, 5795.

[176] A. Friedmann, A. Baertel, C. Schmitt, C. Ludtka, J. Milosevic, H.-J. Meisel, F. Goehre, S. Schwan, *International journal of molecular sciences* **2021**, *22*, 4248.

[177] J. Claus, A. Brietzke, C. Lehnert, S. Oschatz, N. Grabow, U. Kragl, *PloS one* **2020**, *15*, e0231421.

[178] J. Siepmann, F. Siepmann, *International journal of pharmaceutics* **2008**, *364*, 328–343.

[179] O. M. Alsaeed, A. A. Bukhari, A. A. Alshehri, F. A. Alsumairi, A. M. Alnami, H. A. Elsheikh, *Cureus* **2022**, *14*, e26731.

A. Supplementary

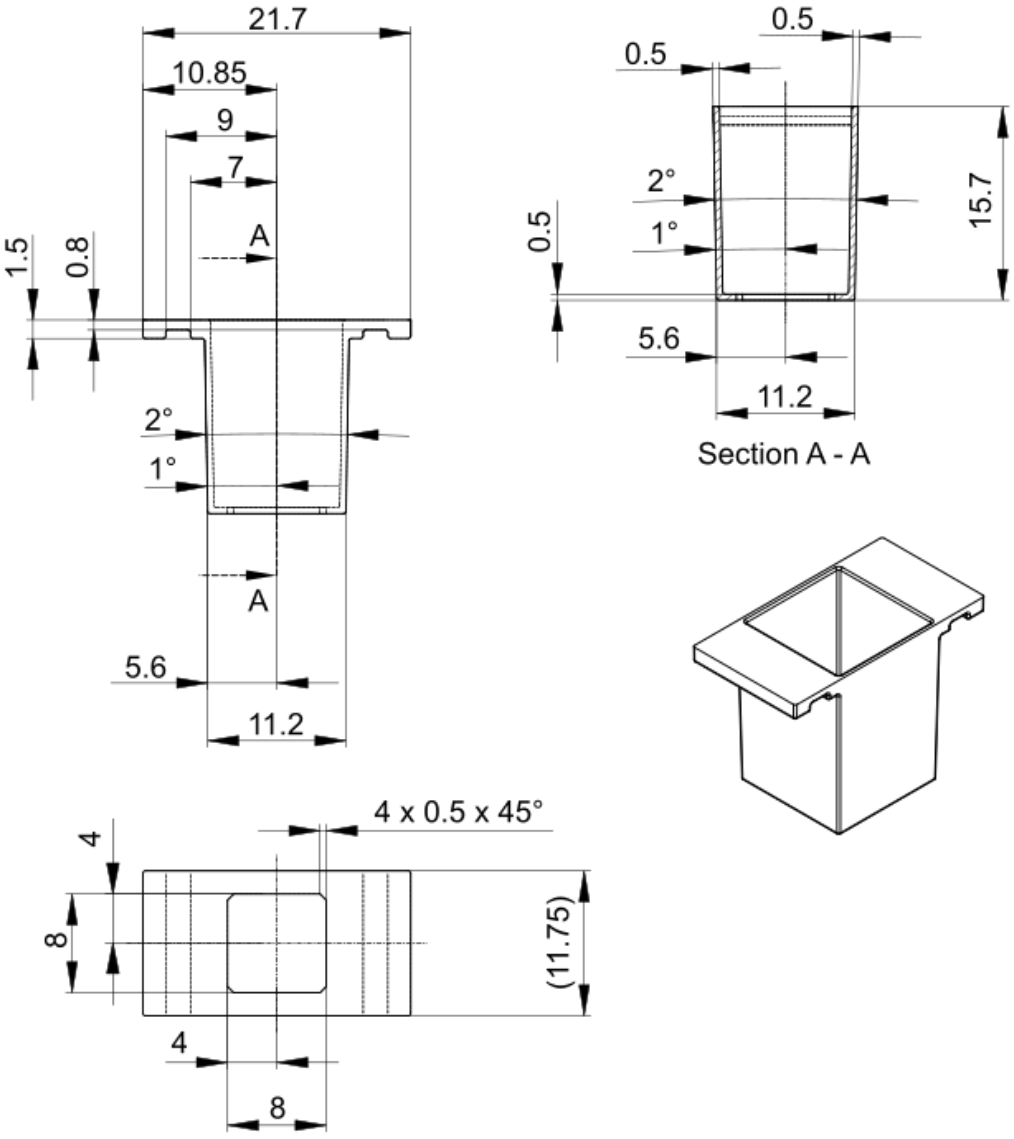

Figure A.1.: Construction drawing of the lower part of the sample holder. The dimensions are displayed in mm. Unspecified radii have a size of 0.2 mm.[127]

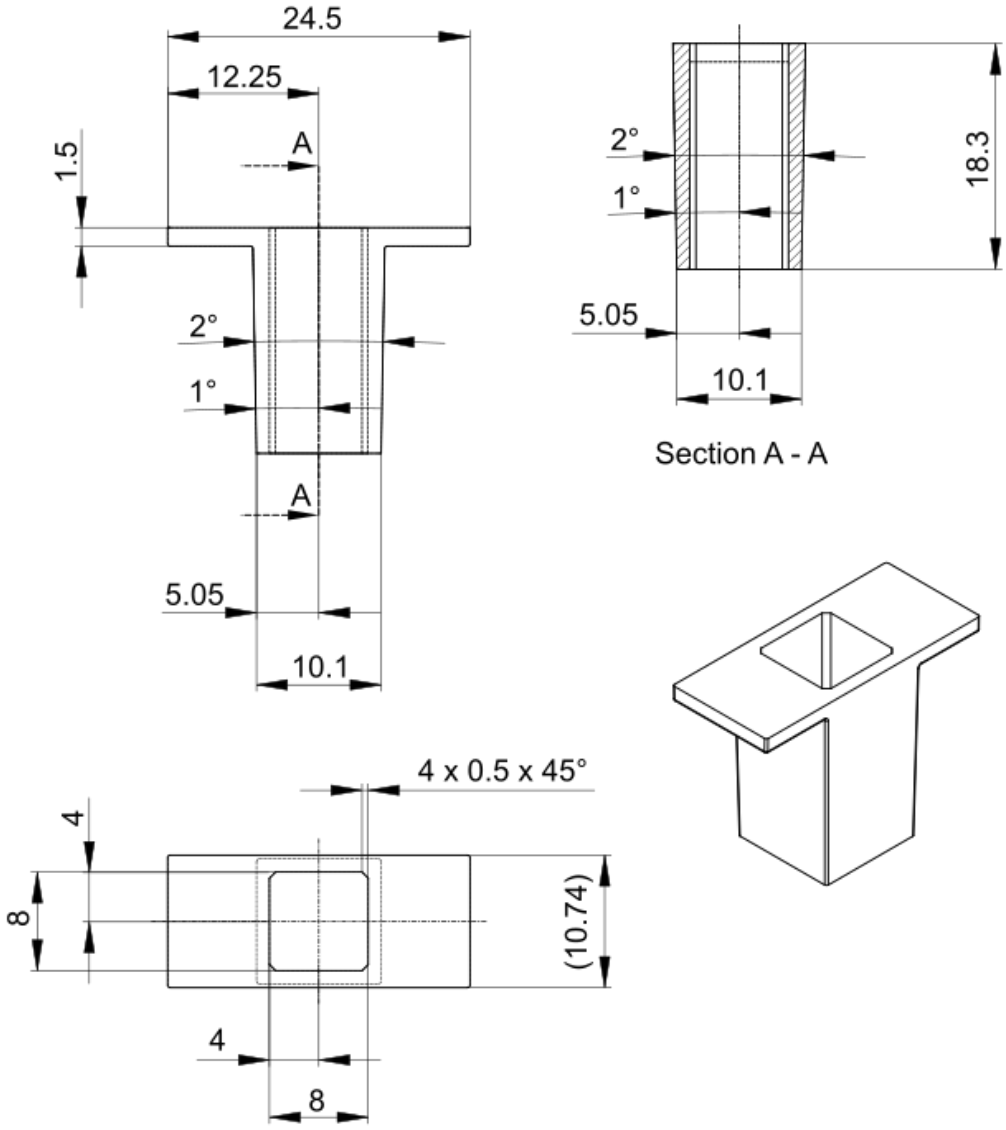

Figure A.2.: Construction drawing of the upper part of the sample holder. The dimensions are displayed in mm. Unspecified radii have a size of 0.2 mm.[127]

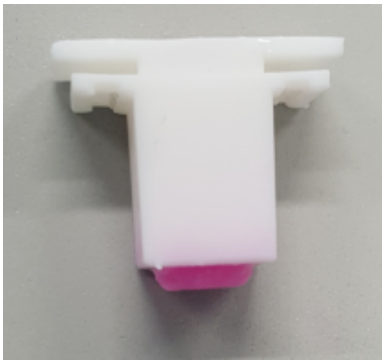

Figure A.3.: Photography of the laminate AAA placed in a white sample holder after 24 h of incubation. The central layer of AAA was loaded with vancomycin. Incubation was performed over 24 h at pH 7.4 and 37 °C.

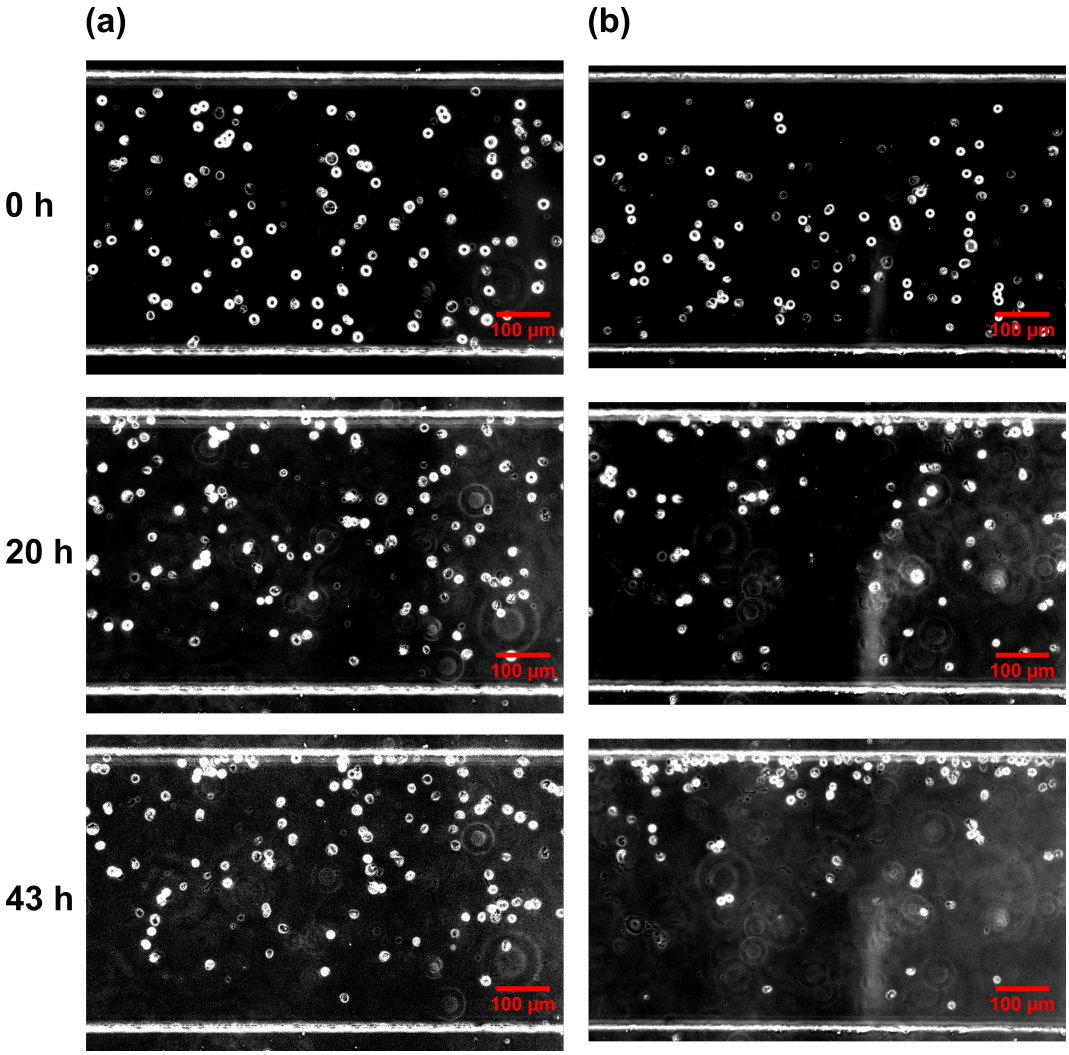

Figure A.4.: Migration of THP-1 cells along an reversibly immobilized CXCL8-gradient in channel section 18 of two microfluidic devices. The microfluidic channels were coated by rotating incubation with dopamine and heparin. The gradient was formed with 8 µM of CXCL8 at a flow rate of 0.8 µL/min for 240 min. After gradient formation, the channel was rinsed from the outlet with loading buffer and $3x10^6$ THP-1 cells were flushed into the channel from the outlet. Images of the channel (900 µm-sections) were taken under the fluorescence microscope with 10x magnification in phase contrast and adjusted in terms of brightness and contrast. (a) First experiment. (b) Second experiment.

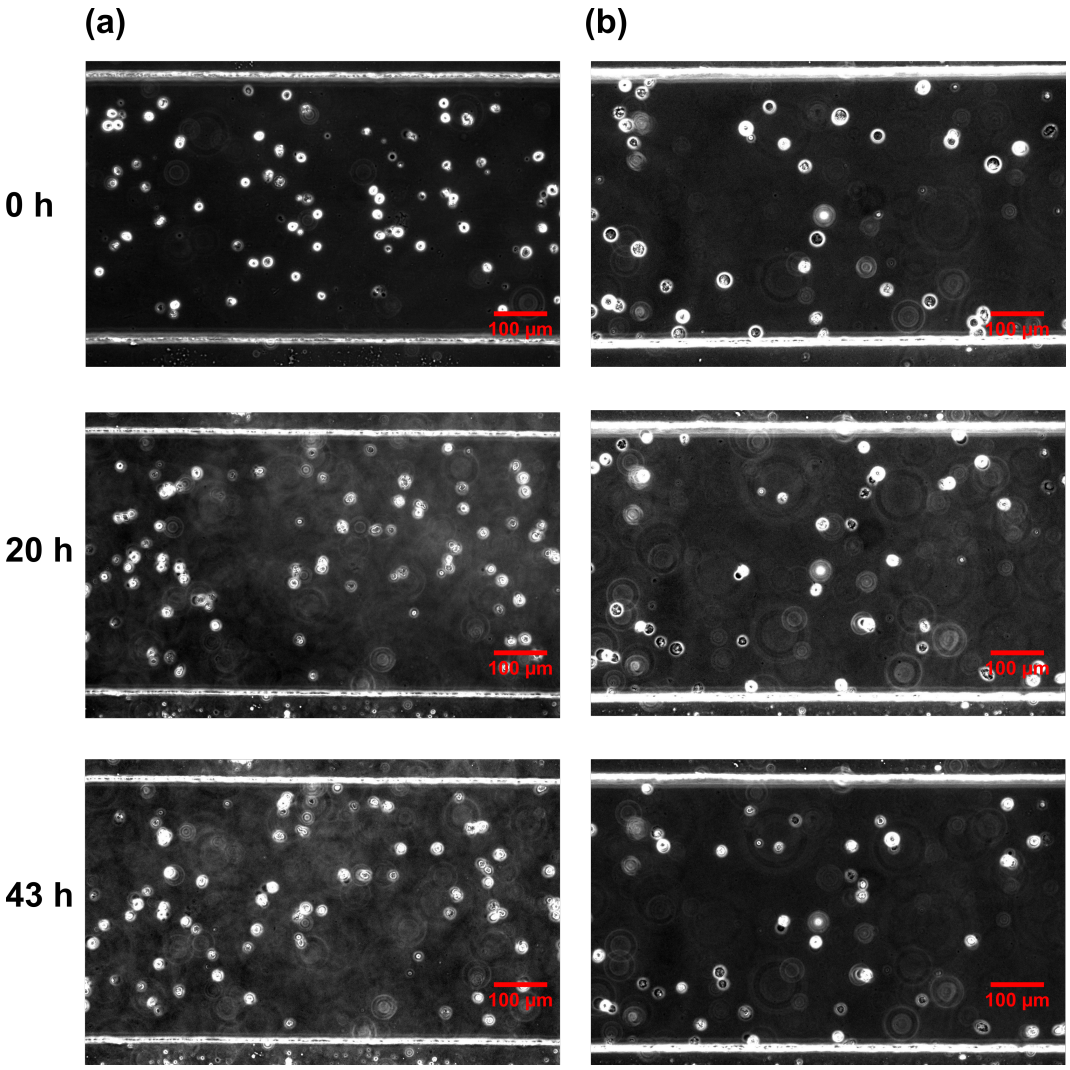

Figure A.5.: Control experiment of THP-1 cell migration in channel section 18. The microfluidic channels were coated by rotating incubation with dopamine and heparin. Loading buffer or 8 µM CXCL8 were flushed into the channel at a flow rate of 0.8 µL/min for 240 min without gradient formation. The channel was rinsed from the outlet with loading buffer and $3x10^6$ THP-1 cells were flushed into the channel from the outlet. Images of the channel (900 µm-sections) were taken under the fluorescence microscope with 10x magnification in phase contrast and adjusted in terms of brightness and contrast. (a) Only loading buffer. (b) Only 8 µM CXCL8 without gradient.

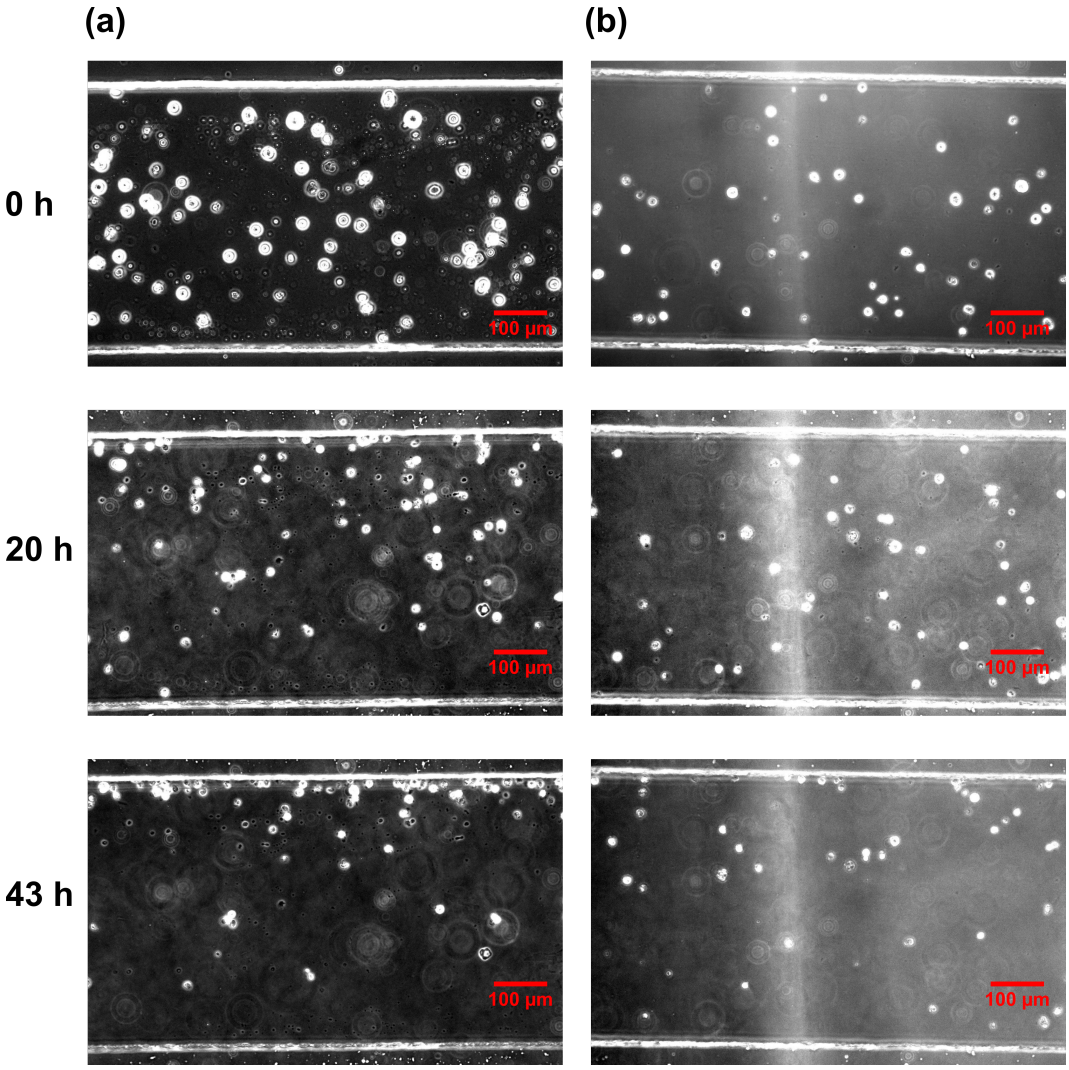

Figure A.6.: Microscopic images of THP-1 cells in the upper and lower channel half of channel sections 15 to 21 before incubation (0 h), after 20 h of incubation and after 43 h of incubation at 37 °C and 5 % CO_2. Channels were coated by rotating incubation with dopamine and heparin. The gradient was formed with 8 µM of CXCL8 at a flow rate of 0.8 µL/min for 240 min. After gradient formation, the channel was rinsed from the outlet with loading buffer and $3x10^6$ THP-1 cells were flushed into the channel from the outlet. The cell suspension was supplemented with 10 nM or 10 µM of soluble CXCL8 directly before flushing the cells into the channel. Images of the channel (900 µm-sections) were taken under the fluorescence microscope with 10x magnification in phase contrast and adjusted according brightness and contrast. (a) Overlay with 10 nM chemokine. (b) Overlay with 10 µM chemokine.

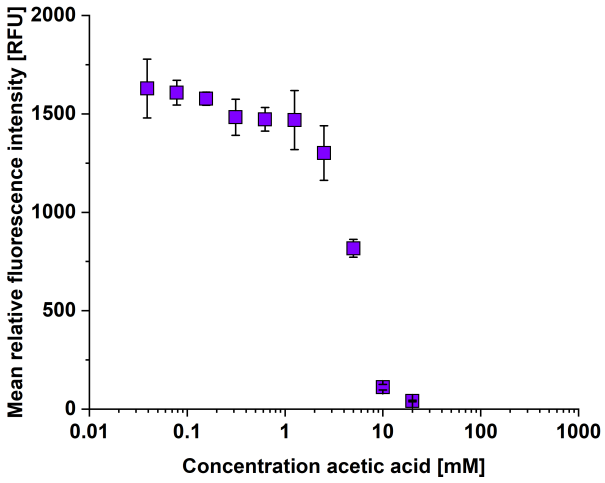

Figure A.7.: Mean relative fluorescence intensity of fluorescein (125 nM) depending on the concentration of acetic acid (0.04-20 mM) at a gain of 100 ($\lambda_{Ex.}$ = 490 nm and $\lambda_{Em.}$ = 525 nm). Error bars represent the standard deviation (*n = 3*).